UNIVERSITÉ PARIS XIII – SORBONNE PARIS NORD

École doctorale Sciences, Technologies, Santé Galilée

Analyse mathématique du blocage des phénomènes d'invasion; applications aux maladies inflammatoires et au remplacement des populations

THÈSE DE DOCTORAT
présentée par

Saoussen Latrach
Laboratoire Analyse, Géométrie et Applications (LAGA)

pour l'obtention du grade de
DOCTEUR EN MATHÉMATIQUES APPLIQUÉES

soutenue le 16/09/2025 devant le jury d'examen constitué de :

Souplet Philippe, Université Sorbonne Paris Nord, Paris ..... Président du jury
Lepoutre Thomas, Inria, Centre de Lyon, Lyon ..... Rapporteur
Griette Quentin, Université Le Havre Normandie, Le Havre ..... Rapporteur
Sasaki Takiko, Université Musashino, Japon ..... Examinatrice
Nouaili Nejla, Université Paris Dauphine-PSL, Paris ..... Examinatrice
Ogier-Denis Eric, INSERM, Paris ..... Examinateur
Vauchelet Nicolas, Université Sorbonne Paris Nord, Paris ..... Directeur
Zaag Hatem, Université Sorbonne Paris Nord, Paris ..... Co-directeur

ABSTRACT

Chronic inflammatory bowel diseases (IBD) and mosquito-borne epidemics pose major public health challenges. This thesis develops and analyses mathematical models based on reaction-diffusion systems to study propagation dynamics and the conditions leading to blockage in these biological phenomena.

In the first study, we focus on ulcerative colitis (UC), an IBD characterised by continuous inflammation of the colon. We establish a model describing the interaction between a pathogen and the immune system, demonstrating the existence of travelling waves that represent the spread of inflammation in a homogeneous medium. We then identify the conditions required to block this propagation in a heterogeneous medium and validate our findings through numerical simulations.

In the second study, we analyse a strategy for controlling mosquito-borne diseases, specifically the spread of Wolbachia, a bacterium that reduces the transmission of pathogens such as dengue. We examine cases where propagation is hindered in a heterogeneous medium, particularly when the carrying capacity varies spatially. We identify the conditions that lead to blockage and validate our results using numerical simulations.

Finally, I have also worked on the project Modelling Compartmentalisation within Intracellular Signaling Pathways, which focusses on modelling receptor-activated signaling pathways while accounting for the dynamics of endosomes and the associated biochemical reactions.

Keywords: Inflammatory bowel diseases, reaction-diffusion system, travelling waves, wave blocking, Wolbachia bacterium, vector-borne diseases, coagulation dynamics, integro-partial differential equations, receptor-activated signaling pathways, compartmentalization.

RÉSUMÉ

Les maladies inflammatoires chroniques de l'intestin (MICI) et les épidémies transmises par les moustiques représentent des défis majeurs en santé publique. Cette thèse développe et analyse des modèles mathématiques basés sur des systèmes de réaction-diffusion afin d'étudier les dynamiques de propagation et les conditions menant au blocage dans ces phénomènes biologiques.

Dans la première étude, nous nous intéressons à la rectocolite hémorragique (RCH), une MICI caractérisée par une inflammation continue du côlon. Nous établissons un modèle décrivant l'interaction entre un pathogène et le système immunitaire, mettant en évidence l'existence d'ondes progressives qui représentent la propagation de l'inflammation dans un milieu homogène. Nous identifions ensuite les conditions nécessaires pour bloquer cette propagation dans un milieu hétérogène et validons nos résultats à l'aide de simulations numériques.

Dans la deuxième étude, nous analysons une stratégie de contrôle des maladies vectorielles, en particulier la propagation de Wolbachia, une bactérie qui réduit la transmission de pathogènes tels que la dengue. Nous examinons les cas où la propagation est entravée dans un milieu hétérogène, notamment lorsque la capacité de charge varie spatialement. Nous identifions les conditions menant au blocage et validons nos résultats à l'aide de simulations numériques.

Enfin, j'ai également travaillé sur le projet Modélisation de la compartimentation dans les voies de signalisation intracellulaire, qui porte sur la modélisation des voies de signalisation activées par les récepteurs en tenant compte de la dynamique des endosomes et des réactions biochimiques associées.

Mots-clés: Maladies inflammatoires de l'intestin, système de réaction-diffusion, ondes progressives, blocage des ondes, bactérie Wolbachia, maladies à transmission vectorielle, dynamique de coagulation, équations aux dérivées partielles intégro-différentielles, voies de signalisation activées par des récepteurs, compartimentalisation.

Remerciements

Avant toute chose, je rends grâce à Dieu, Le Très-Haut, pour m'avoir accordé la patience, la force et la persévérance nécessaires pour mener à bien ce travail. Rien n'aurait été possible sans sa volonté.

Quelles que soient les formules que je pourrais écrire ici, elles ne sauraient jamais exprimer toute ma reconnaissance envers ceux qui ont rendu cette thèse possible. J'ai eu la chance d'être entourée des bonnes personnes au bon moment, et je mesure pleinement l'importance de leur présence à chaque étape de ce parcours.

Ce travail n'aurait pu être mené à bien sans le financement apporté par l'École Universitaire de Recherche (EUR). Je remercie les responsables, notamment pour la confiance qu'ils m'ont accordée et pour les moyens mis à disposition tout au long de ces années de thèse.

Je tiens à exprimer ma sincère gratitude à mes directeurs de thèse, Monsieur Nicolas Vauchelet et Monsieur Hatem Zaag, pour la confiance qu'ils m'ont accordée en me proposant de travailler sur ce projet de thèse à la fois pluridisciplinaire et novateur. Leur encadrement bienveillant, leur disponibilité, ainsi que la richesse de nos échanges scientifiques ont été essentiels tout au long de ce parcours. Je les remercie chaleureusement pour leur soutien constant qu'il soit intellectuel, moral ou administratif, pour leur patience dans les moments difficiles, et pour le temps qu'ils m'ont consacré sans compter. J'ai beaucoup appris à leurs côtés, et je tiens à souligner plus particulièrement l'effort fourni pour m'aider à comprendre les enjeux biologiques de ma thèse. Je leur adresse tous mes remerciements.
Je tiens tout particulièrement à remercier Monsieur Nicolas Vauchelet pour son aide précieuse dans le développement et la compréhension des aspects numériques, ainsi que pour le temps qu'il a pris pour m'expliquer avec clarté des points qui m'échappaient parfois.

Je voudrais tout particulièrement remercier les rapporteurs de ma thèse, Monsieur Thomas Lepoutre, Chargé de recherches HDR à Inria, Centre de Lyon, au sein de l'équipe-projet DRACULA, rattachée à l'Institut Camille Jordan (Université Claude Bernard Lyon 1), et Monsieur Quentin Griette, Professeur au Laboratoire de Mathématiques Appliquées du Havre, Université Le Havre Normandie, pour l'intérêt qu'ils ont porté à mon travail. Leurs remarques enrichissantes, leurs appréciations et leurs validations ont été pour moi une marque d'encouragement précieuse. Leurs rapports ont été, chacun à leur manière, une source de grande motivation, tant sur le plan personnel que scientifique. Je les en remercie sincèrement.

Je souhaite vivement remercier Monsieur Éric Ogier-Denis, Directeur de recherche à l'Institut national de la santé et de la recherche médicale (INSERM), Madame Takiko Sasaki, Professeure à l'Université Musashino au Japon, Madame Nejla Nouaili, maître de conférences HDR à l'Université Paris Dauphine ainsi que Monsieur Philippe Souplet, Professeur à l'Université Sorbonne Paris Nord, pour avoir accepté de faire partie de mon jury de thèse.

Je tiens à remercier chaleureusement le personnel administratif du LAGA, notamment Laila, Yolande et Monia, pour les facilités apportées lors de la préparation de mes missions.

Je tiens à exprimer toute ma gratitude à Monsieur Thomas Duyckaerts pour son soutien constant durant mon master, en particulier pour son aide dans le choix du sujet et sa disponibilité à répondre à mes questions.

Je tiens à remercier chaleureusement Madame Hella Ounaies Khalgui pour son soutien inestimable depuis mes débuts en Tunisie jusqu'à aujourd'hui. Ses encouragements et son aide précieuse ont été essentiels tout au long de mon parcours. Je lui suis profondément reconnaissante pour toute la confiance qu'elle m'a témoignée.

L'amitié est l'une des plus belles histoires que l'on puisse vivre dans une vie. Je tiens à exprimer ma gratitude envers celles qui ont contribué à rendre ces années plus légères et plus humaines:

Je souhaite tout particulièrement remercier chaleureusement Laila Baroukh, avec qui j'ai partagée quatre années dans le même bureau. Son amitié et son soutien ont été des facteurs importants pour détendre l'atmosphère de travail et déstresser ensemble au quotidien. Nous avons souvent fait face à des situations stressantes, mais grâce à notre complicité, nous avons toujours su trouver des moments pour rire et oublier la fatigue. Elle a toujours été présente pour m'aider à résoudre mes questions de dernière minute. Je lui suis reconnaissante pour sa gentillesse et sa présence tout au long de ces années.

Je tiens également à remercier Safa El-Ali, avec qui j'ai partagée le bureau pendant une année. Même après son départ de l'université, nous sommes restées amies, et elle a toujours continué à m'apporter son aide avec beaucoup de gentillesse. Elle a répondu à de nombreuses de mes questions, toujours avec patience et disponibilité. Je garde un très bon souvenir de notre complicité et de sa bienveillance tout au long de ces années.

Je tiens à remercier Sami pour l'amitié que nous avons partagée au cours de ma thèse et pour avoir pris le temps de répondre à mes questions, ce qui a rendu cette période plus légère et plus humaine.

Je tiens également à remercier tous mes amis rencontrés au fil de ces années (Nesrine, Samar, Laila, Cyrine, Ikram). Chacun, à sa manière, a contribué à rendre ce parcours plus léger et plus humain.

Je tiens à remercier sincèrement ma famille pour sa présence, son soutien et ses encouragements tout au long de ce parcours. Votre soutien, aussi bien dans les périodes d'incertitude que dans les moments de joie, m'a été d'une grande aide. Merci d'avoir toujours été là, chacun à votre manière, pour m'aider à avancer vers cette étape.

CONTENTS

LIST OF FIGURES

LIST OF TABLES

CHAPTER 1

GENERAL INTRODUCTION

"Research is to see what everybody else has seen,
and to think what nobody else has thought."

Albert Szent-Györgyi

This work was motivated by two concrete problems that arise from biology. The first concern the study of blocking the propagation of inflammation in chronic inflammatory diseases of the digestive tract, such as ulcerative colitis. The second relates to a mosquito population replacement technique that involves the bacterium Wolbachia. Although these two problems may seem distinct, they share a common mathematical foundation: reaction-diffusion equations, population dynamics, and the study of stationary solutions. This mathematical approach constitutes the main thread of this manuscript.

Before delving into the problems and main results in Sections 2 and 3 of this Introduction, Section 1 provides an overview of the fundamental mathematical concepts underpinning the work in this thesis. Finally, Section 4 briefly outlines the general structure of the manuscript.

1.1 Basic Mathematical Concepts

1.1.1 Fundamental Concepts of Reaction-Diffusion Equations

Reaction-diffusion equations play a key role in modeling biological, chemical, and physical phenomena involving spatial and temporal dynamics. These equations are used to describe a variety of processes, such as spreading diseases, interaction between populations or substances, and chemical reactions in heterogeneous environments. They combine two fundamental mechanisms: diffusion and reaction. Diffusion describes the dispersion of a substance or population under the effect of concentration gradients, in accordance with Fick's law. In contrast, the reaction term models local interactions, such as growth, mortality, or competition between species. A classic form of the diffusion equation is a parabolic equation, which can be expressed in the following general form, derived from the conservation of mass and Fick's law:

$$\partial_t u(t,x) = D\Delta u(t,x); \quad t \geq 0, \quad x \in \Omega \subseteq \mathbb{R}^n, \quad u(t,x) \in \mathbb{R}.$$

Where $u(t,x)$ represents the density of the population as a function of time t and space x, and D is the diffusion rate. This diffusion model is fundamental in many contexts, but it does not necessarily capture the interaction between the population or substance and the factors that locally modify their density. To account for these reaction effects, it is necessary

to complement the equation with a reaction term that depends on the density $u(t,x)$. As demonstrated by Kolmogorov, Petrovskii, and Piskunov in [53], assuming that diffusion is accompanied by a variation of the amount of substance, which is a function of the density, one obtains a semilinear parabolic equation, also known as a reaction-diffusion equation:

$$\partial_t u(t,x) = D\Delta u(t,x) + f(u(t,x)); \quad t \geq 0, \quad x \in \Omega \subseteq \mathbb{R}^n, \quad u(t,x) \in \mathbb{R}. \tag{1.1}$$

Where $f(u(t,x))$ is the reaction term that captures biological, chemical, or ecological dynamics, such as individual growth or mortality, or species interactions. This model, often used in various fields, requires initial conditions to define the state at time zero $u(0,x) = u_0(x)$, as well as boundary conditions to describe the behavior at the boundaries of the domain when it is bounded.

We have thus introduced the fundamental concepts of reaction-diffusion equations. We now proceed to study the existence of solutions to these equations, which is the focus of the next subsection.

1.1.2 Existence of Solutions to the Reaction-Diffusion Equation

To establish the existence of solutions to the reaction-diffusion equation, various theoretical approaches can be employed, depending on the properties of the reaction term $f(u)$. When this term is Lipschitz continuous, the existence and uniqueness of local weak solutions can be guaranteed using Banach's fixed-point theorem. Once these local solutions are established, they can be extended over time to define a maximal solution, which may or may not be global depending on the system's properties.

At the same time, specific techniques, such as subsolution and supersolution methods, prove particularly effective in demonstrating the existence of solutions while analyzing their asymptotic behavior. In addition, the shooting method, which transforms a boundary value problem into an initial value problem, is a valuable tool. These two techniques will be employed in this manuscript to emphasize the existence of stationary solutions to the reaction-diffusion equation. However, before presenting these methods, it is essential to introduce stationary solutions, as their existence will be examined in all subsequent chapters.

Definition 1 (Stationary Solution)**.**

A stationary solution of a reaction-diffusion equation is a time-independent solution, where the temporal variation of the modeled quantity vanishes. These solutions satisfy the equation obtained by setting:

$$\frac{\partial u}{\partial t} = 0,$$

which leads to an algebraic equation in space. Mathematically, a stationary solution $u(x)$ for the reaction-diffusion equation is obtained by solving:

$$D\Delta u + f(u) = 0,$$

where $f(u)$ represents the local reaction function.

Stationary solutions, particularly in the context of biological models, are essential to understand the behaviour of reaction-diffusion systems. As illustrated by Nadin et al., a stationary solution can also act as a natural boundary, defining a threshold beyond which the solutions of the equation cannot evolve. Thus, the existence of a stationary solution imposes strong constraints on the dynamics of equation solutions (1.1). For more details, see

[68]. This property shows that stationary solutions influence the behaviour of the solution to the reaction-diffusion equation.

After we present stationary solutions and their fundamental role in the analysis of reaction-diffusion systems, we now turn to the methods used to study their existence. In particular, we introduce the sub- and super-solution method as well as the shooting method, which will be applied to the two models studied in this manuscript. These techniques will play a key role in demonstrating the existence of stationary solutions.

Monotone Methods for monotone Reaction-Diffusion Systems:

The monotone method, also known as the method of super-solutions and sub-solutions, is a powerful tool for establishing existence results for differential equations. Moreover, this method can also be applied to coupled systems of parabolic and elliptic equations. The basic idea of this method is to use a supersolution or a subsolution as an initial iteration in an appropriate iterative process, such that the resulting sequence of iterations is monotone and converges to a solution of the problem. The underlying monotone iterative scheme can also be used for the computation of numerical solutions when these equations are replaced by suitable finite difference equations.

Since we will apply this method to a coupled system of parabolic equations in Chapter 2 of this manuscript, this section presents the results of its application to such systems. However, for coupled systems of equations, the definition of super-solutions and sub-solutions, as well as the construction of monotone sequences, depends on the quasi-monotone property of the reaction functions in the system. To illustrate the basic idea of this method, we consider a coupled system of two parabolic equations of the form:

$$\begin{cases} \partial_t u - D\Delta u = F_1(u,v), & (x,t) \in \mathbb{R} \times \mathbb{R}_+, \\ \partial_t v - D\Delta v = F_2(u,v), & (x,t) \in \mathbb{R} \times \mathbb{R}_+. \end{cases} \tag{1.2}$$

Let $D_i \subset \mathbb{R}$, $i = 1, 2$. We have:

Definition 2. *(Quasi-monotonic reaction function)*

A function $F_i = F_i(u_1, u_2)$ is said to be quasi-monotonic increasing (resp decreasing) in $D_1 \times D_2$, if for all $u_i \in D_i$ fixed, F_i is increasing (resp decreasing) with respect to $u_j \in D_j$ for $i \neq j$.

Definition 3.

A vector function $F = (F_1, F_2)$ is said to be quasimonotone nondecreasing (or quasi-monotone nonincreasing) in $D_1 \times D_2$, if both F_1 and F_2 are quasimonotone nondecreasing (or quasimonotone nonincreasing) in $D_1 \times D_2$.

If F_1 is quasimonotone nonincreasing and F_2 is quasimonotone nondecreasing in $D_1 \times D_2$ (or vice versa), then F is said to be mixed quasimonotone.

The function F is said to be *quasimonotone* in $D_1 \times D_2$ if it has any one of the above quasimonotone properties.

Definition 4 (super-solutions and sub-solutions)**.**

A pair of functions $(\bar{u}, \bar{v})$ and $(\underline{u}, \underline{v})$ in $C^2(\mathbb{R} \times \mathbb{R}_+) \times C^2(\mathbb{R} \times \mathbb{R}_+)$ are called ordered supersolution and subsolution of problem (1.2), if they satisfy

$$(\bar{u}(x,t), \bar{v}(x,t)) \geq (\underline{u}(x,t), \underline{v}(x,t)), \quad x \in \mathbb{R}, \ t \in \mathbb{R}_+$$

and if

$$\begin{cases} \frac{\partial \bar{u}}{\partial t} - D\Delta\bar{u} - F_1(\bar{u},\bar{v}) > 0 > \frac{\partial \underline{u}}{\partial t} - D\Delta\underline{u} - F_1(\underline{u},\underline{v}), \\ \frac{\partial \bar{v}}{\partial t} - D\Delta\bar{v} - F_2(\bar{u},\bar{v}) > 0 > \frac{\partial \underline{v}}{\partial t} - D\Delta\underline{v} - F_2(\underline{u},\underline{v}). \end{cases} \tag{1.3}$$

When (F_1, F_2) *is quasi-monotone non-decreasing;*

$$\begin{cases} \frac{\partial \bar{u}}{\partial t} - D\Delta\bar{u} - F_1(\bar{u},\underline{v}) > 0 > \frac{\partial \underline{u}}{\partial t} - D\Delta\underline{u} - F_1(\underline{u},\bar{v}), \\ \frac{\partial \bar{v}}{\partial t} - D\Delta\bar{v} - F_2(\underline{u},\bar{v}) \geq 0 \geq \frac{\partial \underline{v}}{\partial t} - D\Delta\underline{v} - F_2(\bar{u},\underline{v}). \end{cases}$$

When (F_1, F_2) *is quasi-monotone non-increasing; and*

$$\begin{cases} \frac{\partial \bar{u}}{\partial t} - D\Delta\bar{u} - F_1(\bar{u},\underline{v}) \geq 0 \geq \frac{\partial \underline{u}}{\partial t} - D\Delta\underline{u} - F_1(\underline{u},\bar{v}), \\ \frac{\partial \bar{v}}{\partial t} - D\Delta\bar{v} - F_2(\bar{u},\bar{v}) \geq 0 \geq \frac{\partial \underline{v}}{\partial t} - D\Delta\underline{v} - F_2(\underline{u},\underline{v}). \end{cases}$$

When (F_1, F_2) *is mixed quasi-monotone.*

We now state the following theorem concerning the existence of solutions using the method of super-solutions and sub-solutions for coupled systems in the case of quasi-monotone increasing functions, as this case is needed in Chapter 2 of this manuscript. The complete proof of this theorem, along with the details of this method, are provided in [98].

Theorem 1.
Let $\bar{W} = (\bar{u}, \bar{v})$, $\underline{W} = (\underline{u}, \underline{v})$ *be ordered super-solution and sub-solution of problem* (1.2), *and* (F_1, F_2) *be quasimonotone nondecreasing in* $D_1 \times D_2$ *and* C^1 *function in* $[\underline{W}, \bar{W}]$. *Then, the problem* (1.2) *has a unique solution* (u, v) *is bounded between the sub and super-solutions.*

The method of super-solutions and sub-solutions is particularly effective for monotone parabolic equations, as it provides a constructive approach to framing the solutions. It serves as a powerful alternative, especially when obtaining explicit solutions for the studied systems is difficult or even impossible. After presenting the first method, the supersolution and subsolution method, which is used in Chapter 2, we now proceed to the second method, the Shooting Method, which will be applied in Chapter 4.

The Shooting Method

The shooting method is a widely used technique for solving boundary value problems. While the previous method focuses on finding solutions through appropriate estimates of sub-solutions and super-solutions, the shooting method addresses boundary conditions by converting them into an initial value problem.

Thus, to solve a boundary value problem, we begin by choosing arbitrary initial conditions and then solve the differential equation using these initial conditions. Once a solution is obtained, we compare the result with the boundary condition and adjust the initial conditions (often in the form of a parameter, called the shooting parameter) until the solution satisfies the boundary conditions. This process is usually carried out through successive iterations.

This method can be effective in applications in the physical sciences and reaction-diffusion models, where the solution of equations with boundary conditions is sought, but where a direct approach is difficult to apply. Among the works that have used this method, there is that of Nadin et al., who applied it in their analysis. For more details, see [68].

Before concluding this section, it is important to highlight the role of reaction-diffusion equations in the modeling of various phenomena. These equations serve as a powerful mathematical tool for describing and analyzing spatiotemporal dynamics.

1.1.3 Modeling with Reaction-Diffusion Equations

Reaction-diffusion equations are essential tools across various disciplines, enabling the modeling of biological, physical, and social phenomena, including population dynamics. In biology, these equations are particularly useful for describing propagation phenomena, often in the form of traveling waves, which represent solutions that move at a constant speed while maintaining their shape. Mathematically, a traveling wave can be described as

$$u(t, x) = \mathbf{w}(\mathbf{x} - \mathbf{ct}),$$

where $\mathbf{c}$ is the propagation speed, and $\mathbf{w}$ is the wave profile, which is a monotonically decreasing function from $\mathbb{R}$ to $\mathbb{R}$. This concept is illustrated in Figure 1.1.

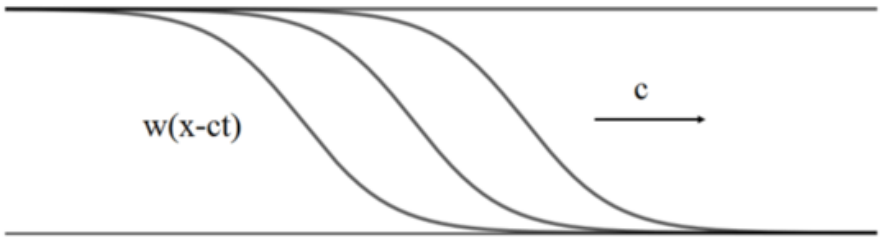

Figure 1.1: Profile of a Traveling Wave.

These phenomena were first studied in the biological context by Kolmogorov and Fisher, who introduced the Fisher-KPP equation to model the spread of a beneficial gene. This equation includes a reaction term describing logistic growth:

$$f(u) = ru(1 - u),$$

where u represents the population density and r is a constant parameter. The Fisher-KPP model has two constant equilibria: $u = 0$ (unstable) and $u = 1$ (stable). The equation is classified as monostable, as any positive initial condition evolves toward the stable equilibrium $u = 1$.

Fisher, Aronson-Weinberger, and Fife-McLeod further demonstrated that these reaction-diffusion equations admit unique traveling waves with a minimum propagation speed given by:

$$c^* = 2\sqrt{rD},$$

where D is the diffusion constant, and r is the population growth rate. In addition to this simple dynamic, more complex models include bistable nonlinearities, described by functions $f(u)$ that have a threshold $\theta \in (0, 1)$, with:

$$f(0) = f(\theta) = f(1) = 0, \ f(u) < 0 \ \text{ for } \ u \in (0, \theta), \text{ and } \ f(u) > 0 \ \text{ for } \ u \in (\theta, 1).$$

A classic example of bistability is given by:

$$f(u) = ru(1 - u)(u - \theta).$$

In this context, $u = 0$ and $u = 1$ are stable equilibria, while $u = \theta$ is unstable. It is generally assumed that the equilibrium $u = 1$ is energetically more favorable than $u = 0$, which is verified if:

$$\int_0^1 f(s)\, ds > 0.$$

This configuration is commonly used to model processes like invasion ($u(t,x) \to 1$ as $t \to \infty$) or extinction ($u(t,x) \to 0$ as $t \to \infty$). Additionally, terms like $(u-\theta)$ can represent biological effects such as the Allee effect, where low population densities reduce survival chances. A well-known example of an Allee nonlinearity is the Allen-Cahn nonlinearity, obtained when $\theta = \frac{1}{2}$. Figure 1.2 highlights the differences between monostable and bistable.

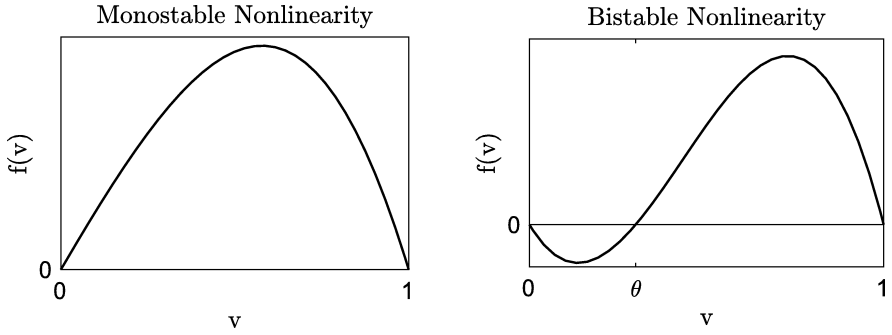

Figure 1.2: Monostable and Bistable Nonlinearities.

In the context of reaction-diffusion equations, it is crucial to ensure that solutions remain within biologically or physically realistic bounds. These bounds are especially important when u represents a density or concentration naturally constrained between 0 and 1. By a classical comparison principle, if the initial data $u(0,x)$ satisfies $0 \leq u(0,x) \leq 1$, then the solution $u(t,x)$ exists for all time $t \geq 0$ and satisfies $0 \leq u(t,x) \leq 1$. This property is essential in mathematical analysis as it restricts the study to biologically admissible solutions.

1.2 A model of inflammation due to Ulcerative Colitis

1.2.1 Inflammatory bowel diseases

Inflammatory Bowel Diseases (IBD) primarily encompass two conditions: ulcerative colitis (UC) and Crohn's disease (CD). While both share common symptoms, such as abdominal pain, diarrhea, and fatigue, they differ significantly in their location within the gastrointestinal tract. UC, first described in 1875, affects only the colon and rectum, causing inflammation and continuous lesions in the inner mucosal layer. In contrast, CD, identified later in 1932, can affect any part of the digestive tract, from the mouth to the anus, with noncontiguous transmural lesions separated by healthy regions. These distinctions are illustrated in the figure 1.3.

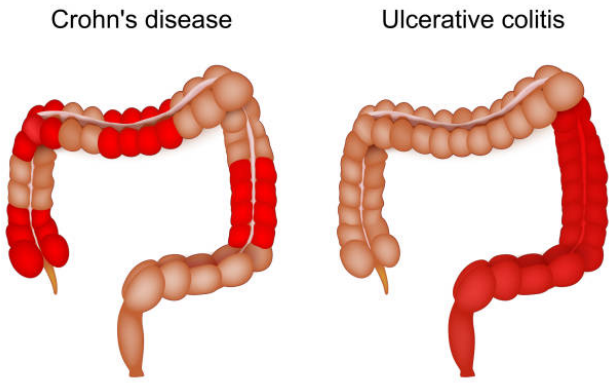

Figure 1.3: Visual Comparison of Affected Regions in Ulcerative Colitis and Crohn's Disease. (Source: drugwatch.com)

Although the exact causes of IBD are unknown, it is widely accepted that these conditions arise from an abnormal immune response against internal factors, such as bacteria. This immune dysfunction, often linked to genetic predispositions, leads to chronic inflammation. UC and CD usually present with digestive symptoms, but can also cause systemic manifestations such as joint pain, skin lesions, and eye involvement.

Treatment aims to manage symptoms and reduce inflammation using medications such as anti-inflammatory drugs, immunosuppressants, biological treatments, and, in severe cases, surgical interventions. These diseases are often chronic and incurable and require continuous monitoring and management of symptoms. Despite advances in treatment aimed at managing symptoms and reducing inflammation, the global prevalence of inflammatory bowel diseases, such as ulcerative colitis (UC) and Crohn's disease, has increased in recent decades. Industrialized regions such as North America, Western Europe, South Asia, and Australia exhibit the highest growth rates. Since Chapter 2 of this manuscript focuses on UC, we will examine the prevalence of this disease. According to GlobalData, the number of diagnosed UC cases in eight countries (US, France, Germany, Italy, Spain, UK, Japan, Canada) is expected to increase from 1.7 million in 2019 to 2 million in 2029, with an annual growth rate of 1.36%. See Figure 1.4 for a global map highlighting regional growth rates of UC.

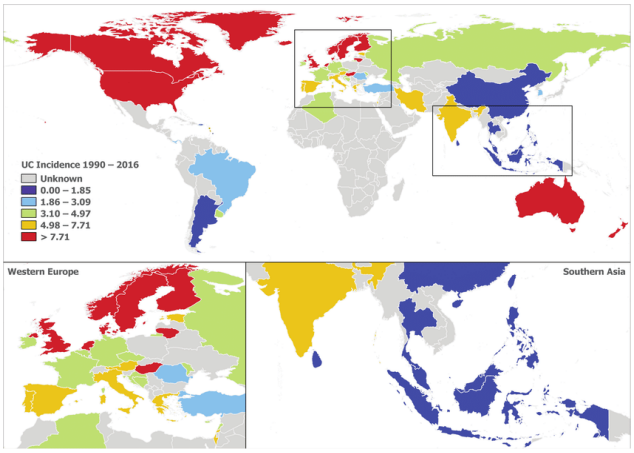

Figure 1.4: A global map highlighting regional growth rates of UC. Countries in dark red show the highest incidence of UC, while those in gray indicate areas with no available data. (Source: [3])

In the context of chronic inflammatory bowel diseases (IBD), the analysis of the mechanisms underlying the onset and progression of these pathologies is of crucial importance. Mathematical modeling is thus an essential tool to explore these complex phenomena. By combining biology, medicine and mathematics, these models quantitatively describe the interactions between intestinal bacteria, immune cells and other biological factors at the origin of chronic inflammation.

Around the world, multidisciplinary research efforts aim to improve treatments and develop early diagnostic tools for IBD. The INFLAMEX excellence cluster in France (ANR-10-LABX-17) brings together top-level researchers conducting interdisciplinary studies. As part of a collaboration between INFLAMEX and Sorbonne Paris North University, the idea of designing and studying a model to explore differences in inflammatory patterns between Crohn's disease and ulcerative colitis emerged.

In chapter 2 of this manuscript, we introduce a reaction-diffusion model inspired by the work of Nadin et al. ([67]). This mathematical model captures the interactions between a pathogen, denoted by u, and immune cells, denoted by v. To simplify, the spatial domain is represented as a one-dimensional interval simulating a segment of the digestive tract. The model is formulated as follows:

$$\begin{cases} \partial_t u - D\Delta u = r_b(1 - \frac{u}{b_i})u - \frac{auv}{s_b+u} + \gamma(1 - \frac{u}{b_i})v - du, \\ \partial_t v - D\Delta v = \beta u - r_c v. \end{cases} \tag{1.4}$$

The primary goal is to describe the propagation in a homogeneous medium in the context of ulcerative colitis (UC). We then study the conditions under which this propagation can be halted in a heterogeneous medium. All the results presented in the aforementioned chapter were obtained through collaboration with N. Vauchelet, H. Zaag and E. Ogier-Denis.

1.2.2 State of the art

In the scientific literature, there are few mathematical models specifically targeting IBD dynamics. For instance, a model presented in [95] constructs a system of 29 ordinary differential equations to represent the interactions between various immune cells and bacteria in the colon. While parameters were chosen to fit existing datasets, it remains difficult to infer qualitative properties due to the system's complexity.
The research on inflammatory bowel disease (IBD) has also been enriched by the data analyses of Morilla et al. ([18]) as well as the innovative image processing research presented in Al-Ali's PhD thesis([3], [4], [5]), which provide essential foundations for understanding IBD. Other researchers, such as Lo and Arsenescu et al. ([63]), have also contributed to this field.

Certain studies have focused on the impact of spatial heterogeneity in modeling inflammation. For instance, El Khatib et al. ([28]) and El Khatib, Génieys et al. ([29]) investigated the process of atherogenesis, while Lauffenburger and Kennedy ([59]) and Penner et al. ([70]) examined tissue inflammation. Meanwhile, Chalmers et al. ([19]) studied acute inflammatory responses. These models are notable for their ability to replicate complex dynamics, considering variables such as immune cell density, pro-inflammatory cytokines, anti-inflammatory mediators, and the presence of bacteria.

However, to the best of my knowledge, no studies have specifically addressed the propagation of this disease or the mechanisms leading to its blockage. These questions constitute the primary focus of Chapter 2 of this manuscript.

1.2.3 Presentation of the main results

In this subsection, we present the main theoretical results of the model (1.4), developed and proved in Chapter 2. These results highlight the ability of the model to represent both the spread and the blocking of the disease. We start with the first result, which deals with the spread of the disease in a homogeneous medium.

Theorem 2.

We assume that $r_b < d < r_b + \frac{\gamma\beta}{r_c}$, *with* $\gamma > a$ *and* $s_b > \max\left(b_i, \frac{1}{r_c}\right)$. *Under these assumptions, there is a spreading speed* $c^* > 0$ *with the properties that for every positive* ϵ, *the following holds:*

$$\lim_{t\to+\infty}\left[\max_{|x|\geq t(c^*+\epsilon)} |\left(u\left(x,t\right),v\left(x,t\right)\right)|\right]=0,$$

and for any strictly positive constant vector w, *there exists a positive* R_w *such that if* $\left(u_0\left(x\right),v_0\left(x\right)\right)\geq w$ *on an interval of length* $2R_w$, *the following holds:*

$$\lim_{t\to+\infty}\left[\max_{|x|\leq t(c^*-\epsilon)} |\left(u_2^+,v_2^+\right)-\left(u\left(x,t\right),v\left(x,t\right)\right)|\right]=0.$$

The pair $\left(u_2^+,v_2^+\right)$ *is a positive equilibrium of the ODE system associated with* (1.4).

The goal of the following theorem is to prove the existence of a stationary solution for the system described by (1.4), by identifying the conditions under which such a solution can exist.

Theorem 3.

Let $d(x)=d_1\mathbb{1}_{x\leq 0}+d_2\mathbb{1}_{x>0}$, $d_k\in\mathbb{R}_+$, $k=1,2$. *If the following conditions hold true:* $r_c>\beta$, $s_b>\max(b_i,\frac{1}{\beta})$, $\gamma>a$, $r_b<d_1<r_b+\frac{\gamma\beta}{r_c}$ *and* $r_b+\gamma<d_2<\min(r_b+\gamma+r_c-\beta, s_b(r_br_c+\beta\gamma))$. *Then, there is a solution* $(\bar{U},\bar{V})$ *of the following system:*

$$\begin{cases} -D\partial_{xx}u = r_bu(1-\frac{u}{b_i})+\gamma(1-\frac{u}{b_i})v-\frac{auv}{s_b+u}-d(x)u,\\ -D\partial_{xx}v=\beta u-r_cv,\\ (u,v)(-\infty)=(u_2^+,v_2^+),\ (u,v)(+\infty)=(0,0),\\ u>0,\ v>0. \end{cases} \tag{1.5}$$

The aim of the following proposition is to prove the comparison principle according to which, under certain conditions, the solution of a system evolving in time always remains framed between a sub-solution and a super-solution.

Proposition 5. *(Comparison principle)*

Assume $\gamma>a$ *and* $s_b>b_i$. *Let* (u,v) *be a solution of* (1.4) *in* $\mathbb{R}$, *supersolution* $(\bar{u},\bar{v})$ *of* (1.4) *in* $\mathbb{R}$ *and subsolution* $(\underline{u},\underline{v})$ *of* (1.4) *in* $\mathbb{R}$, *such that* $(0,0)<(\bar{u},\bar{v})\leq(\frac{b_i}{2},\frac{\beta b_i}{2r_c})$, $(0,0)<(\underline{u},\underline{v})\leq(\frac{b_i}{2},\frac{\beta b_i}{2r_c})$ *and* $(0,0)<(u,v)\leq(\frac{b_i}{2},\frac{\beta b_i}{2r_c})$. *Then*

$$(\underline{u}(t=0,x),\underline{v}(t=0,x))\leq(u(t=0,x),v(t=0,x))\leq(\bar{u}(t=0,x),\bar{v}(t=0,x)),$$

implies that

$$(\underline{u}(t,x),\underline{v}(t,x))\leq(u(t,x),v(t,x))\leq(\bar{u}(t,x),\bar{v}(t,x)),\quad\forall t\geq 0,\ \ \forall x\in\mathbb{R}.$$

The following corollary shows that if the model (1.4) admits a stationary solution and satisfies the comparison principle, it leads to the blockage of the propagation.

Corollary 6. *(Blocking of the Wave)*
Under the assumptions of Theorem 3, any solution to the initial problem (1.4) *with an initial condition* $(u(0,x), v(0,x))$ *such that*
$(0,0) \leq (u(0,x), v(0,x)) \leq (\bar{U}, \bar{V})$ *exhibits limited propagation.*

1.2.4 Perspectives and work in progress

A natural continuation of this research would be to study the stability of the stationary solutions of Model (1.4). Another perspective would be to explore a three-species model: u, representing the density of bacteria; v, the pro-inflammatory immune cells fighting bacteria; and w, the anti-inflammatory immune cells limiting the action of pro-inflammatory immune cells. This extended model can be formulated as follows:

$$\begin{cases} \partial_t u - D\Delta u = r_b u(1 - \frac{u}{b_i}) - a(x)vu, \\ \partial_t v - D\Delta v = B_i + \alpha u - \mu_1 v - \gamma vw, \\ \partial_t w - D\Delta w = \beta v - \mu_2 w. \end{cases}$$

In this system, B_i represents the birth term of immune cells, while $a(x)$ is a spatially heterogeneous parameter describing the action of immune cells v on bacteria u. A fundamental assumption of this model is the constant presence of immune cells in the environment. While they naturally degrade, these cells develop in response to the presence of bacteria, as reflected by the birth term in the second equation.

We will discuss this model with the biologist E. Ogier-Denis for validation. Once validated, the main objective will be to study the propagation and blocking phenomena in a more biologically realistic framework. This extended model also enables an analysis of how interactions between pro-inflammatory and anti-inflammatory immune cells influence the overall dynamics of the system. The theoretical and numerical analysis of this model, particularly in environments where $a(x)$ is spatially heterogeneous, represents a promising direction for future research.

1.3 Mathematical Models and Vector Control Strategies

The problem addressed in Part II is inspired by an innovative technique recently implemented in several countries to combat vector-borne diseases transmitted by mosquitoes. In this subsection, we will begin by presenting these diseases and the technique used to address them, explaining their principles and impacts, before discussing the existing works related to this topic. Finally, we will state all the main results of this part, placing them in the context of current research.

1.3.1 What is Dengue Virus?

Dengue, also known as tropical flu, is a viral disease transmitted by mosquitoes, with symptoms typically lasting 2 to 7 days. While many dengue infections are asymptomatic or

present with only mild manifestations such as high fever (40 °C/104 °F), retro-orbital pain, muscle and joint pain, nausea, and vomiting, there are also more severe forms. These severe forms can lead to critical complications such as intense abdominal pain and the presence of blood in vomit or stool. Though rare, these severe cases can result in death.

Dengue is found in tropical and subtropical climates worldwide, mainly in urban and semi-urban areas. Over recent decades, the number of dengue cases has significantly increased globally. According to the World Health Organization (WHO), approximately 505,000 cases were recorded in 2000, a number that increased to 5.2 million in 2019. Today, dengue is present in more than 100 countries, primarily in Africa, the Americas, the Eastern Mediterranean, Southeast Asia, and the Western Pacific. The most affected regions are Asia, accounting for 70% of global cases, as well as the Americas and the Western Pacific. Recently, the disease has reached new areas such as Europe, the Eastern Mediterranean, and South America. In 2023, the number of cases reached a record high of 4.5 million reported in the Americas Region, with 2,300 deaths. Significant cases were also reported in Asia: 321,000 in Bangladesh, 111,400 in Malaysia, 150,000in Thailand, and 369,000 in Vietnam. The spread of dengue is well illustrated on the following map (Figure 1.5), which highlights the endemic regions for this disease.

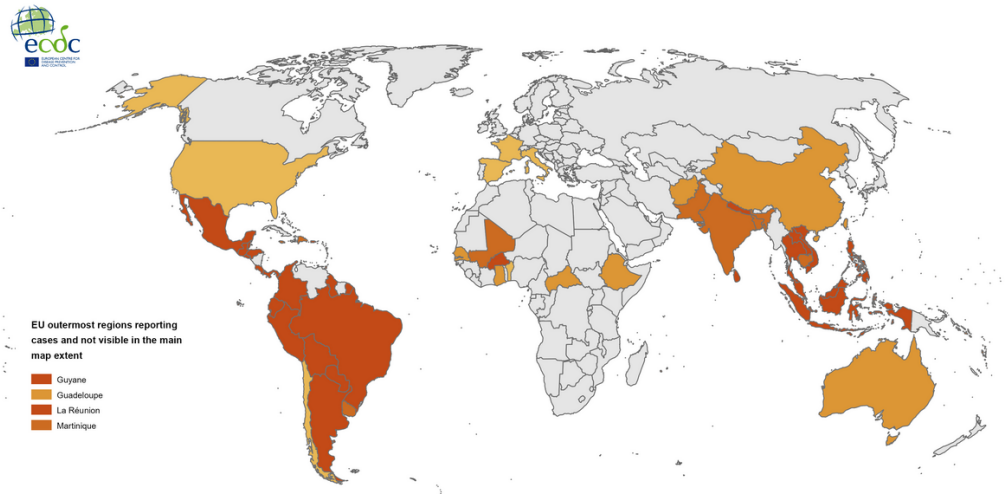

Figure 1.5: Geographical distribution of dengue endemic areas. (European Center for Disease prevention and Control).

The disease is transmitted through the bites of infected female mosquitoes, particularly of the Aedes aegypti species. Other species of the Aedes aegypti genus can also act as vectors, but their contribution is generally secondary compared to that of Aedes aegypti. However, in 2023, a significant increase in the local transmission of the dengue virus by Aedes albopictus (tiger mosquito) was observed in Europe. Mosquitoes become infected by biting an infected person. An infected person is contagious only during the viral phase, which lasts about a week. However, there is an incubation period of several days before mosquitoes can transmit the virus. Once this period has passed, the mosquito remains infectious for the rest of its life.

1.3.2 Vector control methods

Since there is no universally approved vaccine or specific treatment for dengue, prevention and control depend entirely on the implementation of effective vector control strategies. There

are several ways to manage mosquito-borne diseases, such as:

Insecticide spraying: This method involves spreading chemicals to eliminate mosquitoes and other insects. However, these products can sometimes be harmful to human health. This method can be used both indoors and outdoors and requires regular reapplication. It has also been observed that some mosquitoes can develop resistance to certain insecticides. Although this is the most widely used method in the world, it remains expensive and is not always effective as a prevention tool.

Sterile Insect Technique (SIT): This method aims to reduce or eliminate mosquito populations by preventing them from reproducing. This method involves sterilizing male mosquitoes using radiation and then releasing them in large numbers into the wild. These sterile mosquitoes mate with females, but the eggs produced cannot hatch. The effectiveness of this technique depends on the number of males released and the regularity of the releases. If these conditions are not met, the mosquito population can increase again. For a mathematical analysis of this technique.

Genetic modification: is a method that involves introducing lethal genes into the targeted mosquito population, which causes their numbers to gradually decrease. This approach can be expensive, as it requires repeated applications. It is currently being used in Brazil, and has shown positive results in decreasing the mosquito population. There is no conclusive evidence yet on its effectiveness in reducing dengue transmission. In addition, a two-year trial is underway in some areas of the United States.

All of the techniques discussed above seek to limit the mosquito population to reduce dengue transmission. However, if interventions stop, the mosquito population can quickly increase again and return to its initial level. These methods require constant action and regular supervision by local authorities to ensure their long-term effectiveness.
There is a relatively new approach that tackles the problem of stopping the transmission of mosquito-borne diseases in a different way. The idea is to prevent the infection by making mosquitoes incapable of transmitting the pathogen to humans. This strategy is based on the bacterium Wolbachia.

Wolbachia Method

Wolbachia is a bacterium naturally present in about 60% of insect species, but absent in Aedes aegypti. Discovered in 1924, it was not until 1997 that researchers began to study its link with mosquito-borne diseases. At that time, it had been shown that a strain of Wolbachia could reduce the life expectancy of Aedes aegypti mosquitoes, thus limiting the transmission of diseases. Subsequent work [63] revealed a crucial fact: Wolbachia competes with viruses such as dengue, zika, chikungunya and yellow fever, significantly reducing their replication in carrier mosquitoes. In addition, it has been established that females infected with Wolbachia transmit the bacteria to their offspring. This hereditary transmission gives this method the potential for autonomy, although several factors must be taken into account to ensure its success. Wolbachia transmission occurs only from females to eggs. However, infected females have slightly reduced fertility compared to uninfected mosquitoes. In addition, a wild female cannot produce offspring if she mates with a male carrying Wolbachia, a phenomenon known

as cytoplasmic incompatibility. see Figure 1.6.

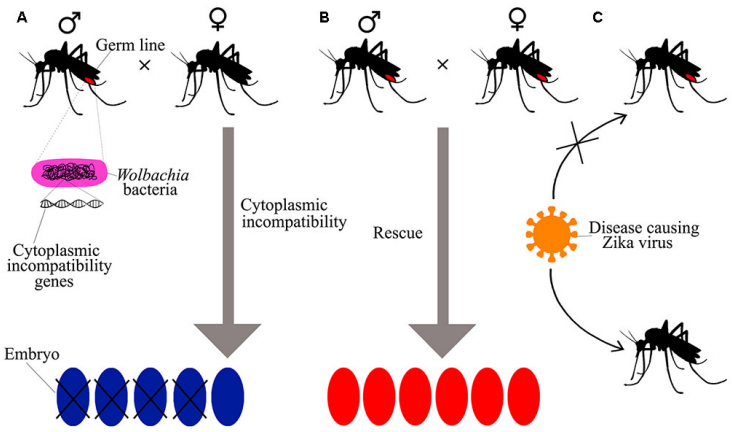

Figure 1.6: Overview of Wolbachia transmission in mosquito populations.

This scientific discovery, combined with the fact that Wolbachia is harmless to humans and other animals, led to the development of what is now known as the Wolbachia method of controlling dengue fever. Researchers raise Wolbachia-infected mosquitoes in the laboratory and then release them into the wild. If this initial population becomes established, it can transmit the bacteria to future generations. Eventually, it is expected that the wild mosquito population will gradually be replaced by mosquitoes carrying Wolbachia, thereby limiting the transmission of dengue and other mosquito-borne diseases. As shown in Figure 1.7.

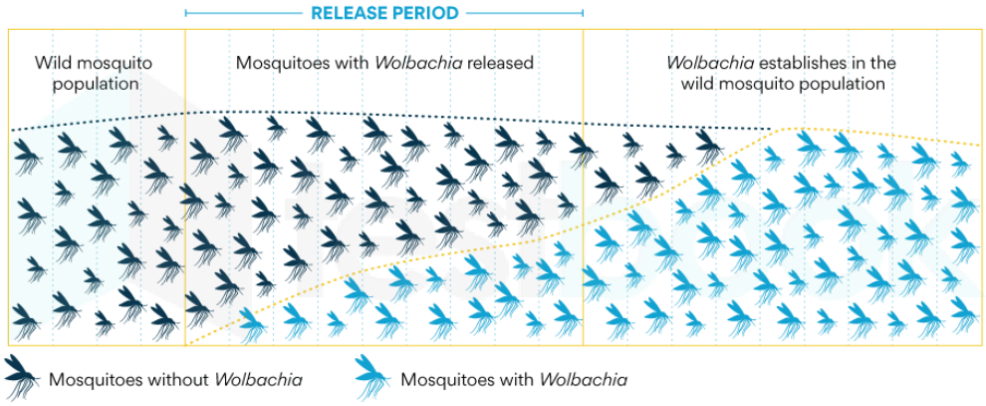

Figure 1.7: Visualization of the Progressive Replacement of Non-Infected Mosquitoes by Wolbachia-Infected Mosquitoes Over Time.

Since the 2000s, the World Mosquito Program (WMP) has coordinated laboratory and field research related to this method. The first releases of Wolbachia-carrying mosquitoes took place in the Cairns region of Australia in 2011, during a 10-week experiment with weekly releases. The results were encouraging and demonstrated the effectiveness of this strategy [78]. In recent years, several regions have joined the program, which now collaborates with more than 10 countries. Clinical trials, risk analyses, economic impact studies and mathematical modeling remain essential to apply this approach on a global scale and effectively control dengue and other mosquito-borne diseases.

1.3.3 State of the art

In this section, we will discuss some relevant studies that have examined the phenomenon of propagation blocking in biological contexts. The observation of biological invasions and the mechanisms used to stop them has inspired numerous studies in the literature. For instance, Nadin et al. ([68]) proposed a simplified mathematical model that supports certain existing analyses. They highlight that differentiated adaptation alone is insufficient to explain this blocking phenomenon. However, a pronounced population gradient could play a crucial role, as suggested by quantitative studies that determine the minimum intensity required to create such blocking. The blocking of propagation is a well-documented phenomenon in various biological contexts, particularly for genetic traits or infections within heterogeneous populations. Previous studies have shown that spatial heterogeneities in population density, or even the Allee effect, can limit the spread of a trait or infection ([12]). This mechanism, often referred to as "pinning" or blocking, is attributed to spatial variations in the environment that hinder invasion ([49]). Although long-term field experiments remain scarce, artificial releases of mosquitoes infected with Wolbachia provide instructive examples. These releases have shown phenomena such as "stable fronts" and blocking ([44]; [69]), which align with theoretical model predictions. These phenomena have been modeled in several studies, particularly using reaction-diffusion models ([13]; [20]) and models accounting for habitat heterogeneity ([38]). In Chapter 4 of the second part of this manuscript, we will study the blocking of propagation in non-homogeneous environments. Specifically, we analyze scenarios where the environmental carrying capacity varies significantly across different regions of the spatial domain.

1.3.4 Presentation of the main results

In this subsection, we present the main results that will be established and proven in Part II. These results prove the model's capacity to simulate the blocking of propagation under particular conditions.

We first introduce a reaction-diffusion model inspired by the work of Vauchelet et al.([68]). This model describes the dynamics of infected mosquitoes (n_i) and uninfected mosquitoes (n_u). It is expressed by the following system of equations:

$$\begin{cases} \partial_t n_i - \Delta n_i = (1-s_f)F_u n_i(1-\frac{n_i+n_u}{K}) - \delta d_u n_i, & in \quad (0,T)\times\mathbb{R}^d, \\ \partial_t n_u - \Delta n_u = F_u n_u(1-s_h\frac{n_i}{n_i+n_u})(1-\frac{n_i+n_u}{K}) - d_u n_u, & in \quad (0,T)\times\mathbb{R}^d. \end{cases} \tag{1.6}$$

The uniform propagation of waves in a homogeneous medium with a constant parameter K is a well-known phenomenon. However, the objective of Part II is to analyze the reduction of system (1.6) to a single closed equation and to study wave blocking in a population replacement technique, particularly in a heterogeneous medium where K varies.
Before stating the main results, it is necessary to establish conditions on K and on the initial data:

First, we assume that K satisfies the following properties: K belongs to $C^2(\mathbb{R}^d)$ and $L^\infty(\mathbb{R}^d)$. Moreover, K is bounded below, i.e., there exists a constant $c'>0$ such that $K>c'$ for all $x\in\mathbb{R}^d$. Additionally, $\nabla K\in L^2(\mathbb{R}^d)$ and $\Delta K\in L^1(\mathbb{R}^d)$.

For the initial data, we assume:

$$n_i^{init,\epsilon} \text{ is uniformly bounded in } L^\infty(\mathbb{R}^d), \quad n_i^{init,\epsilon} \geq 0, \tag{1.7}$$

$$n_u^{init,\epsilon} \text{ is uniformly bounded in } L^\infty(\mathbb{R}^d), \quad n_u^{init,\epsilon} > 0, \tag{1.8}$$

$$\text{and } p^{\text{init}} \in L^2(\mathbb{R}^d), \quad p^{init,\epsilon} = \frac{n_i^{init,\epsilon}}{n_i^{init,\epsilon} + n_u^{init,\epsilon}} \xrightarrow{\epsilon \to 0} p^{init,0} = \frac{n_i^{init,0}}{n_i^{init,0} + n_u^{init,0}} \text{ weakly in } L^2(\mathbb{R}^d). \tag{1.9}$$

Furthermore, we assume that the initial conditions are well-prepared, which means:

$$n_i^{init,\epsilon} + n_u^{init,\epsilon} = K + \epsilon K_0^\epsilon, \quad \text{with } \|K_0^\epsilon\|_\infty \leq C'. \tag{1.10}$$

We now state the convergence result, which establishes the limiting behavior of the solution when $\epsilon \to 0$.

Theorem 4.

Let $T > 0$. Under Assumptions (1.7), (1.8), (1.9), and (1.10) on the initial data, as well as the assumptions on K stated above, it follows that as $\epsilon \to 0$, we have $p^\epsilon := \frac{n_i^\epsilon}{n_i^\epsilon + n_u^\epsilon} \to p^0$ strongly in $L^2(0,T,L^2(\mathbb{R}^d))$, weakly in $L^2(0,T,H^1(\mathbb{R}^d))$ where p^0 is the unique solution of

$$\begin{cases} \partial_t p^0 - \Delta p^0 - 2\frac{\nabla K}{K}\nabla p^0 = f(p^0) + \frac{\Delta K}{K} g(p^0), & \text{in } (0,T)\times\mathbb{R}^d, \\ p^0(t=0,x) = p^{init}(x), & \text{in } \mathbb{R}^d. \end{cases} \tag{1.11}$$

With

$$f(p^0) = p^0(1-p^0)\left[\frac{d_u(\delta s_h p^0 - s_f + 1 - \delta)}{(1-s_f)p^0 + (1-p^0)(1-s_h p^0)}\right],$$

and

$$g(p^0) = \frac{-p^0(1-p^0)(s_h p^0 - s_f)}{(1-s_f)p^0 + (1-p^0)(1-s_h p^0)}.$$

This result shows that the system (1.6) can be reduced to a scalar equation (1.11). Therefore, we will focus on the study of this scalar equation, which is easier than analyzing a system. When K is homogeneous, equation (1.11) becomes:

$$\partial_t p - \Delta p = f(p),$$

where $f(p)$ is a bistable function. This equation was studied in the work of Barton-Turrelli [13]. In particular, it is known that propagation occurs if

$$\int_0^1 f(p)\,dp > 0,$$

and we will assume that this condition is always satisfied in what follows.

We are now interested in studying the blocking of propagation in equation (1.11), in heterogeneous medium where K varies significantly between different regions of the spatial domain. We consider equation (1.11) in one dimension, and K increases exponentially in a specific region of the spatial domain and remains constant elsewhere. More precisely, for certain constants $C > 0$, $L > 0$, we have:

$$K(x) = \begin{cases} A, & \text{if } x < 0, \\ Ae^{Cx}, & \text{if } x \in [0,L], \\ Ae^{CL}, & \text{if } x > L. \end{cases} \tag{1.12}$$

Before stating this result, we introduce a fundamental concept for our analysis: propagation barrier. This concept refers to a boundary beyond which the propagation of Wolbachia is halted, despite favorable conditions existing in other regions of the spatial domain. From a mathematical point of view, this barrier corresponds to the stationary solution of the scalar equation. However, the existence of such a barrier is not systematic. In particular, when C is small enough, propagation remains possible, and no blockage occurs. This is precisely what we establish in the following lemma.

Lemma 7.
If $\frac{K'}{K}$ and $\frac{K''}{K}$ are sufficiently small, then there exists a sub-solution p_A of equation (1.11) that is not blocked, i.e p_A converges to 1 as $t \to +\infty$ uniformly on every compact.

On the contrary, for large enough C and L, there exist barriers.

Theorem 5.
Let $C > 0$, $L > 0$ and assume that the following conditions hold:

$$s_h \leq 1, \quad s_f \leq 1 - s_h, \quad \text{and} \quad \int_0^1 f(t)\, dt > 0.$$

Assume also that K is given by (1.12). $\exists c_* > 0$ such that for all $C > c_*$ there exists L^* such that for all $L > L^*$ we have $(C, L) \in B(f)$.

Lastly, we use a comparison principle to demonstrate how a barrier affects the propagation of $p(t)$. The following proposition formalizes this principle, ensuring that $p(t)$ remains bounded below the barrier for all $t \geq 0$.

Proposition 8.
Suppose that there exists a barrier (C, L) denoted by $\bar{P}$ and that K is given by (1.12). Then every weak solution of

$$\partial_t p - \partial_{xx} p - 2\frac{K'}{K}\partial_x p = f(p) + \frac{K''}{K} g(p),$$

with initial data such that $p^{ini} \leq \bar{P}$, stops spreading, meaning $\forall t \geq 0$, $p(t) \leq \bar{P}$.

1.3.5 Perspectives and work in progress

A natural continuation of this research would be to extend the study to a system involving two coupled populations governed by reaction-diffusion equations. Although such an extension significantly increases the mathematical complexity, the monotonicity properties observed in these systems provide a promising perspective for further analysis.

Another potential avenue would be to expand the study to higher spatial dimensions. Until now, our investigations have been limited to one spatial dimension, where the structure and behavior of solutions can be more intuitively examined. By considering higher-dimensional contexts, we aim to explore how spatial heterogeneity affects the system's dynamics, thereby offering richer insights into the mechanisms of propagation and blocking.

1.4 Dissertation outline

The remainder of the manuscript is structured as follows:

⊙ Chapter 2 is dedicated to the study of a mathematical model of inflammation in the context of inflammatory bowel diseases, such as ulcerative colitis (UC). From a mathematical point of view, the propagation of the disease in a homogeneous environment and its blocking in heterogeneous environments are studied. The paper has been published in Mathematical Biosciences. [57].

⊙ Part II is dedicated to the study of a mathematical model for controlling mosquito-borne diseases, such as dengue, through the introduction of the Wolbachia bacterium. It is divided into two chapters: the first focuses on the reduction of a 2×2 reaction-diffusion system to a single closed equation, while the second analyzes the phenomenon of wave propagation blocking in a population replacement technique. The paper is being prepared for submission [56].

⊙ Part III presents a mathematical model of G-protein coupled receptor signaling systems, incorporating compartment dynamics and biochemical reactions. It also introduces a finite volume scheme to simulate the model, with applications on receptor trafficking and second messenger signaling. This work was carried out during my participation in a summer school and has been published in ESAIM. [1].

Part I

Mathematical Analysis of Ulcerative Colitis

Abstract

The results presented in this chapter came from a multidisciplinary collaboration with Nicolas Vauchelet, Eric Ogier-Denis, and Hatem Zaag and has been published, [57].

Ulcerative colitis (UC) is a chronic inflammatory bowel disease (IBD) with mechanisms that are still partially unclear. Unlike other types of IBD, inflammation in UC is limited to the inner lining of the large intestine and rectum, spreading continuously without breaks between affected areas, creating a uniform pattern of inflammation along the colon.

In this chapter, we develop a mathematical model based on a reaction-diffusion system to describe the inflammation caused by the interaction between a pathogen and immune cells in the context of UC. Our contributions are both theoretical and numerical. We demonstrate the existence of traveling wave solutions, showing how the disease progresses in a homogeneous environment. We then identify the conditions under which the spread of inflammatory waves can be stopped in a heterogeneous environment. Numerical simulations are used to highlight and validate these theoretical results.

CHAPTER 2

MATHEMATICAL STUDY OF THE SPREAD AND BLOCKING IN INFLAMMATORY BOWEL DISEASE

"The more we know, the more we realize how much remains to be discovered."

Isaac Newton

2.1 Introduction

Inflammatory Bowel Diseases (IBD), such as ulcerative colitis (UC) and Crohn's disease, are characterized by persistent inflammation of the intestines. UC affects the large intestine and rectum, while Crohn's disease can affect any part of the gastrointestinal tract. Crohn's disease is marked by patchy damage with complications like narrowing or fistulas, impacting deeper layers of tissue. In contrast, ulcerative colitis only affects the surface of the colon, with no healthy areas between inflamed regions. The exact causes of IBD are not well understood, but they may be linked to an excessive immune response influenced by genetic factors, epithelial barrier issues, and environmental factors. Stress and certain foods do not directly cause IBD, but they can trigger flare-ups (see [100]).

IBD illustrate an acute inflammatory response in body tissues caused by harmful factors like pathogens or damaged cells. This defensive response is also related to other well-known conditions, such as rheumatoid arthritis, inflammation of diabetic wounds, or tissue inflammation in general, and has been the subject of many studies. Currently, this topic continues to interest researchers. Although mathematical models have been developed in recent decades to clarify the causes of acute inflammation, ongoing research continues to refine and expand our understanding of this complex phenomenon. Foundational analyses on the causes of acute inflammation are provided in [89] and [90].

Our goal was to propose a simplified mathematical model, inspired by the model presented in [67], which simulates the immune response that triggers inflammation. Specifically, in the case of ulcerative colitis, we aim to demonstrate the existence of progressive waves in a uniform environment, representing the spread of inflammation or the pathological activity associated with UC throughout the intestinal tissue. In the second phase of our study, we explore the conditions that lead to the blockage of these waves in heterogeneous environments. The blockage of waves refers to the stopping or significant reduction of inflammation spread in the intestinal tissue. Currently, the stopping point of disease spread in the colon remains unexplained and cannot be effectively identified by videos obtained during colono-

scopies. Further research is needed to determine this endpoint of inflammation. While this topic is extensively explored, the mathematical modeling of this phenomenon continues to evolve. Previous work on this disease includes the initial data analyses of Morilla et al. (see [66]), as well as the innovative image processing research presented in Al-Ali's PhD thesis (see [3], [4], [5]), which provide essential foundations for our understanding of inflammatory bowel disease (IBD). Additionally, the work of Rebai et al. (see [74]) explores the use of physics-based neural networks to solve the equations modeling these diseases.

Many mathematical studies on inflammation develop models based on ordinary differential equations ([76]; [58]; [65]; [75]). Most of this research incorporates pro-inflammatory and anti-inflammatory mediators, as well as pathogens and other physiological variables, with various levels of realism. Depending on the parameters and initial conditions, these models reproduce different observable scenarios both experimentally and clinically. This includes situations where the host successfully eradicates the infection, others where the immune system fails to control the disease, and cases where oscillatory solutions lead to a cycle of chronic inflammation.

In modeling the inflammatory response, several studies consider spatial heterogeneity. For instance, El Khatib et al.([28]); El Khatib, Génieys, et al.[29] study the process of atherogenesis, while Lauffenburger and Kennedy ([59]) and Penner et al.([70]) examine tissue inflammation. Chalmers et al.([19]) focus on acute inflammatory responses. These models stand out for the dynamics they seek to replicate, incorporating variables like immune cell density, pro-inflammatory cytokines, anti-inflammatory mediators, and the presence of bacteria. Although mathematical modeling of inflammation attracts considerable attention, it continues to evolve. In our study, we also consider spatial heterogeneity, which is crucial for explaining the blockage phenomenon observed in the spread of ulcerative colitis (UC). In the presence of variations in the properties of the intestinal tissue, our reaction-diffusion model simulates waves of inflammation that, when they encounter heterogeneous areas, are either blocked or significantly slowed down. These heterogeneous areas act as barriers, realistically reproducing the obstacles faced by inflammation in clinical situations. Analyzing the impact of heterogeneity helps us better understand the mechanisms behind the blockage of inflammatory waves in UC.

Like models based on ordinary differential equations, the stability of systems is rigorously studied in these approaches. For example, Chalmers et al.([19]), Porras et al.([73]), and Lauffenburger and Kennedy ([58]) conduct thorough analyses of different possible scenarios based on model parameters. These studies provide biological interpretations of the observed behaviors and numerical simulations that illustrate the results. Furthermore, El Khatib, Génieys, et al.([29]) prove the existence of progressive wave solutions, highlighting their role in triggering a chronic inflammatory response.

2.2 Mathematical model

In this section, we propose a reaction-diffusion system modeling the dysfunctional immune response underlying chronic inflammatory bowel diseases (IBD), with a particular focus on ulcerative colitis (UC). This type of model is relevant because it captures the complex interactions between pathogens, immune cells, and biological tissues.
Fundamentally, the first line of defense in the mucosal immune system is the epithelial barrier, a single polarized layer covered in mucus, where commensal microbes are anchored. A decrease in epithelial resistance and an increase in mucosal permeability, whether inflamed or not, are observed in UC patients. This leads to a disruption of the epithelial barrier, allowing

luminal antigens to access the underlying tissue of the mucosa.
In a healthy intestine, immune cells such as intestinal phagocytes eliminate external agents, thereby limiting inflammation. In contrast, in a pathological state, this finely regulated immune system balance is disrupted, contributing to both acute and chronic inflammation. Excessive migration of immune cells to the affected area may worsen the permeability of the epithelial barrier, thereby facilitating the infiltration of microbial flora and exacerbating inflammation. This complex mechanism triggers an inflammatory cascade characteristic of the progression of diseases such as UC.
To model these phenomena, we focus on two main components that vary with time t and space x: the number of non-resident bacteria crossing the intestinal epithelial barrier, denoted by u (also called microbes, pathogens, or antigens), and the number of immune cells, denoted by v (often referred to as phagocytic cells). Additionally, to simplify the analysis, we consider the intestine as a tube, which allows us to limit ourselves to a single spatial dimension. Thus, the domain of study is defined for $t > 0$ and $x \in \mathbb{R}$.
The model we propose is inspired by that of Nadin et al. ([67]), which studies the interactions between pathogenic bacteria and immune cells in an inflammatory context. It highlights Turing-type instabilities, explaining the formation of spatial patterns, notably in diseases such as Crohn's disease. In this reaction-diffusion model, bacteria act as activators and immune cells as inhibitors. Bacteria multiply at a rate r_b, while immune cells neutralize them and regulate their lifespan via a parameter r_c. The analysis shows that small perturbations can grow and generate stable patterns characteristic of Turing-type phenomena, provided certain conditions are met, including the absence of unbounded growth modes or population extinction.
However, although this model is relevant for Crohn's disease, it has certain limitations when analyzing the dynamics of inflammation propagation or blockage. Indeed, the study of Turing-type instabilities primarily focuses on the emergence of stationary patterns under the influence of diffusion and local interactions, but it does not precisely characterize whether inflammation propagates or is blocked under certain conditions. This model is relevant for Crohn's disease because this disease is often characterized by segmented and discontinuous patterns of inflammation in the intestine, which can be explained by the diffusion mechanisms and local interactions.
On the other hand, ulcerative colitis (UC) presents characteristics different from Crohn's disease: it manifests as contiguous inflammation, progressing continuously from the rectum, in contrast to the segmented and discontinuous patterns often observed in Crohn's disease. Thus, the model of Nadin et al. [67], which emphasizes mechanisms favoring the appearance of stationary spatial structures, is not suitable for studying the propagation and blocking phenomena specific to UC.
To better understand and model the dynamics of inflammation propagation in UC, we propose adapting the model by modifying the bacterial reproduction rate. Specifically, we divide the reproduction rate into a birth rate minus a mortality rate. The modified model is defined by the following equations:

$$\begin{cases} \partial_t u - D\partial_{xx} u = r_b u(1 - \frac{u}{b_i}) + \gamma(1 - \frac{u}{b_i})v - \frac{au}{s_b+u}v - du, \\ \partial_t v - D\partial_{xx} v = \beta u - r_c v. \end{cases} \tag{2.1}$$

We complete by considering initial data $u(0, x) = u_0(x)$ and $v(0, x) = v_0(x)$ for all $x \in \mathbb{R}$.
We emphasize that this modeling choice is not directly based on a specific biological mechanism. Rather, it is intended to mathematically explore how allowing the net growth term to become negative can lead to a blocking of traveling wave solutions. This serves as a theoretical hypothesis to explain how such blocking may occur in the context of ulcerative colitis

(UC).
During an immune response, the first phase involves the migration of non-resident phagocytes from the blood vessels to the intestinal mucosa. Then, in the second phase, these phagocytes move to the damaged area to combat the bacteria. Since the first phase, which involves transvascular transport, occurs almost instantly compared to the second phase, we choose to omit it in this simplified model.

In this work, we assume the same diffusion constant D for the bacteria and the phagocytes. When the diffusion coefficients for bacteria and phagocytes differ, the model can exhibit Turing instabilities, as shown in the article by Nadin, et al. (see [67]).
The parameter r_b represents the rate at which bacteria reproduce, and d represents the bacterial mortality rate.
Under healthy conditions, the number of bacteria present in the intestinal lumen remains nearly constant and cannot cross the epithelial barrier. This quantity is denoted by b_i. It is important to note that b_i may be seen as a carrying capacity. In the absence of the epithelial barrier, the maximum number of bacteria in the colon does not exceed b_i. This is why we include the logistic term $1 - \frac{u}{b_i}$ in the first equation, ([71]; [86]).
The parameter $\beta > 0$ represents the immune response rate of the organism, which sends phagocytes to damaged areas when pathogens are detected. Although their activation is not instantaneous, phagocytes rapidly appear and migrate to infected zones to combat bacteria. The term $-\frac{auv}{s_b+u}$, where $a > 0$ and $s_b > 0$, describes the effect of the immune system on pathogens. In particular, $\frac{au}{s_b+u}$ represents the rate of phagocytosis, which is the speed with which immune cells ingest bacteria. This rate depends on the density of the pathogens. It takes into account the rate p_c at which phagocytes encounter bacteria, given by $p_c := \frac{a}{s_b}$, and the average time τ required for a phagocyte to neutralize a bacterium, calculated as $\tau := \frac{1}{a}$. These dynamics are supported by the experiments described in [62].
We consider $\gamma > 0$ as a measure of the negative effect of phagocyte concentration on epithelial resistance. Therefore, the larger the epithelial gap, the more bacteria are present. As the concentration of bacteria increases, more immune cells are attracted to the damaged zone, exacerbating epithelial permeability.
The term du in our model represents the mortality of bacteria in the intestinal tract, illustrating that these bacteria do not persist indefinitely. This dynamic is essential to avoid excessive accumulation of pathogens and maintain microbial balance. This mechanism is intrinsically linked to the natural defenses of the intestine, such as phagocytosis by immune cells and the action of antimicrobial peptides, which contribute to the regulation of the bacterial population. Finally, a self-regulating mechanism of anti-inflammatory cells limits their lifespan, resulting in an intrinsic mortality rate of immune cells, denoted as $r_c > 0$ in the model.

After understanding the model, we analyze the decomposition of the reproduction rate and justify its relevance in our case. To do this, we consider the equation for u when $v = 0$. In this case, the equation becomes:

$$\partial_t u - D\partial_{xx} u = r_b u \left(1 - \frac{u}{b_i}\right) - du.$$

Expanding this equation, we get:

$$\partial_t u - D\partial_{xx} u = r_b u - \frac{r_b u^2}{b_i} - du = \underbrace{(r_b - d)\, u \left(1 - \left(\frac{r_b}{r_b - d}\right) \frac{u}{b_i}\right)}_{g(u)}.$$

This is a Fisher-KPP type equation. In the case where $r_b - d > 0$, it is well known that this equation exhibits a hair-trigger effect: as soon as the initial condition is positive, the solution rapidly converges to $u = \frac{b_i(r_b-d)}{r_b}$ (see [10]). Thus, to expect to observe a blockage of the propagation, it is necessary that $r_b - d < 0$, as shown in Figures 2.1 and 2.2.

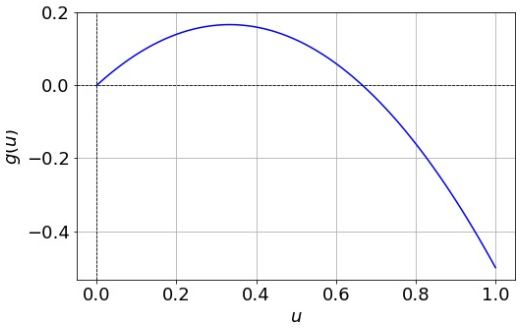

Figure 2.1: Case $r_b - d > 0$.

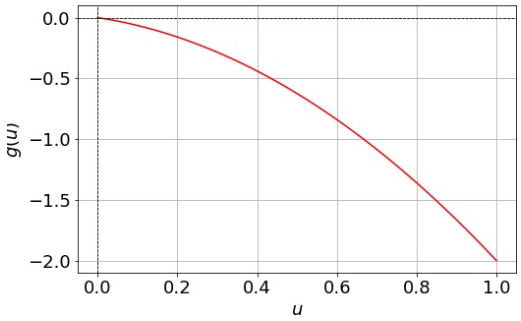

Figure 2.2: Case $r_b - d < 0$.

In our case, this "hair-trigger effect" is all the more significant since, at first order, the action of v on the bacteria is positive, as mentioned in Nadin et al. [67].

The first objective of this chapter is to prove that in a homogeneous medium, there is propagation of the inflammation. Then, our second objective is to prove that in a heterogeneous environment the propagation can be blocked. We describe more precisely in the next section these two main results.

2.3 Main results

In this section, we state the two main results of this chapter. Our first result concerns the homogeneous case, where we show the existence of propagation. This is our statement:

Theorem 6.

We assume that $r_b < d < r_b + \frac{\gamma\beta}{r_c}$, with $\gamma > a$, and $s_b > \max(b_i, \frac{1}{r_c})$. Under these assumptions, there is a spreading speed $c^* > 0$ with the properties that for every positive ϵ, the following holds:

$$\lim_{t\to+\infty}\Big[\max_{|x|\geq t(c^*+\epsilon)} |(u(x,t), v(x,t))|\Big] = 0,$$

and for any strictly positive constant vector w there exists a positive R_w such that if $(u_0(x), v_0(x)) \geq w$ on an interval of length $2R_w$, the following holds:

$$\lim_{t\to+\infty}\Big[\max_{|x|\leq t(c^*-\epsilon)} |(u_2^+, v_2^+) - (u(x,t), v(x,t))|\Big] = 0.$$

The pair (u_2^+, v_2^+) is a positive equilibrium of the ODE system associated with (2.1). It is defined in lemma 11.

In order to prove Theorem 6, we first show that the system under study is cooperative and monostable, which implies the existence of a stable equilibrium. We then establish the propagation of the solution by applying ideas from Weinberger's paper [94]. The detailed proof of this result is presented in Part 2.6.1.

Our second result refers to the heterogeneous case. More precisely, when the death rate of bacteria is heterogeneous, we show that blocking of the propagation occurs, as observed in the homogeneous case. Our result is as follows.

Theorem 7.

Let $d(x) = d_1 \mathbb{1}_{x\leq 0} + d_2 \mathbb{1}_{x>0}$, $d_k \in \mathbb{R}_+$, $k = 1, 2$. If the following conditions hold true : $r_c > \beta$, $s_b > \max(b_i, \frac{1}{\beta})$, $\gamma > a$, $r_b < d_1 < r_b + \frac{\gamma\beta}{r_c}$ and $r_b + \gamma < d_2 < \min(r_b + \gamma + r_c - \beta, s_b(r_b r_c + \beta\gamma))$. Then, there is a solution $(\bar{U}, \bar{V})$ of the following system:

$$\begin{cases} -D\partial_{xx}u = r_b u(1 - \frac{u}{b_i}) + \gamma(1 - \frac{u}{b_i})v - \frac{auv}{s_b+u} - d(x)u, \\ -D\partial_{xx}v = \beta u - r_c v, \\ (u, v)(-\infty) = (u_2^+, v_2^+), \ (u, v)(+\infty) = (0, 0), \\ u > 0, \ v > 0. \end{cases} \tag{2.2}$$

Our proof of this statement reduces to the construction of stationary solutions. That construction represents a particular case of a traveling wave front at constant speed, linking two equilibria of the system. More specifically, for $d = d_1$, we have a stable positive equilibrium, while for $d = d_2$, the system reaches the stable equilibrium at $(0, 0)$. These equilibrium points and their stability are analyzed in detail in subsection 2.4.2. To demonstrate the existence of stationary solutions, we use the method of subsolutions and supersolutions and construct explicitly such solutions.

Corollary 9. *(Blocking of the Wave)*

Under the assumptions of Theorem 7, any solution to the initial problem (2.1) with an initial condition (u_0, v_0) such that $(0, 0) \leq (u_0, v_0) \leq (\bar{U}, \bar{V})$ exhibits limited propagation.

Note that Corollary 9 is a direct consequence of Theorem 7 and the fact that there is a comparison principle for the system (2.1). Its proof is given in Subsection 2.6.3.

Before proving the main results of the existence of propagation and the blocking of this propagation, let us start with some preliminary results that will be used throughout this chapter.

2.4 Preliminary results

2.4.1 Non-negativity property

We first show the persistence of the non-negativity property of our model, which is a crucial requirement for any population dynamics model. In other words, it is crucial that when the initial data holds a biologically plausible interpretation, the solution of the differential equation maintains this feature.

Proposition 10.

If the initial conditions $(u(0, x), v(0, x))$ are nonnegative, then $(u(t, x), v(t, x))$ remains nonnegative for all $t \geq 0$.

Proof.

We consider the following model:

$$\begin{cases} \partial_t u - D\partial_{xx}u = r_b u\left(1 - \frac{u}{b_i}\right) + \gamma\left(1 - \frac{u}{b_i}\right)v - \frac{au}{s_b+u}v - du, \\ \partial_t v - D\partial_{xx}v = \beta u - r_c v. \end{cases} \tag{2.3}$$

With initial conditions $u(0, x) = u_0(x)$ and $v(0, x) = v_0(x)$ for all $x \in \mathbb{R}$.

Consider t_1 the first instant when either $u(t_1, x)$ or $v(t_1, x)$ becomes negative, then for some $x_1 \in \mathbb{R}$ we have $u(t_1, x_1)\, v(t_1, x_1) = 0$.

If $u(t_1, x_1) = 0$ and $v(t, x) > 0$ for all $(t, x) \in (0, t_1] \times \mathbb{R}$. The function $u = 0$ is a sub solution of the first equation in (2.3), As long as $v > 0$, the right-hand side is strictly positive when $u = 0$, By the strong maximum principle, this implies that $u(t, x) > 0$ for all $(t, x) \in (0, t_1] \times \mathbb{R}$, which contradicts $u(t_1, x_1) = 0$.

Similarly, if $v(t_1, x_1) = 0$ and $u(t, x) > 0$ for all $(t, x) \in (0, t_1] \times \mathbb{R}$. The function $v = 0$ is a sub solution of the second equation in (2.3). As long as $u > 0$, the right-hand side is strictly positive when $v = 0$, By the strong maximum principle, this implies that $v(t, x) > 0$ for all $(t, x) \in (0, t_1] \times \mathbb{R}$, which contradicts $v(t_1, x_1) = 0$. Therefore, the solution remains strictly positive for all $t > 0$ and $x \in \mathbb{R}$. □

2.4.2 Equilibria and Their Stability in the Dynamical System

In this subsection, we closely examine the equilibria of the dynamical system and study their stability, which enables us to gain a better understanding of the system without diffusion. Consider the ODE system associated with (2.1) with positive real parameters r_b, b_i, γ, a, s_b, β and r_c and $d \in \mathbb{R}_+$.

$$\begin{cases} \partial_t u^* = r_b u^*(1 - \frac{u^*}{b_i}) + \gamma(1 - \frac{u^*}{b_i})v^* - \frac{a u^* v^*}{s_b + u^*} - d u^*, \\ \partial_t v^* = \beta u^* - r_c v^*. \end{cases} \tag{2.4}$$

Lemma 11. *(Existence of equilibria)*
Let $d \in \mathbb{R}_+$. Suppose that $d < s_b(r_b r_c + \beta\gamma)$ and $s_b > \frac{1}{r_c}$. Then, we have the two following cases:

- ***Case 1:*** *$d < r_b + \frac{\gamma\beta}{r_c}$. In this case, equation (2.4) has three equilibria: a negative equilibrium (u_1^*, v_1^*), and a positive equilibrium $\left(u_2^+, v_2^+\right)$ and $(0, 0)$.*
- ***Case 2:*** *$d > r_b + \frac{\gamma\beta}{r_c}$. In this case, equation (2.4) has three equilibrium: two negative equilibria (u_1^*, v_1^*), $\left(u_2^-, v_2^-\right)$ and $(0, 0)$.*

Remark 1. *The decay parameter was chosen to ensure that $(0, 0)$ is the only stationary point of equation (2.4).*

Remark 2. *We note that negative stationary states are not biologically meaningful because they do not correspond to realistic population densities. Therefore, our analysis focuses on nonnegative solutions.*

Proof.
We note that (u^*, v^*) is the critical point of (2.4) if it satisfies the following system:

$$\begin{cases} r_b u^*(1 - \frac{u^*}{b_i}) + \gamma(1 - \frac{u^*}{b_i})v^* - \frac{a u^* v^*}{s_b + u^*} - d u^* = 0, & (2.5) \\ v^* = \dfrac{\beta}{r_c} u^*. & (2.6) \end{cases}$$

By substituting (2.6) into (2.5), we get:

$$\begin{aligned} & r_b u^*(1-\frac{u^*}{b_i}) - du^* + \frac{\gamma\beta}{r_c}u^*(1-\frac{u^*}{b_i}) - \frac{a\beta(u^*)^2}{r_c(s_b+u^*)} \\ &= u^*[r_b(1-\frac{u^*}{b_i}) - d + \frac{\gamma\beta}{r_c}(1-\frac{u^*}{b_i}) - \frac{a\beta u^*}{r_c(s_b+u^*)}] \\ &= 0 \end{aligned}$$

which yields

$$u^* = 0$$

or

$$r_b(1-\frac{u^*}{b_i}) - d + \frac{\gamma\beta}{r_c}(1-\frac{u^*}{b_i}) - \frac{a\beta u^*}{r_c(s_b+u^*)} = 0.$$

We can simplify the previous equation to obtain a more concise expression. The following equation represents this simplification:

$$\begin{aligned} & (u^*)^2[-r_c r_b - \gamma\beta] + u^*[r_c r_b(b_i - s_b) - db_i r_c + \gamma\beta(b_i - s_b) - a\beta b_i] + r_b r_c b_i s_b \\ & - db_i r_c s_b + \gamma\beta b_i s_b = 0. \end{aligned} \tag{2.7}$$

To find the nonzero equilibria, it suffices to determine the values of u^* for which equation (2.7) vanishes. We then solve equation (2.7), we calculate the discriminant Δ of (2.7).

$$\Delta = [(r_b r_c + \beta\gamma)(b_i - s_b) - ab_i\beta - db_i r_c]^2 + 4(r_b r_c + \beta\gamma)(s_b b_i(r_b r_c + \beta\gamma) - db_i).$$

According to the hypothesis of the lemma, we have $\Delta > 0$. Therefore equation (2.7) has two solutions

$$u_1^* = \frac{(r_b r_c + \beta\gamma)(b_i - s_b) - ab_i\beta - db_i r_c - \sqrt{\Delta}}{2(r_b r_c + \beta\gamma)},$$

$$u_2^* = \frac{(r_b r_c + \beta\gamma)(b_i - s_b) - ab_i\beta - db_i r_c + \sqrt{\Delta}}{2(r_b r_c + \beta\gamma)}.$$

We conclude that (2.4) has three equilibria $(0,0)$, (u_1^*, v_1^*) and (u_2^*, v_2^*),

$$where \quad v_1^* = \frac{\beta}{r_c}u_1^* \; and \; v_2^* = \frac{\beta}{r_c}u_2^*.$$

For all $k \in \{1,2\}$, u_k^* are the solutions of equation (2.7), and thus we have the following relations:

$$\begin{cases} u_1^* u_2^* = \frac{s_b b_i[r_b r_c + \beta\gamma] - db_i r_c s_b}{-r_b r_c - \beta\gamma}, \\ u_1^* + u_2^* = \frac{(b_i - s_b)(r_c r_b + \gamma\beta) - a\beta b_i - db_i r_c}{r_b r_c + \gamma\beta}. \end{cases}$$

- Case 1: $u_1^* u_2^* < 0$. Since $d < r_b + \frac{\gamma\beta}{r_c}$, we have that u_1^* and u_2^* are of opposite sign. Therefore, we have a negative equilibrium (u_1^*, v_1^*) and a positive equilibrium (u_2^*, v_2^*), which will be denoted (u_2^+, v_2^+).

- Case 2: $u_1^* u_2^* > 0$ and $u_1^* + u_2^* < 0$. Since $d > r_b + \frac{\gamma\beta}{r_c}$, u_1^* and u_2^* are both negative. Therefore, we have two negative equilibria.

□

Let us discuss the stability of the equilibria in the following statement:

Lemma 12. *(Stability of equilibria)*

Let $d \in \mathbb{R}_+$. Suppose that $d < s_b(r_b r_c + \beta\gamma)$ and $s_b > \frac{1}{r_c}$

a) If $r_b < d < r_b + \frac{\gamma\beta}{r_c}$ and $f'\left(u_2^+\right) > \max\left(\frac{-r_b r_c}{\beta b_i} - \frac{d}{v_2^+}, \frac{-2r_b r_c}{\beta b_i} - \frac{d}{v_2^+} + \frac{(r_b - r_c)}{v_2^+}\right)$ where $f(u^*) = -\gamma\left(1 - \frac{u^*}{b_i}\right) + \frac{au^*}{s_b + u^*}$, then $(0,0)$ is an unstable equilibrium and $\left(u_2^+, v_2^+\right)$ is a stable positive equilibrium of (2.4).

b) If $d > r_b + \frac{\gamma\beta}{r_c}$, then $(0,0)$ is a stable equilibrium
Moreover, there is no positive equilibrium of (2.4).

Proof.

We consider the following ODEs:

$$\begin{cases} \partial_t u^* = r_b u^*\left(1 - \frac{u^*}{b_i}\right) - du^* - f(u^*)\, v^* = F_1(u^*, v^*), \\ \partial_t v^* = \beta u^* - r_c v^* = F_2(u^*, v^*). \end{cases}$$

With $F(u^*, v^*) = (F_1(u^*, v^*), F_2(u^*, v^*))$ and $f(u^*) = -\gamma\left(1 - \frac{u^*}{b_i}\right) + \frac{au^*}{s_b + u^*}$.
We define $DF(u^*, v^*)$ the differential of the function F at the equilibrium point (u^*, v^*):

$$DF(u^*, v^*) = \begin{pmatrix} \frac{\partial F_1}{\partial u^*} & \frac{\partial F_1}{\partial v^*} \\ \frac{\partial F_2}{\partial u^*} & \frac{\partial F_2}{\partial v^*} \end{pmatrix} = \begin{pmatrix} r_b\left(1 - \frac{2u^*}{b_i}\right) - f'(u^*)\, v^* - d & -f(u^*) \\ \beta & -r_c \end{pmatrix}.$$

We compute the determinant and the trace of this matrix:

$$\mathrm{Tr}\left(DF(u^*, v^*)\right) = r_b\left(1 - \frac{2u^*}{b_i}\right) - f'(u^*)\, v^* - d - r_c,$$

$$\det\left(DF(u^*, v^*)\right) = -r_c r_b\left(1 - \frac{2u^*}{b_i}\right) + r_c f'(u^*)\, v^* + dr_c + \beta f(u^*).$$

Then, we consider the two cases in the statement of the Lemma:

a) $\mathrm{Tr}\left(DF(0,0)\right) = r_b - d - r_c < 0$, since $r_b < d$ and $\det\left(DF(0,0)\right) = -r_b r_c + dr_c - \beta\gamma < 0$, since $d < r_b + \frac{\gamma\beta}{r_c}$. Hence, $(0,0)$ is an unstable equilibrium of (2.4).
Similarly,

$$\mathrm{Tr}\left(DF\left(u_2^+, v_2^+\right)\right) = r_b\left(1 - \frac{2u_2^+}{b_i}\right) - f'\left(u_2^+\right) v_2^+ - d - r_c,$$

$$\det\left(DF\left(\left(u_2^+, v_2^+\right)\right)\right) = -r_b r_c\left(1 - \frac{2u_2^+}{b_i}\right) + r_c f'\left(u_2^+\right) v_2^+ + r_c d + \beta f\left(u_2^+\right).$$

As we have $f'\left(u_2^+\right) > \max\left(\frac{-r_b r_c}{\beta b_i} - \frac{d}{v_2^+}, \frac{-2r_b r_c}{\beta b_i} - \frac{d}{v_2^+} + \frac{(r_b - r_c)}{v_2^+}\right)$,
then $\mathrm{Tr}\left(DF\left(u_2^+, v_2^+\right)\right) < 0$ and $\det\left(DF\left(u_2^+, v_2^+\right)\right) > 0$, thus $\left(u_2^+, v_2^+\right)$ is a stable positive equilibrium of (2.4).

b) $\mathrm{Tr}\left(DF(0,0)\right) = r_b - d - r_c < 0$, since $r_b < d$ and $\det\left(DF(0,0)\right) = r_b r_c + dr_c - \beta\gamma > 0$, since $d > r_b + \frac{\gamma\beta}{r_c}$. Thus, $(0,0)$ is a stable equilibrium.

□

Remark 3.

This lemma confirms that the mere existence of a nontrivial positive equilibrium implies the instability of the trivial equilibrium $(0,0)$*. However, the stability of this positive equilibrium is not automatic: it requires an additional condition on the derivative* f' *at this point.*

After studying the stability of the equilibrium points, we now analyze how they evolve as a function of the parameter d. In particular, we plot a bifurcation diagram to visualize the critical thresholds where a qualitative change occurs in the system dynamics.

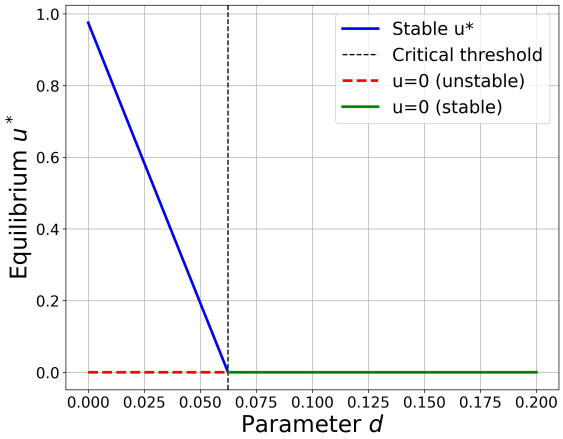

Figure 2.3: Bifurcation diagram of u as a function of d.

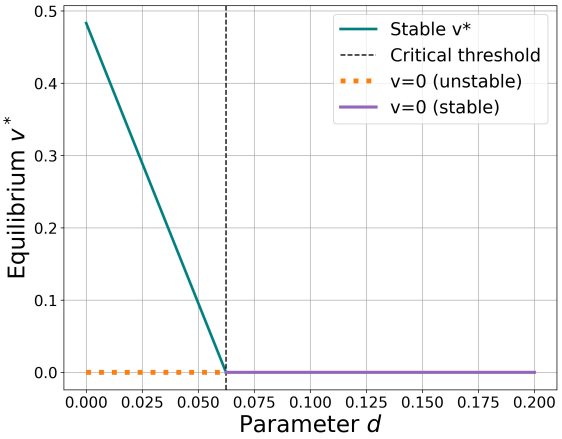

Figure 2.4: Bifurcation diagram of v as a function of d.

Following the preliminary results obtained in the previous section, we now present the estimation of the wave speed for the model, the existence of which was demonstrated in Theorem 6.

2.5 Estimation of the wave speed for the model

In this subsection, we analytically determine the wave speed based on the model parameters. Thanks to Theorem 6, we can affirm that model (2.1) exhibits solutions in the form of progressive waves. Consequently, the variables $u(x,t)$ and $v(x,t)$ can be represented as progressive waves, i.e., $u(x,t) = U(x-ct)$ and $v(x,t) = V(x-ct)$. It is noteworthy that we employ the same strategy as in [27] to analyze the wave speed in our context. To find the minimum speed, we begin by linearizing the system (2.1) at $(0,0)$ to find positive solutions. Subsequently, we search for the minimum value of the wave speed for which positive solutions exist. After this linearization at $(0,0)$, we obtain the system:

$$\begin{cases} -cU' - DU'' = (r_b - d)U + \gamma V, \\ -cV' - DV'' = \beta U - r_c V. \end{cases} \tag{2.8}$$

We are looking for solutions in the form

$$U(x-ct) = p_1 e^{-\lambda(x-ct)}, \quad V(x-ct) = p_2 e^{-\lambda(x-ct)}.$$

Hence, system (2.8) yields:

$$\begin{cases} c\lambda p_1 - D\lambda^2 p_1 = (r_b - d)p_1 + \gamma p_2, \\ c\lambda p_2 - D\lambda^2 p_2 = \beta p_1 - r_c p_2. \end{cases} \tag{2.9}$$

To determine the minimum wave speed, it is necessary to find the minimum value of c for which the system 2.9 admits a positive solution λ. Introducing the parameter $X = c\lambda - D\lambda^2$ and eliminating the variables p_1 and p_2, we obtain the following equation :

$$X^2 + (r_c + d - r_b)X + r_c(d - r_b) - \beta\gamma = 0.$$

Hence,

$$c^* = \min_{\lambda>0} D\lambda + \frac{X_+}{\lambda} = 2\sqrt{DX_+},$$

where $X_+ = \frac{-r_c-d+r_b+\sqrt{(r_c-d+r_b)^2+4\beta\gamma}}{2}$.

We are studying the dependence of the analytical wave speed on several parameters, particularly the parameter d, which represents the mortality rate. We consider the range of values for d to be $(0.021, 0.03712)$. In addition to the analysis of the analytical wave speed's dependence, we are calculating and graphically representing the numerical wave speed, which is calculated using the formula for dividing distance by time (see Figure 2.5). A detailed explanation of the values of all parameters used in this simulation is provided later in Section 2.7 of the paper.

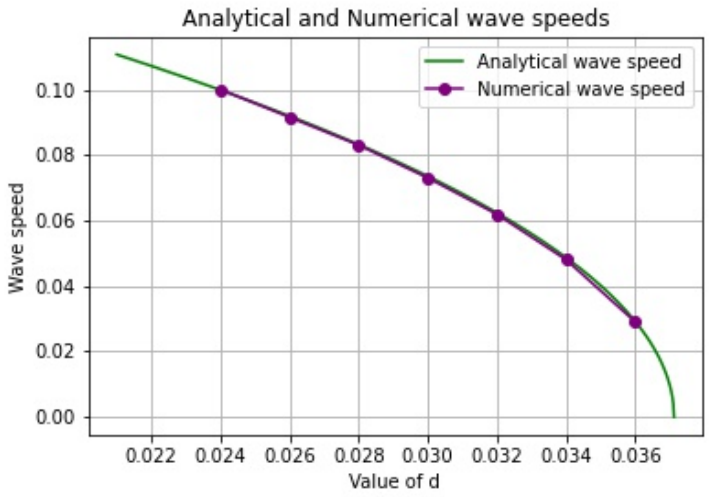

Figure 2.5: Dependence of the wave speed on the parameter $d \in (0.021, 0.03712)$. Wave speed in numerical simulations and analytical formula (curves coincide) for the values of parameters : $r_b = 0.02$, $r_c = 0.3129$, $\beta = 0.06258$, $D = 0.2$, $\gamma = 0.0856$.

2.6 Proof of the main results

In this section, we prove our main results. We will start by presenting the proof of the first result.

2.6.1 Proof of Theorem 6

Before proving the theorem, let us first show that our system is cooperative, then we define the concept of invariant sets and introduce some notations, as they are necessary for the proof.

Lemma 13.

If $\gamma > a > 0$, $\beta > 0$, $s_b > b_i$, and $0 < u \leq \frac{b_i}{2}$, then the system (2.1) is cooperative.

Proof.

As introduced in Lemma 12, the functions $F_1(u, v)$ and $F_2(u, v)$ are given by:

$$F_1(u, v) = r_b u \left(1 - \frac{u}{b_i}\right) + \gamma \left(1 - \frac{u}{b_i}\right) v - \frac{au}{s_b + u} v - du,$$

$$F_2(u, v) = \beta u - r_c v.$$

We aim to demonstrate that the system is cooperative by showing that $\frac{\partial F_1}{\partial v}(u, v)$ and $\frac{\partial F_2}{\partial u}(u, v)$ are positive. First, we compute the partial derivatives:

$$\frac{\partial F_1}{\partial v}(u, v) = \gamma \left(1 - \frac{u}{b_i}\right) - \frac{au}{s_b + u}.$$

Next, we rewrite the expression for $\frac{\partial F_1}{\partial v}(u, v)$ as follows:

$$\frac{\partial F_1}{\partial v}(u, v) = \frac{1}{s_b + u} \left(\gamma \left(1 - \frac{u}{b_i}\right) (s_b + u) - au\right).$$

Now, we observe that since $0 \leq u \leq \frac{b_i}{2}$ and $\gamma > a$, it follows that:

$$\gamma \left(1 - \frac{u}{b_i}\right) (s_b + u) > \frac{a (s_b + u)}{2}.$$

From this, under the assumption that $s_b > b_i$, $u \leq \frac{b_i}{2}$, and $a > 0$, we can conclude:

$$\gamma \left(1 - \frac{u}{b_i}\right) (s_b + u) > au.$$

This implies that:

$$\frac{\partial F_1}{\partial v}(u, v) > 0.$$

Next, we compute the partial derivative of $F_2(u, v)$ with respect to u:

$$\frac{\partial F_2}{\partial u}(u, v) = \beta.$$

Since $\beta > 0$, we conclude that:

$$\frac{\partial F_2}{\partial u}(u, v) > 0.$$

Thus, both partial derivatives are positive, which proves that the system is cooperative.

□

The monotonicity of the system guarantees the existence of traveling wave solutions in both bistable and monostable cases, our paper focusing mainly on the latter.

2.6.1.1 Definition and Notations

Definition 14. *(Definition of Invariant Set)*
Let Ω be an open subset of $\mathbb{R}^n$. A closed subset $I \subset \mathbb{R}^n$ is called a (positively) invariant region for the solution defined by equations (2.1) *if the following condition holds: Any solution $(u(x,t), v(x,t))$ with all its boundary and initial values in I satisfies $(u(x,t), v(x,t)) \in I$ for all $x \in \Omega$ and for all $t \in [0, \infty)$.*

This definition is found in [82]. More precisely, we consider a set of the form:

$$I = \{V \in \mathbb{R}^n \mid G_i(V) \leq 0, \quad \forall i = 1, \ldots, n\}. \tag{2.10}$$

To show that I is an invariant region, we verify that the associated vector field points strictly inward on the boundary ∂I. That is, the smooth function $G : \mathbb{R}^n \to \mathbb{R}$ satisfies:

$$dG_i(F) < 0 \quad \text{at} \quad V_0, \quad \text{where} \quad G_i(V_0) = 0. \tag{2.11}$$

This condition ensures that any trajectory of the system starting in I remains in I for all $t \geq 0$, thus proving that I is an invariant region.

Notation 1.
In the following sections, the vector $X := (X_1, X_2)$ is said to be positive if $X_1 \geq 0$ and $X_2 \geq 0$ and we note it $(X_1, X_2) \geq (0,0)$. The vector $X := (X_1, X_2)$ is said to be strictly positive if $X_1 > 0$ and $X_2 > 0$ and we note it $(X_1, X_2) \gg (0,0)$. For any $(X_1, X_2) \gg (0,0)$, we define $C_{(X_1,X_2)} = \{(u,v),\ 0 \leq u \leq X_1,\ 0 \leq v \leq X_2\}$.

2.6.1.2 Proof of Theorem 6

To establish the existence of a propagation speed, we follow the approach of Theorem 4.1 from [94], which ensures the existence of a well-defined asymptotic speed under certain conditions. Before verifying these conditions, let us briefly recall the underlying intuition: the idea is to identify an invariant region that constrains the evolution of the solution and to demonstrate that the system admits a well-defined propagation speed. In what follows, we verify the hypotheses of Theorem 4.1.

i) Since $d < r_b + \frac{\gamma\beta}{r_c}$, then from Lemma 11, we see that (2.1) has a positive equilibrium (u_2^+, v_2^+), i.e $(u_2^+, v_2^+) \gg (0,0)$.

ii) Next, we show that

$$C_{(u_2^+, v_2^+)} = \{(u,v), 0 \leq u \leq u_2^+, 0 \leq v \leq v_2^+\}$$

is an invariant set of (2.1). We use Definition 14. Let $(u,v) \in C_{(u_2^+, v_2^+)}$ and define $G_1(u,v) = -u$. Now, since

$$F(u,v) = \left(r_b u \left(1 - \frac{u}{b_i}\right) + \gamma \left(1 - \frac{u}{b_i}\right) v - \frac{auv}{s_b + u} - du, \beta u - r_c v\right),$$

and by taking the differential of G_1, we obtain

$$dG_1(F)|_{u=0} = -\gamma v < 0,$$

since $v > 0$ and $-\gamma < 0$. Moreover, if we set $G_2(u,v) = -v$, we obtain that

$$dG_2(F)|_{v=0} = -\beta u < 0,$$

since $u \geq 0$ and $\beta > 0$. Similarly, if $G_3(u,v) = v - v_2^+$, and $G_4(u,v) = u - u_2^+$, we obtain that

$$dG_3(F)|_{v=v_2^+} = \beta u - r_c v_2^+ = \beta(u - u_2^+) \leq 0,$$

and

$$dG_4(F)|_{u=u_2^+} = r_b u_2^+(1 - \frac{u_2^+}{b_i}) - du_2^+ + \gamma(1 - \frac{u_2^+}{b_i})v - \frac{au_2^+ v}{s_b + u_2^+}.$$

Rewriting the above expression, we get:

$$dG_4(F)|_{u=u_2^+} = r_b u_2^+(1 - \frac{u_2^+}{b_i}) - du_2^+ - \frac{r_b r_c(1 - \frac{u_2^+}{b_i})v}{\beta} + \frac{dr_c v}{\beta}.$$

Further simplifying, we have:

$$dG_4(F)|_{u=u_2^+} = \frac{r_b}{\beta}[1 - \frac{u_2^+}{b_i}][\beta u_2^+ - r_c v] + d[\frac{r_c}{\beta}v - u_2^+].$$

Rearranging terms, we obtain:

$$dG_4(F)|_{u=u_2^+} = \frac{r_b r_c}{\beta}(1 - \frac{u_2^+}{b_i})[v_2^+ - v] + \frac{r_c d}{\beta}[v - v_2^+].$$

Finally, the concluding statement about the inequality:

$$dG_4(F)|_{u=u_2^+} = \frac{r_c}{\beta}[v - v_2^+][d - r_b + \frac{r_b u_2^+}{b_i}] < 0,$$

respectively, since $u \leq u_2^+$, $v \leq v_2^+$, $\beta > 0$ and $d > r_b$. By using the definition of an invariant set, we conclude that $C_{(u_2^+, v_2^+)} = \{(u,v), 0 \leq u \leq u_2^+, 0 \leq v \leq v_2^+\}$ is an invariant set of (2.1).

iii) In this step, we will verify the hypotheses of [94, proposition 2.1].

- $F(0,0) = F(u_2^+, v_2^+) = (0,0)$ and $(u_2^+, v_2^+) \gg (0,0)$ which is minimal in the sense that there is no other equilibrium than $(0,0)$ and (u_2^+, v_2^+) in the set $C_{u_2^+, v_2^+}$, when $d < r_b + \frac{\gamma\beta}{r_c}$.
- $F(\xi_1, \xi_2)$ is a continuous and piecewise continuously differentiable in (ξ_1, ξ_2) for $(0,0) < (\xi_1, \xi_2) \leq (u_2^+, v_2^+)$ and differentiable at $(0,0)$.
- Since $\gamma > a$; $\beta > 0$; $s_b > b_i$ and $0 < u \leq \frac{b_i}{2}$, we can conclude from Lemma 13 that the system (2.1) is cooperative.
- F does not depend explicitly on either x or t.
- The Jacobian matrix $DF(0,0) = \begin{pmatrix} r_b - d & \gamma \\ \beta & -r_c \end{pmatrix}$ is in Frobenius form. The principal eigenvalue
  $\gamma_1(0) = \frac{r_b - d - r_c + \sqrt{(-r_b + d + r_c)^2 - 4(-r_b r_c + d r_c - \gamma\beta)}}{2} > 0$, since $d < r_b + \frac{\gamma\beta}{r_c}$.

Then according to Theorem 4.1 in [94], there is a spreading speed $c^* > 0$ with the properties that for every positive ϵ:

- For any initial function $(u_0(x), v_0(x))$ in $C_{(u_2^+, v_2^+)} = \{(u,v), 0 \leq u \leq u_2^+, 0 \leq v \leq v_2^+\}$ which vanishes outside a bounded set, the solution of (2.1) satisfies

$$\lim_{t \to +\infty} [\max_{|x| \geq t(c^* + \epsilon)} |(u(x,t), v(x,t))|] = 0, \quad \forall \epsilon > 0.$$

- For any strictly positive constant vector w, there exists a positive R_w with the property that if $(u_0(x), v_0(x)) \geq w$ on an interval of length $2R_w$, then

$$\lim_{t\to+\infty}[\max_{|x|\leq t(c^*-\epsilon)}|(u_2^+, v_2^+) - (u(x,t), v(x,t))|] = 0.$$

We are now in a position to establish our second main result.

2.6.2 Proof of Theorem 7

In this subsection, our goal is to prove the existence of a stationary solution for problem (2.1). This solution corresponds to a solution of the associated elliptic problem, which can be formulated as follows:

$$\begin{cases} -D\partial_{xx}u = r_b u(1-\frac{u}{b_i}) + \gamma(1-\frac{u}{b_i})v - \frac{auv}{s_b+u} - du = F_1(u,v), \\ -D\partial_{xx}v = \beta u - r_c v = F_2(u,v), \\ (u,v)(-\infty) = (u_2^+, v_2^+),\ (u,v)(+\infty) = (0,0), \\ u > 0,\ v > 0,\ x \in \mathbb{R}. \end{cases} \tag{2.12}$$

The proof is done by four steps. First, we begin by proving a comparison principle. Then, we construct the super and subsolution and finally we show the existence of the stationary solution.

2.6.2.1 Comparison principle

Before proving the comparison principle, we start by presenting the following property :

Lemma 15.
Assume that $(0,0) < (u,v) \leq \left(\frac{b_i}{2}, \frac{\beta b_i}{2r_c}\right)$. *Then*

$$|\frac{\partial F_1}{\partial u}(u,v)| \leq 2r_b + d + \frac{\beta b_i}{2r_c}\|f'\|_\infty = \Gamma_1,$$

where $\|f'\|_\infty = \sup_{0\leq u\leq \frac{b_i}{2}} |\ f'(u)\ |$.

Proof.
The proof of this result is based on a straightforward calculation. In fact, let $0 \leq u \leq \frac{b_i}{2}$ and $F_1(u,v) = r_b u\left(1-\frac{u}{b_i}\right) - f(u)v - du$, where$f(u) = -\gamma\left(1-\frac{u}{b_i}\right) + \frac{au}{s_b+u}$.
Since the function F_1 and f are C^∞, we calculate:

$$\frac{\partial F_1}{\partial u}(u,v) = r_b\left(1-\frac{2u}{b_i}\right) - f'(u)v - d.$$

Therefore, we obtain:

$$|\frac{\partial F_1}{\partial u}(u,v)| \leq 2r_b + d + \frac{\beta b_i}{2r_c}\|f'\|_\infty = \Gamma_1.$$

□

Proposition 16. *(Comparison principle)*

Assume $\gamma > a$ and $s_b > b_i$. Let (u, v) be a solution of (2.1) in $\mathbb{R}$, supersolution $(\bar{u}, \bar{v})$ of (2.1) in $\mathbb{R}$ and subsolution $(\underline{u}, \underline{v})$ of (2.1) in $\mathbb{R}$, such that $(0,0) < (\bar{u}, \bar{v}) \leq (\frac{b_i}{2}, \frac{\beta b_i}{2r_c})$, $(0,0) < (\underline{u}, \underline{v}) \leq (\frac{b_i}{2}, \frac{\beta b_i}{2r_c})$ and $(0,0) < (u, v) \leq (\frac{b_i}{2}, \frac{\beta b_i}{2r_c})$. Then

$$(\underline{u}(t=0,x), \underline{v}(t=0,x)) \leq (u(t=0,x), v(t=0,x)) \leq (\bar{u}(t=0,x), \bar{v}(t=0,x)),$$

implies that

$$(\underline{u}(t,x), \underline{v}(t,x)) \leq (u(t,x), v(t,x)) \leq (\bar{u}(t,x), \bar{v}(t,x)), \quad \forall t \geq 0, \quad \forall x \in \mathbb{R}.$$

Proof.

Suppose that $(\underline{u}(t=0,x), \underline{v}(t=0,x)) \leq (u(t=0,x), v(t=0,x)) \leq (\bar{u}(t=0,x), \bar{v}(t=0,x))$. We use the strategy in [[71], Chapter 1], we have $(\bar{u}, \bar{v})$ a supersolution of (2.1) and (u, v) a solution of (2.1), then we have

$$\partial_t(u - \bar{u}) - D\partial_{xx}(u - \bar{u}) \leq F_1(u, v) - F_1(\bar{u}, \bar{v}). \tag{2.13}$$

We multiply ((2.13)) by $(u - \bar{u})_+$ and integrate on $\mathbb{R}$, we obtain

$$\partial_t \int_{\mathbb{R}} \frac{(u - \bar{u})_+^2}{2} dx + D \int_{\mathbb{R}} (\partial_x (u - \bar{u})_+)^2 dx \leq \int_{\mathbb{R}} [F_1(u, v) - F_1(\bar{u}, \bar{v})](u - \bar{u})_+ dx.$$

Implies that

$$\begin{aligned} &\partial_t \int_{\mathbb{R}} \frac{(u - \bar{u})_+^2}{2} dx + D \int_{\mathbb{R}} (\partial_x (u - \bar{u})_+)^2 dx \\ &\leq \int_{\mathbb{R}} [F_1(u, v) - F_1(u, \bar{v})](u - \bar{u})_+ dx + \int_{\mathbb{R}} \underbrace{[F_1(u, \bar{v}) - F_1(\bar{u}, \bar{v})](u - \bar{u})_+}_{I_1} dx. \end{aligned} \tag{2.14}$$

Since $(0,0) \leq (u, v) \leq (\frac{b_i}{2}, \frac{\beta b_i}{2r_c})$, $\frac{\partial F_1}{\partial u}(u, v)$ is bounded. Then the term I_1 is bounded by $\Gamma_1 (u - \bar{u})_+^2$. Hence

$$\begin{aligned} &\partial_t \int_{\mathbb{R}} \frac{(u - \bar{u})_+^2}{2} dx + D \int_{\mathbb{R}} (\partial_x (u - \bar{u})_+)^2 dx \\ &\leq \Gamma_1 \int_{\mathbb{R}} (u - \bar{u})_+^2 dx + \int_{\mathbb{R}} \underbrace{[F_1(u, v) - F_1(u, \bar{v})](u - \bar{u})_+}_{I_2} dx. \end{aligned}$$

According to the cooperativity property proven in the lemma 13, we have $\frac{\partial F_1}{\partial v}(u, v) = -f(u) \geq 0$. Then I_2 is bounded by $\|f\|_\infty (u - \bar{u})_+ (v - \bar{v})_+$. Hence

$$\begin{aligned} &\partial_t \int_{\mathbb{R}} \frac{(u - \bar{u})_+^2}{2} dx + D \int_{\mathbb{R}} (\partial_x (u - \bar{u})_+)^2 dx \\ &\leq \Gamma_1 \int_{\mathbb{R}} (u - \bar{u})_+^2 dx + \|f\|_\infty \int_{\mathbb{R}} (u - \bar{u})_+ (v - \bar{v})_+ dx. \end{aligned}$$

Which implies that

$$\partial_t \int_{\mathbb{R}} \frac{(u - \bar{u})_+^2}{2} dx \leq \max(\Gamma_1, r_c) \int_{\mathbb{R}} (u - \bar{u})_+^2 dx + \max(\beta, \|f\|_\infty) \int_{\mathbb{R}} (u - \bar{u})_+ (v - \bar{v})_+ dx. \tag{2.15}$$

Similarly, we can prove that

$$\partial_t \int_{\mathbb{R}} \frac{(v - \bar{v})_+^2}{2} dx \leq \max(\Gamma_1, r_c) \int_{\mathbb{R}} (v - \bar{v})_+^2 dx + \max(\beta, \|f\|_\infty) \int_{\mathbb{R}} (u - \bar{u})_+ (v - \bar{v})_+ dx. \tag{2.16}$$

$$\partial_t \int_{\mathbb{R}} \frac{(\underline{v}-v)_+^2}{2} dx \leq \max(\Gamma_1, r_c) \int_{\mathbb{R}} (\underline{v}-v)_+^2 dx + \max(\beta, \|f\|_\infty) \int_{\mathbb{R}} (\underline{u}-u)_+ (\underline{v}-v)_+ dx. \quad (2.17)$$

$$\partial_t \int_{\mathbb{R}} \frac{(\underline{u}-u)_+^2}{2} dx \leq \max(\Gamma_1, r_c) \int_{\mathbb{R}} (\underline{u}-u)_+^2 dx + \max(\beta, \|f\|_\infty) \int_{\mathbb{R}} (\underline{u}-u)_+ (\underline{v}-v)_+ dx. \quad (2.18)$$

We define

$$z(t) = \int_{\mathbb{R}} [(v-\bar{v})_+^2 + (u-\bar{u})_+^2 + (\underline{v}-v)_+^2 + (\underline{u}-u)_+^2] dx. \quad (2.19)$$

By summing ((2.15)), ((2.16)), ((2.17)) and ((2.18)), and using the fact $2ab \leq a^2 + b^2$, we obtain

$$\begin{cases} \partial_t z(t) \leq \Gamma z(t), \\ z(0) = 0. \end{cases} \quad (2.20)$$

Where $\Gamma = 2\max(\Gamma_1, r_c) + 2\max(\beta, \|f\|_\infty)$.

System ((2.20)) admits unique nonnegative solution $z(t) = 0$, $\forall t \geq 0$ which implies $\int_{\mathbb{R}} [(v - \bar{v})_+^2 + (u-\bar{u})_+^2 + (\underline{v}-v)_+^2 + (\underline{u}-u)_+^2] dx = 0$.

Since $(v-\bar{v})_+^2$, $(u-\bar{u})_+^2$, $(\underline{v}-v)_+^2$ and $(\underline{u}-u)_+^2$ are four continuous and positive functions, we have the result. □

2.6.2.2 Construction of the supersolution

The objective of this subsection is to construct a supersolution for equation (2.12) on $\mathbb{R}$. We choose (u_2^+, v_2^+) as a supersolution on the interval $(-\infty, 0)$, given that $C_{(u_2^+, v_2^+)}$ remains invariant for $d > r_b$. The next step is to construct a supersolution on the interval $(0, +\infty)$ for $d = d_2$. Before proceeding with the construction of the supersolution on the interval $(0, +\infty)$, we begin by stating the following property.

Lemma 17.
Let $d_2 > r_b + \gamma$. There exists (ϕ_1, ϕ_2) satisfying

$$\begin{cases} -D\partial_{xx}\phi_1 + \phi_1(-r_b - \gamma + d_2) = 0, \\ D\partial_{xx}\phi_2 - r_c\phi_2 = 0, \\ \phi_1(0) = u_2^+, \ \phi_1(+\infty) = 0, \\ \phi_2(0) = u_2^+ - v_2^+, \ \phi_2(+\infty) = 0, \\ \phi_1 > 0, \ \phi_2 > 0. \end{cases} \quad (2.21)$$

Indeed, for all $x \in (0, +\infty)$, $\phi_1(x) = u_2^+ e^{-\sqrt{\frac{1}{D}(-r_b-\gamma+d_2)}x}$ and $\phi_2(x) = (u_2^+ - v_2^+)e^{-\sqrt{\frac{r_c}{D}}x}$ are solutions to system (2.21).

Lemma 18.
Under the assumptions that $r_b + \gamma < d_2 < \min(r_b + \gamma + r_c - \beta, s_b(r_b r_c + \beta\gamma))$, $s_b > \frac{1}{\beta}$, and $\beta < r_c$, we have that $(\bar{u}, \bar{v}) = (\phi_1, \phi_1 - \phi_2)$ is a supersolution of (2.12) on $(0, +\infty)$.

Proof.
Let $(\bar{u}, \bar{v})$ be a supersolution of (2.12), such as $\bar{v} \leq \bar{u}$. For all $x > 0$, we show that

$$\begin{cases} -D\partial_{xx}\bar{u} - F_1(\bar{u}, \bar{v}) \geq 0, \\ -D\partial_{xx}\bar{v} - F_2(\bar{u}, \bar{v}) \geq 0. \end{cases} \quad (2.22)$$

Before proving system (2.22), note that $\bar{u} = \phi_1$ and $\bar{v} = \phi_1 - \phi_2$ are positive since $r_b + \gamma < d_2 < r_b + \gamma + r_c - \beta$ and $\beta < r_c$. Now, let us demonstrate system (2.22). Starting with the first equation, we have:

$$-D\partial_{xx}\bar{u} - F_1(\bar{u},\bar{v}) = -D\partial_{xx}\bar{u} - r_b\bar{u}(1 - \frac{\bar{u}}{b_i}) + d_2\bar{u} + f(\bar{u})\bar{v}.$$

With the definition of f, we get:

$$-D\partial_{xx}\bar{u} - F_1(\bar{u},\bar{v}) = -D\partial_{xx}\bar{u} - r_b\bar{u} - \gamma\bar{v} + d_2\bar{u} + \underbrace{\frac{r_b(\bar{u})^2}{b_i} + \frac{\gamma\bar{u}\bar{v}}{b_i} + \frac{a\bar{u}\bar{v}}{s_b + \bar{u}}}_{J_2}.$$

Since $J_2 > 0$, we have

$$-D\partial_{xx}\bar{u} - F_1(\bar{u},\bar{v}) \geq -D\partial_{xx}\bar{u} - r_b\bar{u} - \gamma\bar{v} + d_2\bar{u}.$$

Under the condition that $\bar{v} \leq \bar{u}$, we have

$$-D\partial_{xx}\bar{u} - F_1(\bar{u},\bar{v}) \geq -D\partial_{xx}\bar{u} + \bar{u}[-r_b - \gamma + d_2].$$

By definition of the function ϕ_1, we have $-D\partial_{xx}\phi_1 + \phi_1[-r_b - \gamma + d_2] = 0$. Therefore,

$$-D\partial_{xx}\bar{u} - F_1(\bar{u},\bar{v}) \geq 0.$$

Now, let us proceed to the second equation of the system. We have:

$$-D\partial_{xx}\bar{v} - F_2(\bar{u},\bar{v}) = -D\partial_{xx}\bar{v} - \beta\bar{u} + r_c\bar{v} = -D\partial_{xx}\phi_1 + [r_c - \beta]\phi_1 + D\partial_{xx}\phi_2 - r_c\phi_2.$$

Based on the definitions of the functions ϕ_1 and ϕ_2, we can deduce that:

$$-D\partial_{xx}\bar{v} - F_2(\bar{u},\bar{v}) = [r_c - \beta + r_b + \gamma - d_2]\phi_1.$$

Considering that $d_2 < r_b + \gamma + r_c - \beta$,we can deduce that:

$$-D\partial_{xx}\bar{v} - F_2(\bar{u},\bar{v}) \geq 0.$$

To complete the proof, we need to prove that $(\bar{u},\bar{v})(+\infty) = (0,0)$ and $(\bar{u},\bar{v})(0,0) = (u_2^+, v_2^+)$. According to the definition of the functions ϕ_i, where $i = 1, 2$, we know that $\phi_i(+\infty) = 0$. Hence, $(\bar{u},\bar{v})(+\infty) = (0,0)$. Furthermore, since $\phi_1(0) = u_2^+$ and $\phi_2(0) = u_2^+ - v_2^+$, we can compute $(\bar{u},\bar{v})(0,0)$ as follows:

$$(\bar{u},\bar{v})(0,0) = (\phi_1, \phi_1 - \phi_2)(0) = (u_2^+, u_2^+ - u_2^+ + v_2^+) = (u_2^+, v_2^+).$$

Therefore, we have shown that $(\bar{u},\bar{v})(+\infty) = (0,0)$ and $(\bar{u},\bar{v})(0,0) = (u_2^+, v_2^+)$. □

2.6.2.3 Construction of a subsolution

The goal of this subsection is to construct a subsolution for the system represented by (2.12) over the entire real line. We choose $(0,0)$ as the subsolution over the interval $(0,+\infty)$ because the system is cooperative. Now, we proceed to establish a subsolution over the interval $(-\infty,0)$.

Lemma 19.

If $\gamma > a$, $s_b > b_i$ and $d_1 > r_b$ then the system defined by (2.12) *admits a subsolution on the interval* $(-\infty,0)$.

Proof.

For $R > 0$, $\lambda \geq \sqrt{\frac{1}{D}[\frac{D}{R^2} + d_1 - \frac{r_b}{2}]}$, $0 < a_1 < u_2^+$ and $z \geq R\pi$. We define the function as follows:

$$\psi(x) = \begin{cases} a_1 e^{-\lambda(x+z)} \sin\left(\frac{x+z}{R}\right), & \text{for } 0 < \frac{x+z}{R} < \pi, \\ 0, & \text{otherwise.} \end{cases}$$

For $0 < \frac{x+z}{R} < \pi$, we show that $(\underline{u}, \underline{v}) = (\psi, \frac{\beta}{r_c}\psi)$ is a subsolution of (2.12), i.e., we show that

$$\begin{cases} -D\partial_{xx}\underline{u} - F_1(\underline{u}, \underline{v}) \leq 0, \\ -D\partial_{xx}\underline{v} - F_2(\underline{u}, \underline{v}) \leq 0. \end{cases} \tag{2.23}$$

Before showing (2.23), note that $\underline{u} = \psi$ and $\underline{v} = \frac{\beta}{r_c}\psi$ are positive, since $a_1 > 0$ and $0 < \frac{x+z}{R} < \pi$. Now, let us demonstrate system (2.23). Starting with the first equation, we have:

$$-D\partial_{xx}\underline{u} - F_1(\underline{u}, \underline{v}) = -D\partial_{xx}\underline{u} + J_1 + d_1\underline{u} - r_b\underline{u}(1 - \frac{\underline{u}}{b_i}),$$

with $J_1 = [-\gamma(1 - \frac{\underline{u}}{b_i}) + \frac{a\underline{u}}{s_b + \underline{u}}]\underline{v}$. Since $\gamma > a$, $s_b > b_i$ and $\underline{u} < \frac{b_i}{2}$, we have $J_1 < 0$, therefore

$$-D\partial_{xx}\underline{u} - F_1(\underline{u}, \underline{v}) \leq -D\partial_{xx}\underline{u} - r_b\underline{u}(1 - \frac{\underline{u}}{b_i}) + d_1\underline{u} \leq -D\partial_{xx}\underline{u} + [d_1 - \frac{r_b}{2}]\underline{u}.$$

Using the definition of $\underline{u}$, we write:

$$-D\partial_{xx}\underline{u} + [d_1 - \frac{r_b}{2}]\underline{u} = a_1 e^{-\lambda(x+z)} \sin\left(\frac{x+z}{R}\right)[-D\lambda^2 + \frac{D}{R^2} + d_1 - \frac{r_b}{2}].$$

Since $\lambda \geq \sqrt{\frac{1}{D}[\frac{D}{R^2} + d_1 - \frac{r_b}{2}]}$ and $a_1 > 0$, we can conclude that

$$-D\partial_{xx}\underline{u} - F_1(\underline{u}, \underline{v}) \leq -D\partial_{xx}\underline{u} + [d_1 - \frac{r_b}{2}]\underline{u} \leq 0,$$

Now, let's proceed to the second equation of the system. We have:

$$-D\partial_{xx}\underline{v} - F_2(\underline{u}, \underline{v}) = -D\partial_{xx}\underline{v} - \beta\underline{u} + r_c\underline{v} = -D\partial_{xx}\underline{u} - \beta\underline{u} + \beta\underline{u} = -D\partial_{xx}\underline{u}.$$

We previously showed that $-D\partial_{xx}\underline{u} \leq [\frac{r_b}{2} - d_1]\underline{u}$. Therefore,

$$-D\partial_{xx}\underline{v} - F_2(\underline{u}, \underline{v}) \leq [\frac{r_b}{2} - d_1]\underline{u}.$$

Since $d_1 > r_b$, thus

$$-D\partial_{xx}\underline{v} - F_2(\underline{u}, \underline{v}) \leq 0.$$

To prove that $(\underline{u}, \underline{v})(-\infty) = (0, 0)$ and $(\underline{u}, \underline{v})(0, 0) = (0, 0) \leq (u_2^+, v_2^+)$, we can refer to the definition of the function ψ. Thus, we have $(\underline{u}, \underline{v})(-\infty) = (0, 0)$ and $(\underline{u}, \underline{v})(0, 0) = (0, 0) \leq (u_2^+, v_2^+)$. □

2.6.2.4 Construction of a stationary solution

To establish the existence of a solution for the system represented by (2.12), we will first show that the subsolutions and supersolutions are ordered. Here are the supersolutions and subsolutions we have identified for equation (2.12):

$$\bar{u} = \begin{cases} u_2^+, & \text{on } (-\infty, 0), \\ u_2^+ e^{-\sqrt{\frac{1}{D}(-r_b-\gamma+d_2)}x}, & \text{on } (0, +\infty), \end{cases} \qquad \bar{v} = \begin{cases} v_2^+ = \frac{\beta u_2^+}{r_c}, & \text{on } (-\infty, 0), \\ \phi_1 - \phi_2, & \text{on } (0, +\infty). \end{cases}$$

$$\underline{u} = \begin{cases} \psi, & \text{on } (-\infty, 0), \\ 0, & \text{on } (0, +\infty), \end{cases} \qquad \underline{v} = \begin{cases} \frac{\beta}{r_c}\psi, & \text{on } (-\infty, 0), \\ 0, & \text{on } (0, +\infty). \end{cases}$$

On the interval $(-\infty, 0)$, we have $(0, 0) < (\underline{u}, \underline{v}) = (\psi, \frac{\beta}{r_c}\psi) < (\bar{u}, \bar{v}) = (u_2^+, v_2^+)$, given that $0 < a_1 < u_2^+$.
On the interval $(0, +\infty)$, we have $(\underline{u}, \underline{v}) = (0, 0)$ and $(\bar{u}, \bar{v}) = (\phi_1, \phi_1 - \phi_2)$. These satisfy the following properties:

$$\bar{v} - \underline{v} = (\phi_1 - \phi_2) - 0 = \phi_1 - \phi_2 > 0, \quad \textit{and} \quad \bar{u} - \underline{u} = \phi_1 > 0.$$

We can construct a solution for equation (2.12) using the above subsolution and supersolution. According to Lemma 18 and Lemma 19, we identify a well-ordered subsolution and supersolution. Application of the method of subsolution and supersolution (as described in subsection 1.1.2 of the Introduction chapter), we conclude that there exists a unique solution for (2.12). Moreover, according to Proposition 16, this solution is within the interval $[(\underline{u}, \underline{v}), (\bar{u}, \bar{v})]$.

2.6.3 Proof of Corollary 9

We would like to emphasize that Corollary 9 is proved using the results of Theorem 7 (existence of a stationary solution) and Proposition 5 (comparison principle). We show that our system admits a stationary solution by applying the method of subsolutions and supersolutions, satisfying the comparison principle as outlined in Proposition 5. According to this principle, if the initial positive solution is smaller than the stationary solution, then for all $t > 0$, the solution remains below the stationary solution.
By applying this principle to our model, we conclude that if the initial positive solution is smaller than the stationary solution, it can never reach or exceed the stationary solution. Indeed, the stationary solution acts as a barrier to propagation. The term 'blocking' is therefore justified because it describes the situation where the solution consistently remains below the stationary solution, thus confirming the phenomenon of propagation blocking.

2.7 Numerical simulations

2.7.1 Parameters estimations

In this section, we aim to estimate the values of the model parameters. Whenever possible, we will rely on values obtained from the article by [67]. However, in some cases, the exact values are unknown due to the difficulty of measuring them in vivo, or even in vitro.
We begin by estimating the bacterial reproduction rate, denoted by r_b. This parameter, expressed in u/min, represents the number of bacterial divisions per unit of time. Its estimation relies on experimental data from studies on bacterial growth, where the doubling time of E. coli is approximately 20 minutes under optimal conditions. According to Nadin et al. [67], for Crohn's disease, r_b is estimated as $3.47 \times 10^{-2}\, u$/min, based on the generation rate of E. coli under standard conditions (Korem et al. [55]). For our ulcerative colitis (UC) model, we choose $r_b = 0.02\, u$/min. This slightly lower value accounts for potential differences

in bacterial dynamics and interactions with the intestinal epithelium specific to UC, which influence the bacterial growth rate. The value of $r_b = 0.02$ complies with the constraints identified in our study for ulcerative colitis (UC). This estimation is therefore consistent with the observations and specific conditions of our model.
After estimating the rate of reproduction of the bacteria, we now focus on the mortality rate of phagocytes, denoted by r_c. Like r_b, this parameter is also expressed in u/min to ensure consistency with experimental data on immune cell turnover in an inflammatory environment. Its value is estimated at $10^{-4}\,u$/min, which corresponds to an average half-life of phagocytes of approximately two days. However, other studies suggest variations ranging from $10^{-3}\,u$/min in cases of severe inflammation to $10^{-6}\,u$/min in early stages of atherosclerosis. For Crohn's disease, a rate of $0.02\,u$/min is used, but this value does not apply to ulcerative colitis (UC). Indeed, the mechanisms involved in UC result in a mortality rate of $0.6258\,u$/min (see Table 2.1), which satisfies the conditions of our study. In our study, The parameter D, which represents diffusion, is used in a dimensionless form in our simulations. We consider the same value for immune cells and bacteria, assuming equivalent mobility in the studied environment. For our simulations, we set $D = 0.2$, ensuring a consistent interpretation of the numerical results.
The bacterial density in the intestinal lumen is approximately $b_i = 10^{15}\,u/m^3$. At the positive equilibrium (u, v), which corresponds to an inflammatory phase, we estimate that about 30% of this density can cross the epithelial barrier. Therefore, we set $u = 0.3 \times b_i$. Experimental data suggest that, in the affected area, the density of immune cells is about ten times lower than that of bacteria, which is consistent with the larger size of phagocytes compared to bacteria. We therefore assume $\kappa = \frac{1}{10}$, which implies that $u = 10v$ and consequently, $v = 3 \times 10^{-2} \times b_i$. For the model of ulcerative colitis (UC), we consider that the immune response rate, represented by β, is less than $10^{-1}\,r_c$. This decision is based on the fact that in UC, the immune response is generally less aggressive and more regulated compared to other inflammatory states. Thus, the parameter β, which represents the rate of immune response mobilizing cells to combat bacteria in damaged areas, is adjusted to be less than $10^{-1}\,r_c$. This reflects a more moderate response and stricter regulation of the immune response compared to the immune cell death rate r_c. This approach better models the balance between bacterial growth and the immune response specific to UC.
The value of γ is calculated in such a way that it satisfies the conditions of our study.

2.7.2 Numerical results

We conduct numerical simulations of the mathematical model that describes the interaction between bacteria and phagocytes (immune cells) to illustrate our theoretical results. We use the parameter values shown in Table 2.1 below, which are estimated in the previous section.

Parameters	Interpretations	Values	Units
r_b	Reproduction rate of bacteria	0.02	(u/min)
b_i	maximum bacterial density	10^{15}	(u/m^3)
γ	Related to the porosity of the epithelium	0.0856	(u/min)
a	coefficient proportional to the rate of phagocytosis	0.0347	(u/min)
s_b	Proportionality coefficient between p_c and a	10^{16}	(u/m^3)
d	mortality rate	0.030	(u/min)
β	immune response rate	0.3129	(u/min)
r_c	intrinsic death rate of phagocytes	0.6258	(u/min)

Table 2.1: Specified parameter values for the model.

After satisfying the conditions stated in Theorem 3.1 with the given parameter values, we proceed to perform numerical simulations of system (2.1) in a one-dimensional space with a diffusion constant $D = 0.2$. The simulation covers a time period from $t = 0$ to $T = 600$ seconds, using the initial conditions $\left(u_2^+, v_2^+\right)$. The numerical domain spans the interval $[-50, 50]$, corresponding to a total length of $2L = 100$ cm. This choice is biologically relevant as it approximates the average length of the human colon. Thus, the domain can be interpreted as a simplified representation of a significant portion of the colon where inflammatory phenomena occur. It was discretized using a semi-implicit finite difference scheme with $J = 1000$ points and a spatial step size of $dx = \frac{2L}{J}$. The scheme treated the right-hand side implicitly. For the simulations, we used a time step of $dt = 0.7$ seconds. To ensure appropriate boundary conditions in the numerical domain, Neumann boundary conditions were imposed at the boundaries. This was necessary as we were dealing with a bounded domain for numerical purposes. Finally, we present in the following the simulation results that visually illustrate the temporal propagation of bacteria and immune cells, as shown in Figure 2.6 and Figure 2.8, along with the corresponding space-time dynamics in Figures 2.7 and 2.9.

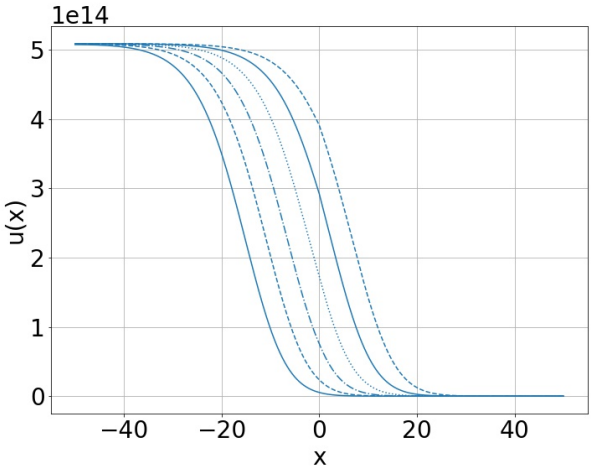

Figure 2.6: Bacterial propagation at constant speed in a homogeneous medium over time.

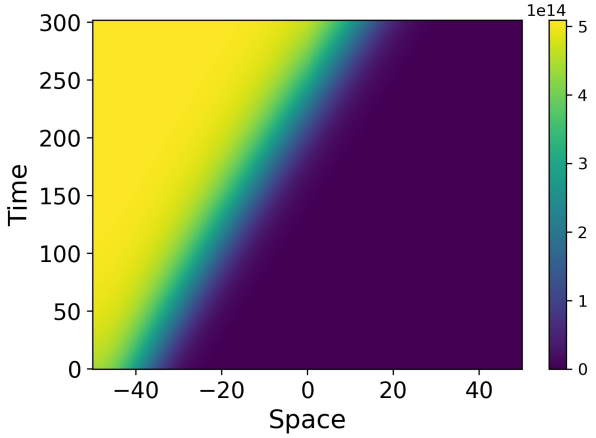

Figure 2.7: Spatiotemporal Dynamics of Bacterial Propagation.

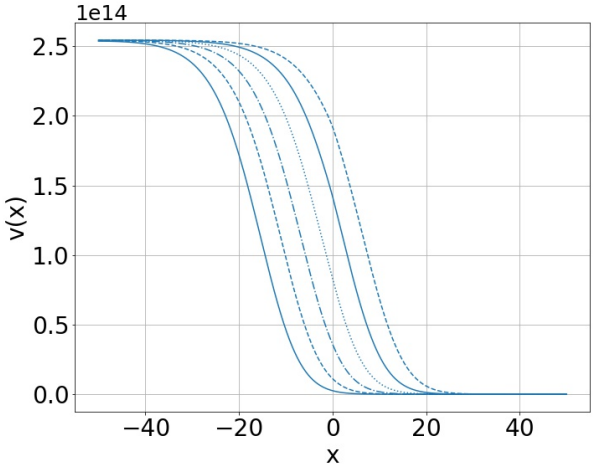

Figure 2.8: ropagation of immune cell at constant speed in a homogeneous medium over time.

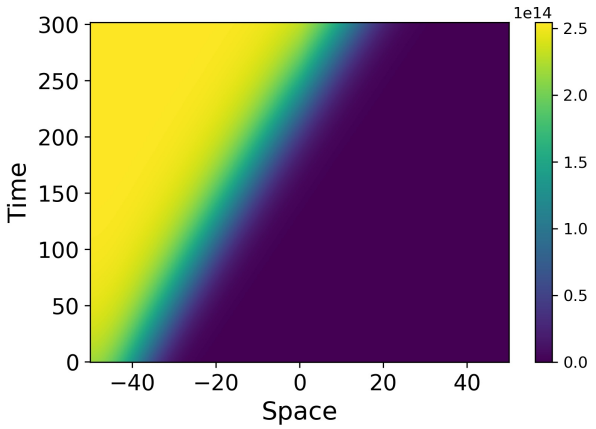

Figure 2.9: Spatiotemporal Dynamics of Immune Cell Propagation.

In the second simulation, we aim to explore the behavior of the system under different conditions, specifically focusing on the blocking of propagation. To achieve this, we extend the final time to 1500 seconds and introduce changes to the value of d at specific spatial points. These modifications are designed to impede the spread of bacteria and immune cells in those particular areas. we define a customized d function to reflect these alterations:

$$d\left(x\right) = \begin{cases} 0.030, & if \quad x \leq 0, \\ 0.1065, & if \quad x > 0. \end{cases}$$

By implementing this modified function d and running the simulation, we observe significant differences in propagation patterns compared to the previous simulation. The results of this simulation, which illustrate the blocked propagation in the specified regions, are presented in the subsequent images.

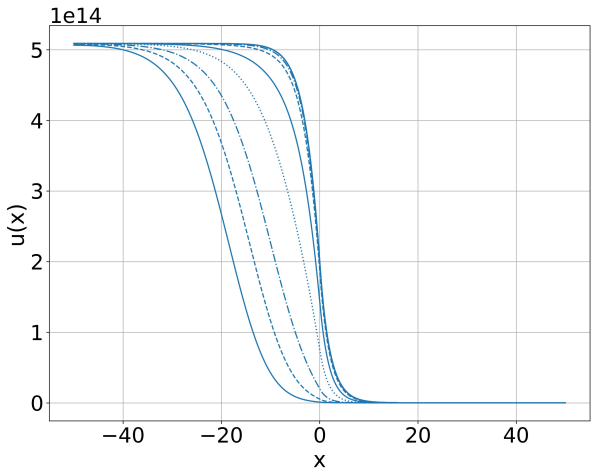

Figure 2.10: Initial spread followed by blockage over time: bacterial dynamics.

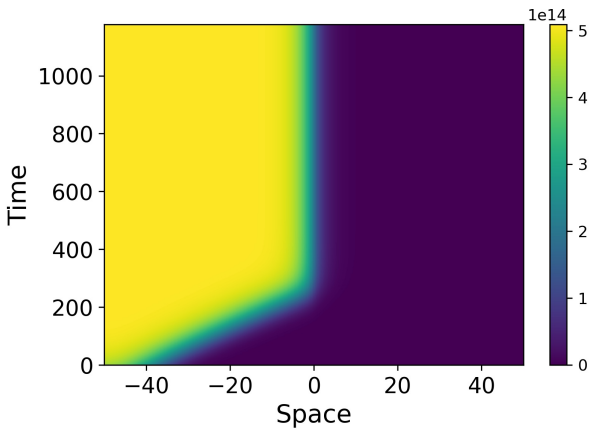

Figure 2.11: Spatiotemporal Dynamics of Bacterial Spread and Blockage.

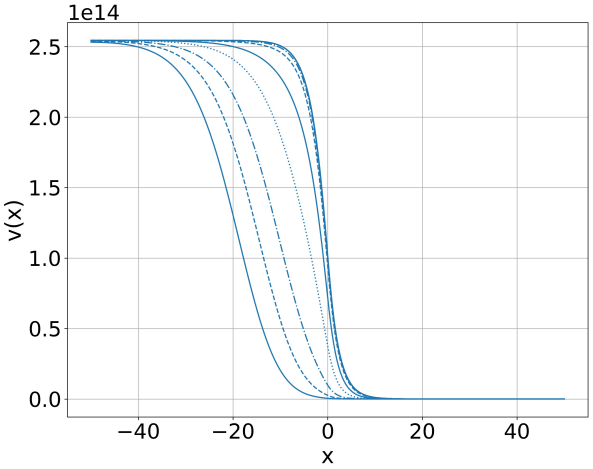

Figure 2.12: Initial Spread Followed by Blockage Over Time: Immune Cell Dynamics.

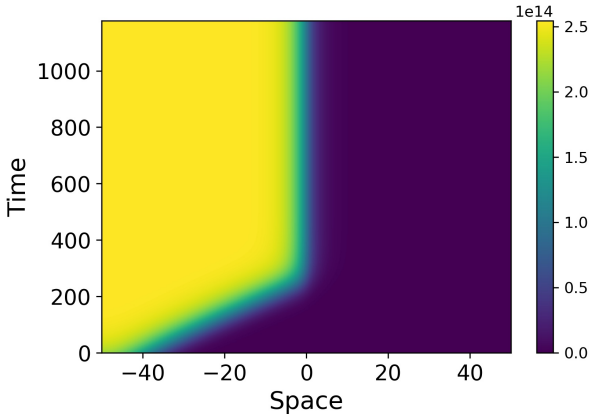

Figure 2.13: Spatiotemporal Dynamics of Immune Cell Spread and Blockage.

2.8 Biological interpretation

In this section, we will biologically interpret the results obtained in our model of wave propagation in a homogeneous medium, as well as the resulting blocking phenomenon in a heterogeneous medium. First, we analyze the propagation of waves in a homogeneous medium. This result has a deep meaning in the biological context, suggesting that homogeneous wave propagation corresponds to uniform diffusion of inflammation throughout the colon. More specifically, in the context of inflammatory bowel diseases such as ulcerative colitis, this model can be interpreted as a mathematical representation of the overall extension of inflammation along the colonic mucosa, thus characterizing pancolitis where the entire colon is affected by inflammation. According to statistics, after 20 years, about 50% patients have cumulative pancolitis [22]. When inflammation spreads evenly, it means that the entire surface of the colon is affected by the disease in the same way, leading to widespread symptoms and impaired bowel function. This interpretation reinforces the importance of holistically treating the disease, targeting not only symptomatic domains but also areas where inflammation is present subclinically, in order to effectively control disease progression and improve the quality of life of patients.

Having explored in detail the homogeneous propagation of waves and its biological corollary, namely the uniform diffusion of inflammation throughout the colon, we now examine the second result of our study: the blocking phenomenon observed in heterogeneous environments. In this configuration, we introduce variability into the model by modifying the mortality coefficient of bacteria. This change leads to a significant alteration in inflammation spread. Where previously the spread is uniform, we now see a progressive blockage. This observation is consistent with clinical findings, in which doctors often report that certain areas of the colon of patients with inflammatory bowel diseases, such as ulcerative colitis, may exhibit localized areas of blockage, leading to resistance to the progression of inflammation. Until now, stopping the spread of the disease in the colon remains inexplicable and cannot be effectively identified by the video obtained after a colonoscopy. More studies are needed to identify the end point of inflammation. In conclusion, our results highlight the crucial role of bacterial mortality in the spread of inflammation. Although constant rates of spread are observed in a homogeneous environment, local variations in this term can result in a blockage of the

progression of inflammation in specific regions of the colon. This observation highlights the important role that interactions between bacteria and local inflammatory processes play in the progression of the disease.

2.9 Conclusion

This work is a simplified approach to modeling the inflammatory response in ulcerative colitis (UC). We make several assumptions to gain a general understanding of the mechanisms of disease spread and blockage, while keeping the model relatively simple in terms of variables and equations. In future research, it is useful to explore the stability of the stationary solution and study how it depends on different parameters. Furthermore, expanding the model to include more factors, such as additional interacting species, can provide a more complete understanding of the complex dynamics involved in the spread and control of inflammatory diseases.

Part II

Analysis of Reduced Models and Wave Blocking in Population Dynamics

Abstract

The results presented in this chapter are the result of a collaboration with Nicolas Vauchelet and Hatem Zaag and are currently being prepared for submission.

To control mosquito-borne diseases such as dengue, for which no effective vaccine is available, several strategies focus on targeting mosquito populations. One such approach involves introducing Wolbachia, a symbiotic bacterium that blocks pathogen transmission, into the mosquito population. A mathematical model describing the introduction of Wolbachia and the subsequent population replacement has demonstrated that, in a homogeneous environment, spatial propagation occurs.

The objective of this part is to prove the blocking of this propagation in a heterogeneous environment. To achieve this goal, we divide this part into two chapters:

The first chapter focuses on the reduction of a 2×2 reaction-diffusion system to a single closed equation, providing a simplified framework for studying the dynamics of Wolbachia propagation.

The second chapter investigates the study of wave blocking in a population replacement technique, where we examine scenarios in which environmental heterogeneity, particularly spatial variations in carrying capacity, may prevent the spread of Wolbachia.

CHAPTER 3

REDUCTION OF A 2×2 REACTION-DIFFUSION SYSTEM TO A SINGLE CLOSED EQUATION

"Nothing in life is to be feared. It is only to be understood."

Marie Curie

3.1 Introduction

We study the dynamics of two biological populations belonging to the same species, which move, reproduce, and compete. Their evolution is described by a reaction-diffusion system with two equations posed in the space $\mathbb{R}^d$ with $d \geq 1$. The reaction terms, generally nonlinear, represent the interactions between these populations, including competition or mutualism effects.

Let $n_1(t,x)$ and $n_2(t,x)$ denote the respective densities of the two variants at time $t > 0$ and position $x \in \mathbb{R}^d$. The model is given by:

$$\begin{cases} \partial_t n_1 - \Delta n_1 = n_1 f_1(n_1, n_2), \\ \partial_t n_2 - \Delta n_2 = n_2 f_2(n_1, n_2). \end{cases} \tag{3.1}$$

The functions f_1 and f_2 model these interactions and are accompanied by initial conditions.

Directly studying such a system is often complex. An alternative approach is to analyze the proportion of one population relative to the total population, defined as:

$$p = \frac{n_1}{n_1 + n_2}.$$

In this framework, it is possible to show that the evolution of p is governed by a reaction-diffusion equation of the form:

$$\partial_t p - \Delta p = pF(p). \tag{3.2}$$

Since the pioneering works of Fisher [32] and Kolmogorov, Petrovskii, and Piskunov [54], such equations have been widely studied in mathematics, particularly concerning the existence of traveling waves and invasion phenomena (see [91]). However, the analysis of competitive reaction-diffusion systems remains challenging and introduces additional difficulties, as illustrated in [35]. This chapter aims to establish a rigorous link between systems (3.1) and

(3.2). More precisely, we seek to determine whether the solutions of system (3.1) can approximate those of system (3.2) for the proportion p. Our main result shows that, under certain assumptions on the reaction terms in (3.1), the proportion

$$p = \frac{n_1}{n_1 + n_2}, \tag{3.3}$$

remains close, in a precise sense, to a solution of (3.2). Specifically, we prove that when the total population becomes large and competition intensifies, the frequency p associated with system (3.1) converges to the solution of equation (3.2), where the nonlinear function F is explicitly derived from f_1 and f_2. The proof relies on a compactness argument based on a priori estimates.

Similar results have been obtained for the reduction of competition-diffusion models in [41] and [40], particularly in bounded domains with a detailed study of boundary conditions.

One of the main motivations for this study arises from the phenomenon of cytoplasmic incompatibility, induced by the endosymbiotic bacterium Wolbachia in certain arthropod species (see [96], [13]). These bacteria are of increasing interest due to their potential as a tool for controlling arboviruses (see [44], [92]). This biological phenomenon can be modeled by a reaction-diffusion system, and we show that if the reaction terms are properly adjusted, then the frequency of Wolbachia infection converges to the solution of a closed reaction-diffusion equation, which is bistable. Such equations have long been proposed to describe this phenomenon (see [80]).

3.2 Modelling

Let $T > 0$ denote a fixed horizon of time.

3.2.1 Model with two compartments

The model for infected and non-infected mosquitoes proposed in [84] can, in a certain sense, be used to derive a two-population model posed on $\mathbb{R}^d$. In this model, n_i represents the density of infected mosquitoes, and n_u represents the density of non-infected mosquitoes. The model is described by the following equations:

$$\begin{cases} \partial_t n_i - \Delta n_i = (1 - s_f) F_u n_i (1 - \frac{n_i + n_u}{K}) - \delta d_u n_i, & in \ \ (0,T) \times \mathbb{R}^d, \\ \partial_t n_u - \Delta n_u = F_u n_u (1 - s_h \frac{n_i}{n_i + n_u})(1 - \frac{n_i + n_u}{K}) - d_u n_u, & in \ \ (0,T) \times \mathbb{R}^d. \end{cases} \tag{3.4}$$

Complemented by initial conditions $n_i(t = 0, x) = n_i(x)^{init} \geq 0$, $n_u(t = 0, x) = n_u(x)^{init} > 0$. The parameters in the model are defined as follows:

- $\star$ d_u, $d_i = \delta d_u$ with $\delta > 1$ represent the death rates for uninfected and infected mosquitoes, respectively. We assume that $d_i > d_u$ because Wolbachia shortens their lifespan;
- $\star$ $s_f \in (0, 1)$ is a dimensionless parameter that reflects the reduced fecundity of infected mosquitoes;
- $\star$ F_u, $F_i = (1 - s_f) F_u$ denote the fecundity rates for uninfected and infected mosquitoes, respectively. We assume that $F_i < F_u$, as Wolbachia reduces fecundity;
- $\star$ $s_h \in (0, 1)$ is the cytoplasmic incompatibility parameter, representing the fraction of eggs from uninfected females fertilized by infected males that do not hatch. In other words, a proportion $1 - s_h$ of the eggs fertilized by infected males actually hatch. Cytoplasmic incompatibility is perfect when $s_h = 1$;

⋆ K denotes the environmental capacity.

All the constants mentioned previously are assumed to be positive. In the literature related to this model, one can find analyses of equilibrium states and their stability. Moreover, the existence and uniqueness of solutions for such a reaction–diffusion system are by now well-known; see, e.g.,[30, 71]. The equations governing the dynamics of n_i and n_u are respectively bistable and monostable reaction-diffusion equations. It is worth noting that in the reaction term of the second equation, the term $-\frac{n_i}{n_i+n_u}$ represents the vertical transmission of the disease, while the coefficient s_h models the imperfection of this transmission due to cytoplasmic incompatibility. In accordance with [6], we will assume moreover that the relation

$$s_f + \delta - 1 < s_h\delta \tag{3.5}$$

holds true. This choice of parameters is relevant, as for Wolbachia-infected Aedes mosquitoes, and more specifically in the case of the `wMel` strain, cytoplasmic incompatibility (CI) is nearly perfect for this species-strain combination (see [26]), implying that s_h is close to 1. Furthermore, these mosquitoes typically have slightly reduced fecundity, which is represented by $s_f \approx 0.1$. In addition, the parameters δ and s_h take the values $\delta \approx 1.1$ and $s_h \approx 0.9$, ensuring the validity of equation (3.5).

3.2.2 Reduction for large fecundity

We assume high fecundity, as described in [84], and introduce a small parameter $\epsilon \ll 1$ such that $F_u = \frac{\tilde{F_u}}{\epsilon}$. When fecundity becomes dominant compared to the other parameters, it is relevant to consider the asymptotic regime $\epsilon \to 0$ in order to simplify the equations of the system (3.4). This reduction method is inspired by [6], where the authors explore a differentiable system. In this section, we elaborate on the reduction procedure of this system in detail. Since n_i and n_u will depend on ϵ, we use the notation n_i^ϵ and n_u^ϵ. Before we begin rigorous reasoning, we use the following assumptions:

Assumptions 20.

1- K *in* $C^2(\mathbb{R}^d)$.

2- $K \in L^\infty(\mathbb{R}^d)$.

3- K *is bounded from below, i.e., there exists* $c' > 0$ *such that* $K > c'$, *for all* $x \in \mathbb{R}^d$.

4- $\nabla K \in L^2(\mathbb{R}^d)$ *and* $\Delta K \in L^1(\mathbb{R}^d)$.

Formal reasoning: we introduce the total population as $N^\epsilon = n_i^\epsilon + n_u^\epsilon$ and the fraction of infected mosquitoes as $p^\epsilon = \frac{n_i^\epsilon}{n_i^\epsilon+n_u^\epsilon}$. After straightforward computations from (3.4), we obtain the system

$$\begin{aligned}\partial_t N^\epsilon - \Delta N^\epsilon = N^\epsilon\Bigg(&F_u(1-\frac{N^\epsilon}{K})((1-s_f)p^\epsilon + (1-p^\epsilon)(1-s_hp^\epsilon)) \\ &- d_u(\delta p^\epsilon + 1 - p^\epsilon)\Bigg).\end{aligned} \tag{3.6}$$

$$\partial_t p^\epsilon - \Delta p^\epsilon - 2\frac{\nabla p^\epsilon \nabla N^\epsilon}{N^\epsilon} = p^\epsilon(1-p^\epsilon)\left(F_u(1-\frac{N^\epsilon}{K})(s_hp^\epsilon - s_f) + d_u(1-\delta)\right). \tag{3.7}$$

We can therefore reformulate equation (3.6) as:

$$\partial_t N^\epsilon - \Delta N^\epsilon = N^\epsilon \Bigg(\frac{\tilde{F}_u}{\epsilon}(1 - \frac{N^\epsilon}{K})((1-s_f)p^\epsilon + (1-p^\epsilon)(1-s_h p^\epsilon)) \\ - d_u(\delta p^\epsilon + 1 - p^\epsilon) \Bigg). \tag{3.8}$$

We expect that, as $\epsilon \to 0$, we have $N^\epsilon(t,x) = K(x)(1 + O(\epsilon))$. Then we introduce an expansion

$$N^\epsilon(t,x) = K(x)(1 - \epsilon z^\epsilon(t,x)).$$

Equating the leading terms in (3.8) yields

$$z^\epsilon(t,x) = \frac{d_u[(\delta-1)p^\epsilon(t,x) + 1] - \frac{\Delta K(x)}{K(x)}}{\tilde{F_u}((1-s_f)p^\epsilon(t,x) + (1-p^\epsilon(t,x))(1-s_h p^\epsilon(t,x)))}.$$

In subsection 3.4.1, we show that z^ϵ is uniformly bounded with respect to ϵ. Equation (3.7) then rewrites

$$\begin{aligned} &\partial_t p^\epsilon - \Delta p^\epsilon - 2\frac{\nabla K}{K}\nabla p^\epsilon - 2\nabla p^\epsilon \nabla \ln(1 - \epsilon z^\epsilon) \\ &= p^\epsilon(1-p^\epsilon)\left((s_h p^\epsilon - s_f) \frac{d_u\left((\delta-1)p^\epsilon + 1\right) - \frac{\Delta K}{K}}{(1-s_f)p^\epsilon + (1-p^\epsilon)(1-s_h p^\epsilon)} - d_u(\delta - 1) \right), \end{aligned}$$

which is equivalent to

$$\partial_t p^\epsilon - \Delta p^\epsilon - 2\frac{\nabla K}{K}\nabla p^\epsilon - 2\nabla p^\epsilon \nabla \ln(1 - \epsilon z^\epsilon) = f(p^\epsilon) + \frac{\Delta K}{K} g(p^\epsilon), \tag{3.9}$$

where

$$f(p^\epsilon) = p^\epsilon(1-p^\epsilon)\left[\frac{d_u(\delta s_h p^\epsilon - s_f + 1 - \delta)}{(1-s_f)p^\epsilon + (1-p^\epsilon)(1-s_h p^\epsilon)} \right],$$

and

$$g(p^\epsilon) = \frac{-p^\epsilon(1-p^\epsilon)(s_h p^\epsilon - s_f)}{(1-s_f)p^\epsilon + (1-p^\epsilon)(1-s_h p^\epsilon)}.$$

Before stating the convergence theorem, we will make a remark on the property of bistability:

Remark 4. *The function f is continuous and Lipschitz, with $f(0) = f(1) = f(\theta_1) = 0$. Furthermore, $f < 0$ on the interval $(0, \theta_1)$ and $f > 0$ on $(\theta_1, 1)$, where $\theta_1 = \frac{(\delta-1)+s_f}{s_h \delta} \in (0,1)$, under the condition $(\delta - 1) + s_f < s_h \delta$.*

Assumptions 21.

We assume that the initial conditions satisfy:

$$n_i^{init,\epsilon} \text{ is uniformly bounded in } L^\infty(\mathbb{R}^d), \quad n_i^{init,\epsilon} \geq 0, \tag{3.10}$$

$$n_u^{init,\epsilon} \text{ is uniformly bounded in } L^\infty(\mathbb{R}^d), \quad n_u^{init,\epsilon} > 0, \tag{3.11}$$

$$\text{and } p^{init} \in L^2(\mathbb{R}^d), \quad p^{init,\epsilon} = \frac{n_i^{init,\epsilon}}{n_i^{init,\epsilon} + n_u^{init,\epsilon}} \xrightarrow{\epsilon \to 0} p^{init,0} = \frac{n_i^{init,0}}{n_i^{init,0} + n_u^{init,0}} \text{ weakly in } L^2(\mathbb{R}^d). \tag{3.12}$$

Furthermore, we assume that the initial conditions are well-prepared, which means:

$$n_i^{init,\epsilon} + n_u^{init,\epsilon} = K + \epsilon K_0^\epsilon, \quad \text{with } \|K_0^\epsilon\|_\infty \leq C'. \tag{3.13}$$

3.3 Main result

We are now able to present our main result, namely the the reduction of system (3.6)-(3.7) to the scalar equation (3.9) as $\epsilon \to 0$. This result extends the one presented in [84], where the carrying capacity is assumed to be constant.

Theorem 8.
Let $T > 0$. Under Assumptions 20 and 21, as $\epsilon \to 0$, we have $p^\epsilon := \frac{n_i^\epsilon}{n_i^\epsilon + n_u^\epsilon} \to p^0$ strongly in $L^2(0,T,L^2(\mathbb{R}^d))$, weakly in $L^2(0,T,H^1(\mathbb{R}^d))$ where p^0 is the unique solution of

$$\begin{cases} \partial_t p^0 - \Delta p^0 - 2\frac{\nabla K}{K}\nabla p^0 = f(p^0) + \frac{\Delta K}{K} g(p^0), & in \quad (0,T)\times\mathbb{R}^d, \\ p^0(t=0,x) = p^{init}(x), & in \quad \mathbb{R}^d, \end{cases} \tag{3.14}$$

with

$$f(p^0) = p^0(1-p^0)\left[\frac{d_u(\delta s_h p^0 - s_f + 1 - \delta)}{(1-s_f)p^0 + (1-p^0)(1-s_h p^0)}\right],$$

and

$$g(p^0) = \frac{-p^0(1-p^0)(s_h p^0 - s_f)}{(1-s_f)p^0 + (1-p^0)(1-s_h p^0)}.$$

3.4 Proof of convergence

In this section, we provide a proof of Theorem 8, which enables us to reduce the system (3.4) to a scalar reaction-diffusion equation for the proportion as the parameter ϵ tends to 0. This approach is inspired by [6], where the authors employ a model consisting of two differential equations. First, we present the system of equations that is satisfied by (N^ϵ, p^ϵ)

$$\begin{cases} \partial_t N^\epsilon - \Delta N^\epsilon = N^\epsilon[\frac{\tilde{F}_u}{\epsilon}(1-\frac{N^\epsilon}{K})((1-s_f)p^\epsilon + (1-p^\epsilon)(1-s_h p^\epsilon)) \\ \qquad\qquad -d_u(\delta p^\epsilon + 1 - p^\epsilon)], \\ \partial_t p^\epsilon - \Delta p^\epsilon - 2\frac{\nabla K}{K}\nabla p^\epsilon - 2\nabla p^\epsilon \nabla \ln(1-\epsilon z^\epsilon) = f(p^\epsilon) + \frac{\Delta K}{K} g(p^\epsilon), \\ N^\epsilon(t=0) = N^{init,\epsilon},\ p^\epsilon(t=0) = p^{init,\epsilon}. \end{cases}$$

Where

$$f(p^\epsilon) = p^\epsilon(1-p^\epsilon)\left[\frac{d_u(\delta s_h p^\epsilon - s_f + 1 - \delta)}{(1-s_f)p^\epsilon + (1-p^\epsilon)(1-s_h p^\epsilon)}\right],$$

and

$$g(p^\epsilon) = \frac{-p^\epsilon(1-p^\epsilon)(s_h p^\epsilon - s_f)}{(1-s_f)p^\epsilon + (1-p^\epsilon)(1-s_h p^\epsilon)}.$$

3.4.1 Uniform a priori estimates

We initially establish some uniform bounds with respect to $\epsilon > 0$.
Before starting with the first lemma which demonstrates that z^ϵ is uniformly bounded with respect to ϵ, we introduce the following system of equations, which is used to demonstrate this property. We have $N^\epsilon = K(x)(1-\epsilon z^\epsilon(t,x))$ and $p^\epsilon = \frac{n_i^\epsilon}{n_i^\epsilon + n_u^\epsilon}$.

Let us replace N^ϵ with its expression in equation (3.6), and then, from straightforward computations, we get

$$\begin{aligned}
&\partial_t z^\epsilon - \Delta z^\epsilon - 2\frac{\nabla K}{K}\nabla z^\epsilon \qquad (3.15)\\
&= -\frac{(1-\epsilon z^\epsilon(t,x))}{\epsilon}\left(\frac{\tilde{F}_u}{\epsilon}(1-\frac{N^\epsilon}{K})((1-s_f)p^\epsilon + (1-p^\epsilon)(1-s_h p^\epsilon))\right)\\
&\quad - \frac{(1-\epsilon z^\epsilon(t,x))}{\epsilon}\left(-d_u(\delta p^\epsilon + 1 - p^\epsilon)\right) - \frac{(1-\epsilon z^\epsilon)}{\epsilon}\frac{\Delta K}{K}.
\end{aligned}$$

Lemma 22.

Assume that the assumptions of Theorem 8 hold, and let (z^ϵ, p^ϵ) be the unique solution of system (3.15)-(3.9). Then z^ϵ is uniformly bounded with respect to ϵ, and $0 \le p^\epsilon \le 1$ on $[0,T]\times\mathbb{R}^d$.

Proof.

By nonnegativity of $n_i^{\text{init},\epsilon}$ and $n_u^{\text{init},\epsilon}$, it is standard to deduce the nonnegativity of n_i^ϵ and n_u^ϵ (Indeed 0 is a subsolution for (3.4)). Moreover, since $\mathbb{R}^+$ is invariant for the equation of n_u^ϵ and $n_u^{\text{init},\epsilon} > 0$, we deduce that $n_u^\epsilon > 0$ on $[0,T]\times\mathbb{R}^d$. Therefore, p^ϵ is well-defined on $[0,T]\times\mathbb{R}^d$ and satisfies by definition $0 \le p^\epsilon \le 1$ on $[0,T]\times\mathbb{R}^d$.

Consider the function h defined as $h(p) = \frac{d_u(\delta p+1-p)}{\tilde{F}_u((1-s_f)p+(1-p)(1-s_h p))}$. We remark that the denominator is positive, since $p\in[0,1]$. Let

$$\tilde{K} = \max\{\max_{p\in[0,1]}(h(p) - \frac{\min\frac{\Delta K}{K}}{\tilde{F}_u((1-s_f)p+(1-p)(1-s_h p))}), \|z^{init,\epsilon}\|_\infty\}.$$

Let ϵ_0 be such that $\tilde{K} \le \frac{1}{\epsilon_0}$ ($\Leftrightarrow 1-\epsilon_0\tilde{K} \ge 0$), then, thanks to this choice we have for $0<\epsilon\le\epsilon_0$:

$$\begin{aligned}
&-\frac{(1-\epsilon\tilde{K})}{\epsilon}(\tilde{F}_u\tilde{K}((1-s_f)p^\epsilon + (1-p^\epsilon)(1-s_h p^\epsilon)) - d_u(\delta p^\epsilon + 1 - p^\epsilon)) - \frac{(1-\epsilon\tilde{K})}{\epsilon}\frac{\Delta K}{K}\\
&= -\frac{(1-\epsilon\tilde{K})}{\epsilon}(\tilde{F}_u[((1-s_f)p^\epsilon + (1-p^\epsilon)(1-s_h p^\epsilon))][\tilde{K} - h(p^\epsilon)] + \frac{\Delta K}{K}).
\end{aligned}$$

According to the definition of $\tilde{K}$, we have

$$\begin{aligned}
&-\frac{(1-\epsilon\tilde{K})}{\epsilon}(\tilde{F}_u[((1-s_f)p^\epsilon + (1-p^\epsilon)(1-s_h p^\epsilon))][\tilde{K} - h(p^\epsilon)] + \frac{\Delta K}{K})\\
&\le 0 = \partial_t\tilde{K} - \Delta\tilde{K} - 2\frac{\nabla K}{K}\nabla\tilde{K}.
\end{aligned}$$

Hence, we have that $\tilde{K}$ is a super-solution for (3.15) for any $0<\epsilon\le\epsilon_0$. Then $z^\epsilon \le \tilde{K}$ for any $0<\epsilon\le\epsilon_0$.

By the same token, we have that the negative constant

$$\underset{\sim}{K} = \min\{\min_{p\in[0,1]}(h(p) - \frac{\max\frac{\Delta K}{K}}{\tilde{F}_u\Big((1-s_f)p+(1-p)(1-s_h p)\Big)}), -\|z^{\text{init},\epsilon}\|_\infty\}$$

is a sub-solution for (3.15). Indeed, Let ϵ_0 be such that $\underset{\sim}{K} \le \frac{1}{\epsilon_0}$ ($\Leftrightarrow 1-\epsilon_0\underset{\sim}{K} \ge 0$), then, thanks to this choice we have for $0<\epsilon\le\epsilon_0$:

$$-\frac{(1-\epsilon\underset{\sim}{K})}{\epsilon}\Big[\tilde{F}_u\underset{\sim}{K}\Big((1-s_f)p^\epsilon+(1-p^\epsilon)(1-s_hp^\epsilon)\Big)-d_u(\delta p^\epsilon+1-p^\epsilon)\Big]-\frac{(1-\epsilon\underset{\sim}{K})}{\epsilon}\frac{\Delta K}{K}$$

$$=-\frac{(1-\epsilon\underset{\sim}{K})}{\epsilon}\bigg(\tilde{F}_u\Big[(1-s_f)p^\epsilon+(1-p^\epsilon)(1-s_hp^\epsilon)\Big]\Big[\underset{\sim}{K}-h(p^\epsilon)\Big]+\frac{\Delta K}{K}\bigg).$$

According to the definition of $\underset{\sim}{K}$, we have:

$$-\frac{(1-\epsilon\underset{\sim}{K})}{\epsilon}\bigg(\tilde{F}_u\Big[(1-s_f)p^\epsilon+(1-p^\epsilon)(1-s_hp^\epsilon)\Big]\Big[\underset{\sim}{K}-h(p^\epsilon)\Big]+\frac{\Delta K}{K}\bigg)$$
$$\geq 0=\partial_t\underset{\sim}{K}-\Delta\underset{\sim}{K}-2\frac{\nabla K}{K}\nabla\underset{\sim}{K}.$$

Hence, we conclude that $\underset{\sim}{K}$ is a sub-solution for (3.15). Thus, z^ϵ is uniformly bounded from below by $\underset{\sim}{K}$. We therefore deduce the uniform bound of z^ϵ. □

Lemma 23.

We assume that Assumptions 20 holds. Let (z^ϵ,p^ϵ) represent the unique solution of the equations (3.15)-(3.9)*. For any sufficiently small $\epsilon>0$, the following uniform estimate holds:*

$$\epsilon\int_0^T\int_{\mathbb{R}^d}|\nabla z^\epsilon|^2dxdt\leq S_1 \tag{3.16}$$

$$\int_0^T\int_{\mathbb{R}^d}|\nabla p^\epsilon|^2dxdt\leq S_2 \tag{3.17}$$

for some positive constant S_k, $k=1,2$.

Proof. We begin by demonstrating the following estimate:

$$\epsilon\int_0^T\int_{\mathbb{R}^d}|\nabla z^\epsilon|^2dxdt\leq S_1.$$

We multiply equation (3.15) by z^ϵ and integrate it over $\mathbb{R}^d$, to get

$$\begin{aligned}&\frac{\epsilon}{2}\frac{d}{dt}\int_{\mathbb{R}^d}(z^\epsilon)^2dx+\epsilon\int_{\mathbb{R}^d}|\nabla z^\epsilon|^2dx\\&\leq\int_{\mathbb{R}^d}|[z^\epsilon(1-\epsilon z^\epsilon(t,x))[\tilde{F}_uz^\epsilon((1-s_f)p^\epsilon+(1-p^\epsilon)(1-s_hp^\epsilon))-d_u(\delta p^\epsilon+1-p^\epsilon)]\\&\qquad+z^\epsilon(1-\epsilon z^\epsilon)\frac{\Delta K}{K}]|dx+2\epsilon\int_{\mathbb{R}^d}|z^\epsilon||\frac{\nabla K}{K}||\nabla z^\epsilon|dx.\end{aligned}$$

We have proved that z^ϵ and p^ϵ are uniformly bounded, and under Assumptions 20, there exist two positive constants S_3 and S_4 such that

$$\frac{\epsilon}{2}\frac{d}{dt}\int_{\mathbb{R}^d}(z^\epsilon)^2dx+\epsilon\int_{\mathbb{R}^d}|\nabla z^\epsilon|^2dx\leq S_3+2S_4\epsilon\int_{\mathbb{R}^d}|\nabla K||\nabla z^\epsilon|dx.$$

Using a Cauchy-Schwarz inequality and a Young inequality, we deduce

$$\frac{\epsilon}{2}\frac{d}{dt}\int_{\mathbb{R}^d}(z^\epsilon)^2dx+(\frac{3\epsilon}{4})\int_{\mathbb{R}^d}|\nabla z^\epsilon|^2dx\leq S_5.$$

We obtain (3.16) through time integration.

Before proving estimation (3.17), we show that $\int_0^T \int_{\mathbb{R}^d} |\nabla \ln(1-\epsilon z^\epsilon)|^2 dxdt$ approaches 0 as ϵ tends to 0. We have

$$\int_0^T \int_{\mathbb{R}^d} |\nabla \ln(1-\epsilon z^\epsilon)|^2 dxdt = \epsilon^2 \int_0^T \int_{\mathbb{R}^d} \frac{|\nabla z^\epsilon|^2}{|1-\epsilon z^\epsilon|^2} dxdt.$$

Since z^ϵ is bounded, there exists a constant S_6 such that,

$$\int_0^T \int_{\mathbb{R}^d} |\nabla \ln(1-\epsilon z^\epsilon)|^2 dxdt \leq \epsilon^2 S_6 \int_0^T \int_{\mathbb{R}^d} |\nabla z^\epsilon|^2 dxdt.$$

Then, according to estimate (3.16), we have $\int_0^T \int_{\mathbb{R}^d} |\nabla \ln(1-\epsilon z^\epsilon)|^2 dxdt$ tends to 0 as ϵ goes to 0.
Now we will demonstrate the estimate (3.17). We multiply equation (3.9) by p^ϵ and integrate it over $\mathbb{R}^d$, we obtain

$$\begin{aligned}
&\frac{1}{2}\frac{d}{dt}\int_{\mathbb{R}^d}(p^\epsilon)^2 dx + \int_{\mathbb{R}^d}|\nabla p^\epsilon|^2 dx - 2\int_{\mathbb{R}^d} p^\epsilon \frac{\nabla K}{K}\nabla p^\epsilon dx \\
&- 2\int_{\mathbb{R}^d} p^\epsilon \nabla p^\epsilon \nabla \ln(1-\epsilon z^\epsilon) dx \\
&\quad \leq \int_{\mathbb{R}^d} p^\epsilon f(p^\epsilon) dx + \frac{\max_{p\in[0,1]}|g(p)|}{c'}\int_{\mathbb{R}^d}|\Delta K| dx.
\end{aligned}$$

Using a Cauchy-Schwarz inequality, we get

$$\begin{aligned}
&\frac{1}{2}\frac{d}{dt}\int_{\mathbb{R}^d}(p^\epsilon)^2 dx + \int_{\mathbb{R}^d}|\nabla p^\epsilon|^2 dx \\
&\leq \quad \frac{1}{c'}\Big(\int_{\mathbb{R}^d}|\nabla p^\epsilon|^2\Big)^{\frac{1}{2}}\Big(\int_{\mathbb{R}^d}|2\nabla K|^2\Big)^{\frac{1}{2}} + \int_{\mathbb{R}^d} p^\epsilon f(p^\epsilon) dx \\
&\quad + \frac{2}{3}\Big(\int_{\mathbb{R}^d}|\nabla p^\epsilon|^2\Big)^{\frac{1}{2}}\Big(\int_{\mathbb{R}^d}|3\nabla ln(1-\epsilon z^\epsilon)|^2 dx\Big)^{\frac{1}{2}} \\
&\quad + \frac{\max_{p\in[0,1]}|g(p)|}{c'}\int_{\mathbb{R}^d}|\Delta K| dx.
\end{aligned}$$

From assumptions 20 and the well-known inequality $2ab \leq a^2 + b^2$, we deduce after an integration in time

$$\frac{1}{2}\int_{\mathbb{R}^d}(p^\epsilon)^2 dx + \frac{1}{6}\int_0^T\int_{\mathbb{R}^d}|\nabla p^\epsilon|^2 dxdt \leq S' + \int_{\mathbb{R}^d} p^\epsilon f(p^\epsilon) dx + \int_0^T\int_{\mathbb{R}^d}|\nabla ln(1-\epsilon z^\epsilon)|^2 dxdt. \quad (3.18)$$

We note that $p^\epsilon f(p^\epsilon) \leq C(p^\epsilon)^2$ for some constant $C > 0$. Therefore,

$$\int_{\mathbb{R}^d} p^\epsilon f(p^\epsilon)\, dx \leq C\int_{\mathbb{R}^d}(p^\epsilon)^2\, dx.$$

Inequality (3.18) can thus be rewritten as:

$$\frac{1}{2}\int_{\mathbb{R}^d}(p^\epsilon)^2 dx + \frac{1}{6}\int_0^T\int_{\mathbb{R}^d}|\nabla p^\epsilon|^2 dxdt \leq S' + C\int_{\mathbb{R}^d}(p^\epsilon)^2\, dx + \int_0^T\int_{\mathbb{R}^d}|\nabla ln(1-\epsilon z^\epsilon)|^2 dxdt.$$

We then apply Grönwall's lemma to the inequality

$$\frac{1}{2}\frac{d}{dt}\int_{\mathbb{R}^d}(p^\epsilon)^2\, dx \leq C\int_{\mathbb{R}^d}(p^\epsilon)^2\, dx.$$

Which provides a uniform bound for $\int_{\mathbb{R}^d}(p^\epsilon)^2\, dx$ in terms of the initial data.

Finally, by taking ϵ small enough, we obtain the desired estimate.

3.4.2 Compactness result and proof of Theorem 8

Before proceeding to prove our theorem, it is relevant to recall the compactness result (see [81]).

Lemma 24. *(Lions-Aubin). Let $T > 0$, $q \in (1, \infty)$, $(\psi_n)_n$ a bounded sequence in $L^q(0, T, H)$, where H is a banach space. If ψ_n is bounded in $L^q(0, T, V)$ and V compactly embeds in H, and if $(\partial_t \psi_n)_n$ is bounded in $L^q(0, T, V')$ uniformly with respect to n, then $(\psi_n)_n$ is relatively compact in $L^q(0, T, H)$.*

The proof of the theorem is divided into several steps.

Step 1 : Local relative Compactness. For $R > 0$, we define the increasing sequence $(B_R)_R$ of balls of radius R with center 0 in $\mathbb{R}^d$. We use lemma (Aubin-Lions) with $q = 2$, $H_R = L^2(B_R)$ and $V_R = H^1(B_R) \cap L^\infty(B_R)$. Then, we apply Lions-Aubin Lemma with $q = 2$. Then the sequence (p^ϵ) is uniformly bounded in $L^2(0, T, V_R)$ from Lemma 23. The compact embedding of V_R in H_R is well-known from the Rellich-Kondrachov theorem. We are left to verify the bound on the time derivative : Let $\phi \in V_R$, we denote $\langle \cdot, \cdot \rangle = \langle \cdot, \cdot \rangle_{V_R', V_R}$, the duality bracket. From equation (3.9), we get

$$\int_0^T |\langle \partial_t p^\epsilon(t), \phi \rangle|^2 dt = \int_0^T |\langle \Delta p^\epsilon + 2\frac{\nabla K}{K} \nabla p^\epsilon + 2\nabla p^\epsilon \nabla \ln(1 - \epsilon z^\epsilon) - \psi^\epsilon, \phi \rangle|^2 dt.$$

Where ψ^ϵ is the function defining the right hand side in equation (3.9), which is uniformly bounded in $L^1((0, T) \times B_R) \cap L^\infty((0, T) \times B_R)$, then

$$\begin{aligned}
&\int_0^T |\langle \Delta p^\epsilon + 2\frac{\nabla K}{K} \nabla p^\epsilon + 2\nabla p^\epsilon \nabla \ln(1 - \epsilon z^\epsilon) - \psi^\epsilon, \phi \rangle|^2 dt \\
< \quad & ||\nabla \phi||^2_{L^2(B_R)} \int_0^T ||\nabla p^\epsilon||^2_{L^2(B_R)} dt \\
& + \frac{2}{c'} ||\phi||^2_{L^\infty(B_R)} ||\nabla K||^2_{L^2(B_R)} \int_0^T ||\nabla p^\epsilon||^2_{L^2(B_R)} dt \\
& + 2||\phi||^2_{L^\infty(B_R)} || \int_0^T ||\nabla \ln(1 - \epsilon z^\epsilon)||^2_{L^2(B_R)} ||\nabla p^\epsilon||^2_{L^2(B_R)} dt + ||\phi||^2_{L^2(B_R)} ||\psi^\epsilon||^2_{L^\infty(B_R)}.
\end{aligned}$$

Step 2 : Global convergence. For all $R \in \mathbb{N}$, one can extract converging in $L^2(0, T, H_R)$ subsequence from $(p^\epsilon)_\epsilon$ by Lions-Aubin lemma. We perform a diagonal extraction process successively in R, so that

$$p^{\epsilon_m^{(R)}} \xrightarrow{m \to +\infty} p^{(R)} \quad in \quad L^2(0, T, H_R)$$

and by construction $(\epsilon_m^{(R_2)})_m$ is a subsequence of $(\epsilon_m^{(R_1)})_m$ if $R_2 > R_1$. This ensures the consistency of the subsequences on increasing nested domains. Since the family $(p^\epsilon)_\epsilon$ is uniformly bounded in $L^2(0, T; H^1(\mathbb{R}^d))$, we can also obtain the weak convergence of the gradient:

$$\nabla p^{\epsilon_m^{(R)}} \xrightarrow{m \to +\infty} \nabla p^{(R)} \quad \text{in } L^2(0, T; H_R).$$

The limits $p^{(R)}$ are well defined, independent of the extracted subsequences, and satisfy the same bounds as $(p^\epsilon)_\epsilon$. Additionally,

$$R_2 > R_1 \implies p^{(R_2)}\Big|_{B_{R_1}} = p^{(R_1)}.$$

This property allows us to define a global limit function $p^0 \in L^2(0,T;L^2(\mathbb{R}^d))$ by combining the local limits $p^{(R)}$ for $R>0$. Finally, we have constructed a subsequence, still denoted as (p^ϵ), such that

$$p^\epsilon \xrightarrow{\epsilon\to 0} p^0 \quad \text{strongly in } L^2(0,T;L^2(B_R)), \quad \forall R>0.$$

To transition from local convergence to global convergence, it is necessary to obtain uniform estimates in ϵ for the tails, i.e., for $|x|>R$. To achieve this, we introduce a function $\phi \in C^\infty(\mathbb{R}^d)$ such that $0\le\phi\le 1$, $\phi(x)=0$ if $|x|<\frac{1}{2}$, and $\phi(x)=1$ if $|x|>1$. We then define $\phi_R(x)=\phi\left(\frac{x}{R}\right)$. Multiplying (3.9) by $p^\epsilon\phi_R$ and integrating over $\mathbb{R}^d$, we obtain:

$$\begin{aligned}\frac{1}{2}\frac{d}{dt}\int_{\mathbb{R}^d}(p^\epsilon)^2\phi_R\,dx \le &-\int_{\mathbb{R}^d}\nabla(p^\epsilon\phi_R)\nabla p^\epsilon\,dx + 2\int_{\mathbb{R}^d}\frac{\nabla K}{K}\nabla p^\epsilon p^\epsilon\phi_R\,dx\\ &+2\int_{\mathbb{R}^d}\nabla p^\epsilon\nabla\ln(1-\epsilon z^\epsilon)p^\epsilon\phi_R\,dx + A\int_{\mathbb{R}^d}(p^\epsilon)^2\phi_R\,dx,\end{aligned}$$

where $A=\sup_{p\in[0,1]}\{|\frac{(1-p)(s_hp-s_f)d_u[(\delta-1)p+1]}{(1-s_f)p+(1-p)(1-s_hp)}-d_u(\delta-1)|+|\frac{\max\left[\frac{\Delta K}{K}\right](1-p)(s_hp-s_f)}{(1-s_f)p+(1-p)(1-s_hp)}|\}$.

We begin by expanding the expression:

$$\int_{\mathbb{R}^d}\nabla(p^\epsilon\phi_R)\cdot\nabla p^\epsilon\,dx=\int_{\mathbb{R}^d}p^\epsilon\nabla\phi_R\cdot\nabla p^\epsilon\,dx+\int_{\mathbb{R}^d}\phi_R|\nabla p^\epsilon|^2\,dx.$$

By bounding $|\nabla\phi_R|$ by its L^∞ norm and applying Hölder's inequality, we get the following.

$$|\int_{\mathbb{R}^d}p^\epsilon\nabla\phi_R\cdot\nabla p^\epsilon\,dx|\le||\nabla\phi_R||_{L^\infty}\int_{\mathbb{R}^d}|p^\epsilon\cdot\nabla p^\epsilon|dx.$$

Then, using Young's inequality, we deduce:

$$|\int_{\mathbb{R}^d}p^\epsilon\nabla\phi_R\cdot\nabla p^\epsilon\,dx|\le\frac{||\nabla\phi||_{L^\infty}}{R}||p^\epsilon||_{L^2}||\nabla p^\epsilon||_{L^2}.$$

Following the same procedure and given that z^ϵ is uniformly bounded, we obtain the following inequality:

$$\begin{aligned}\frac{1}{2}\frac{d}{dt}\int_{\mathbb{R}^d}(p^\epsilon)^2\phi_R\,dx\le&\frac{||\nabla\phi||_{L^\infty}}{R}||p^\epsilon||_{L^2}||\nabla p^\epsilon||_{L^2}+2\max\left|\frac{\nabla K}{K}\right|\int_{\mathbb{R}^d}|\nabla p^\epsilon p^\epsilon\phi_R|\,dx\\&+\epsilon\int_{\mathbb{R}^d}|\nabla p^\epsilon|^2\,dx+\epsilon^2S'\int_{\mathbb{R}^d}|\nabla z^\epsilon|^2\,dx+A\int_{\mathbb{R}^d}(p^\epsilon)^2\phi_R\,dx.\end{aligned}$$

This implies:

$$\begin{aligned}\frac{1}{2}\frac{d}{dt}\int_{\mathbb{R}^d}(p^\epsilon)^2\phi_R\,dx\le&\left(\frac{1}{R}+\epsilon\right)\left(||\nabla\phi||_{L^\infty}||p^\epsilon||_{L^2}||\nabla p^\epsilon||_{L^2}+\epsilon S'\int_{\mathbb{R}^d}|\nabla z^\epsilon|^2\,dx\right)\\&+2\max\left|\frac{\nabla K}{K}\right|\int_{\mathbb{R}^d}|\nabla p^\epsilon p^\epsilon\phi_R|\,dx+A\int_{\mathbb{R}^d}(p^\epsilon)^2\phi_R\,dx.\end{aligned}$$

Let us define:

$$\begin{aligned}h_{R,\epsilon}(t)=&\left(\frac{1}{R}+\epsilon\right)\left(||\nabla\phi||_{L^\infty}||p^\epsilon||_{L^2}||\nabla p^\epsilon||_{L^2}+\epsilon S'\int_{\mathbb{R}^d}|\nabla z^\epsilon|^2\,dx\right)\\&+2\max\left|\frac{\nabla K}{K}\right|\int_{\mathbb{R}^d}|\nabla p^\epsilon p^\epsilon\phi_R|\,dx.\end{aligned}$$

Thanks to Lemma 23, we know that $h_{R,\epsilon} \in L^1(0,T)$, so we obtain:

$$\frac{1}{2}\frac{d}{dt}\int_{\mathbb{R}^d}(p^\epsilon)^2\phi_R\,dx \le h_{R,\epsilon}(t) + A\int_{\mathbb{R}^d}(p^\epsilon)^2\phi_R\,dx.$$

Using Gronwall's Lemma, this inequality implies:

$$\int_{\mathbb{R}^d}(p^\epsilon)^2\phi_R\,dx \le e^{2At}\int_{\mathbb{R}^d}(p^{\text{init}})^2\phi_R\,dx + \int_0^t h_{R,\epsilon}(\tau)e^{2A(t-\tau)}\,d\tau.$$

By the definition of ϕ_R (where $\phi_R(x) = 1$ on $\mathbb{R}^d \setminus B_R$), we deduce that for all $\epsilon > 0$ sufficiently small and for all $R > 0$, we have:

$$\begin{aligned}&\int_0^T\int_{\mathbb{R}^d\setminus B_R}(p^\epsilon)^2\,dx\,dt \\ &\le \int_0^T\int_{\mathbb{R}^d}(p^\epsilon)^2\phi_R\,dx\,dt \le \frac{1}{2A}\left(e^{2AT}-1\right)\left(\int_{\mathbb{R}^d\setminus B_{\frac{R}{2}}}(p^{\text{init}})^2\,dx + \int_0^T h_{R,\epsilon}(t)\,dt\right).\end{aligned} \tag{3.19}$$

This result implies a uniform bound, as $p^{\text{init}} \in L^2(\mathbb{R}^d)$. Therefore, we conclude that the subsequence $(p^\epsilon)_\epsilon$ converges strongly to p^0 in $L^2(0,T;L^2(\mathbb{R}^d))$ as $\epsilon \to 0$.

The reasoning is as follows:

$$\int_0^T\int_{\mathbb{R}^d}|p^\epsilon - p^0|^2\,dx\,dt = \int_0^T\int_{B_R}|p^\epsilon - p^0|^2\,dx\,dt + \int_0^T\int_{\mathbb{R}^d\setminus B_R}|p^\epsilon - p^0|^2\,dx\,dt.$$

This inequality leads to:

$$\begin{aligned}\int_0^T\int_{\mathbb{R}^d}|p^\epsilon - p^0|^2\,dx\,dt \le \int_0^T\int_{B_R}|p^\epsilon - p^0|^2\,dx\,dt + 2\int_0^T\int_{\mathbb{R}^d\setminus B_R}|p^\epsilon|^2\,dx\,dt \\ + 2\int_0^T\int_{\mathbb{R}^d\setminus B_R}|p^0|^2\,dx\,dt.\end{aligned}$$

The second term on the right-hand side is uniformly bounded for sufficiently large R due to inequality (3.19) and the fact that $p^0 \in L^2(0,T;L^2(\mathbb{R}^d))$. Regarding the first term, we rely on local convergence.

Step 3 : Passing to the limit. Using the strong convergence of the sequence (p^ϵ) in $L^2(0,T;L^2(\mathbb{R}^d))$ and the Lipschitz continuity of the function I, we deduce that $(I(p^\epsilon))$ converges strongly in $L^2(0,T;L^2(\mathbb{R}^d))$ to $I(p^0)$.

Where $I(p) = p(1-p)\left[(s_h p - s_f)\frac{d_u[(\delta-1)p+1]-\frac{\Delta K}{K}}{(1-s_f)p+(1-p)(1-s_h p)} - d_u(\delta-1)\right]$.

Using the weak formulations of the equations concerning p^ϵ (3.9), we derive the equation satisfied by p^0. Let $\chi \in C_C^\infty((0,T)\times\mathbb{R}^d)$, we have

$$\begin{aligned}&\int_0^T\int_{\mathbb{R}^d} p^\epsilon\partial_t\chi - \nabla p^\epsilon\nabla\chi - 2\frac{\nabla K}{K}\nabla p^\epsilon\chi - 2\nabla p^\epsilon\nabla\ln(1-\epsilon z^\epsilon)\chi dxdt \\ &= \int_0^T\int_{\mathbb{R}^d} I(p^\epsilon)\chi dxdt,\end{aligned} \tag{3.20}$$

from the above convergence it is straightforward to pass into the first two terms of the left hand side. For the fourth term, we use

$$\int_0^T \int_{\mathbb{R}^d} |\nabla p^\epsilon|^2 dxdt \leq S'$$

and a Cauchy Schwarz inequality to get

$$\int_0^T \int_{\mathbb{R}^d} \nabla p^\epsilon \nabla \ln(1-\epsilon z^\epsilon)\chi dxdt \leq S' ||\chi||_{L^\infty} ||\nabla \ln(1-\epsilon z^\epsilon)||_\infty \xrightarrow{\epsilon \to 0} 0.$$

In the case where p^ϵ converges strongly, we can take the limit for the first term on the right-hand side of (3.20). Finally, by letting $\epsilon \to 0$ in (3.20), we obtain

$$\partial_t p^0 - \Delta p^0 - 2\frac{\nabla K}{K}\nabla p^0 = f(p^0) + \frac{\Delta K}{K} g(p^0). \tag{3.21}$$

Where

$$f(p^0) = p^0(1-p^0)\left[\frac{d_u(\delta s_h p^0 - s_f + 1 - \delta)}{(1-s_f)p^0 + (1-p^0)(1-s_h p^0)}\right],$$

and

$$g(p^0) = \frac{-p^0(1-p^0)(s_h p^0 - s_f)}{(1-s_f)p^0 + (1-p^0)(1-s_h p^0)}.$$

□

3.5 Conclusion

In this chapter, we have proven the rigorous convergence, under appropriate assumptions, of a two-equation reaction-diffusion model to a reduced model describing the frequency of a variant. This result legitimizes the use of simplified models in practice. However, while the bistable model approach is mathematically justified, its validity relies on specific scaling conditions, particularly regarding population size and fecundity. Bistable equations are widely used to model the spatial spread of Wolbachia, as they allow the analysis of traveling waves and the estimation of invasion speed.

CHAPTER 4

BLOCKING OF BISTABLE FRONT PROPAGATION: APPLICATION TO WOLBACHIA POPULATION REPLACEMENT

"It always seems impossible until it's done."

Nelson Mandela

4.1 Introduction

The fight against dengue, a global scourge [14], and other arboviruses has mobilized significant efforts within the scientific community. The development of innovative vector control techniques is a particularly dynamic field of research. Among these approaches, the use of Wolbachia in Aedes mosquitoes to limit disease transmission [92, 7] has attracted growing interest. The artificial infection of mosquitoes with Wolbachia can be achieved in laboratory settings, and its vertical transmission enables the rapid and large-scale spread of the infected strain.

The first mathematical models of this strategy include the works of Barton et al. [13], Hughes et al. [45], and Hancock et al. [39], which have contributed to a better understanding of the dynamics of this infection and its population-level implications. The impact of spatial dimensions in vector control processes has also attracted significant attention from researchers. Several studies have explored the conditions under which mathematical models incorporating spatial variations can predict the blocking of a biological invasion, particularly in the context of Wolbachia-infected mosquito releases.

The observation of biological invasions and the mechanisms used to stop them is a widely studied topic in the literature. For example, the experimental study conducted by Atyame et al. [11] demonstrated that stable coexistence between multiple natural Wolbachia strains could be observed in a Culex pipiens population. Several hypotheses have been proposed to explain this stability. Nadin et al. [68], through a simplified mathematical model, supported some of the analyses derived from these studies.

Our results in this chapter support these analyses. We show that the environmental carrying capacity K plays a crucial role in propagation. When spatial variations, represented by the terms $K^{'}/K$ and $K^{''}/K$, are small, blocking propagation is impossible. However, when these variations are sufficiently pronounced, they can halt the invasion. This result highlights the

importance of environmental gradients in controlling biological invasions and opens new perspectives for explaining experimental observations.
Although long-term field experiments remain limited, artificial releases of Wolbachia-infected mosquitoes [44, 69] have revealed phenomena such as stable fronts and blockages [43, 99]. These phenomena have been modeled in several studies, notably using reaction-diffusion equations [13, 20] and models accounting for habitat heterogeneity [38].
Our approach is based on the analysis of a modified equation in one spatial dimension that accounts for spatial variations:

$$\partial_t p - D\partial_{xx} p - 2D\frac{K^{'}}{K}\partial_x p = f(p) + \frac{K^{''}}{K}g(p). \tag{4.1}$$

This formulation explicitly integrates spatial heterogeneity through the term $\frac{K''}{K}$, a determining factor in blocking propagation. Mathematically, our study relies on demonstrating the existence of stationary solutions for this equation, using the shooting method, a commonly employed approach for solving partial differential equations. In particular, we show that when $\frac{K'}{K}$ and $\frac{K''}{K}$ are of small amplitude, propagation is not blocked. On the other hand, if these terms are sufficiently large, propagation is blocked. To simplify the analysis, we assume that the diffusion coefficient is normalized, meaning that $D = 1$ and will maintain this assumption throughout the remainder of the work.

4.2 Results on the blocking

In this section, we present our main result, which addresses blocking the propagation of Wolbachia in heterogeneous environments where the environmental carrying capacity varies significantly across different regions of the spatial domain. Before presenting our main result for equation (3.21), we introduce the concept of propagation barrier (referred to simply as barrier below). We consider the domain to be one-dimensional and therefore study the differential equation :

$$\partial_t p - \partial_{xx} p - 2\frac{K^{'}}{K}\partial_x p = f(p) + \frac{K^{''}}{K}g(p), \quad t \geq 0, \quad x \in \mathbb{R}. \tag{4.2}$$

Where

$$f(p) = p(1-p)\left(\frac{d_u(\delta s_h p - s_f + 1 - \delta)}{(1-s_f)p + (1-p)(1-s_h p)}\right),$$

and

$$g(p) = \frac{-p(1-p)(s_h p - s_f)}{(1-s_f)p + (1-p)(1-s_h p)}.$$

To proceed, let us define the function $F(x)$ as

$$F(x) = \int_0^x f(t)\, dt,$$

On the one hand, under hypothesis

$$(\delta - 1) + s_f < s_h \delta,$$

the function f is bistable meaning that it is continuous and Lipschitz, and satisfies

$$f(0) = f(1) = f(\theta_1) = 0, \quad where \;\; \theta_1 = \frac{(\delta - 1) + s_f}{s_h \delta} \in (0, 1).$$

Furthermore, $f < 0$ on the interval $(0, \theta_1)$ and $f > 0$ on $(\theta_1, 1)$.
On the other hand, throughout this chapter, we assume that

$$F(1) = \int_0^1 f(t)\, dt > 0.$$

In the case where K is homogeneous, it is well known that a unique traveling wave exists. Its speed has the sign of

$$F(1) = \int_0^1 f(t)\, dt,$$

which is positive. Depending on the initial conditions, the solution may converge to 1, leading to an invasion phenomenon.

In this chapter, we are interested in what happens when K depends on x. To obtain a tractable problem, we assume that K increases exponentially in a given region of the spatial domain and remains constant elsewhere. Specifically, for certain constants $C > 0$, $L > 0$:

$$K(x) = \begin{cases} A, & \text{for } x < 0, \\ Ae^{Cx}, & \text{for } x \in [0, L], \\ Ae^{CL}, & \text{for } x > L. \end{cases} \tag{4.3}$$

In this context, our goal is to prove the blocking of Wolbachia propagation where K varies significantly across different regions of the spatial domain. To achieve this, we will show that equation (4.2) admits a stationary solution and satisfies the comparison principle. The existence of a stationary wave for this problem boils down to the existence of a solution to

$$\begin{cases} -p'' - Cp' - C^2 g(p) = f(p), & on \ \ ]0, L[, \\ -p'' = f(p), & on \ \ [0, L]^c, \\ p'(0^-) - p'(0^+) = Cg(p(0)), & \\ p'(L^-) - p'(L^+) = -Cg(p(L)), & \\ p(-\infty) = 1, \ p(+\infty) = 0, \ p > 0. & \end{cases} \tag{4.4}$$

In our study, stationary solutions of equation (4.2), which exhibit specific behavior at infinity as described by the solutions of equation (4.4), act as barriers that prevent propagation. Before presenting the main results, we first introduce the definition of a barrier and the assumptions.

Definition 25.
We name a (C, L)-barrier any solution to (4.4)*. For any bistable function f we define the barrier set*

$$B(f) = \{(C, L) \in (0, +\infty)^2, \ \textit{there exists a } (C, L) - \textit{barrier}\}.$$

Assumptions 26.

- $s_h \leq 1$.
- $s_f \leq 1 - s_h$.

Before presenting the Barrier Existence Theorem, it is important to note that if C is small enough, there is no blockage. This is the objective of the following lemma.

Lemma 27.
If $\frac{K'}{K}$ and $\frac{K''}{K}$ are sufficiently small, then there exists a sub-solution that is not blocked.

On the contrary, for large enough C and L, there exist barriers.

Theorem 9.
Let $C > 0$, $L > 0$, and assume that K is given by (4.3), that assumption 26 holds and that $F(1) > 0$. $\exists c_* > 0$ such that for all $C > c_*$ there exists L^* such that for all $L > L^*$ we have $(C, L) \in B(f)$.

The existence of a barrier significantly and directly influences the asymptotic behavior of the solutions of equation (4.2), as established by the following proposition.

Proposition 28.
Suppose that there exists a barrier (C, L) denoted by $\bar{P}$ and that K is given by (4.3). Then every weak solution of

$$\partial_t p - \partial_{xx} p - 2\frac{K'}{K}\partial_x p = f(p) + \frac{K''}{K} g(p),$$

with initial data such that $p^{ini} \leq \bar{P}$, stops spreading, meaning $\forall t \geq 0$, $p(t) \leq \bar{P}$.

4.3 Preliminary result

In this section, we present a fundamental result on barriers, as defined in Definition 25. Specifically, we prove that the barriers are decreasing. Since $F(1) = \int_0^1 f(t)\,dt > 0$, we introduce θ_c, the unique real number such that

$$F(\theta_c) = \int_0^{\theta_c} f(t)\,dt = 0.$$

We assume that the following inequality holds:

$$(\delta - 1) + s_f < s_h \delta.$$

Lemma 29.
If $(C, L) \in B(f)$, $p(L) \leq \frac{s_f}{s_h}$ and p is a (C, L)-barrier, then p is decreasing.

Proof.
Consider the following system:

$$\begin{cases} -p'' - Cp' - C^2 g(p) = f(p), & \text{on }]0, L[, \\ -p'' = f(p), & \text{on } [0, L]^c, \\ p'(0^-) - p'(0^+) = Cg(p(0)), \\ p'(L^-) - p'(L^+) = -Cg(p(L)), \\ p(-\infty) = 1, \quad p(+\infty) = 0, \quad p > 0. \end{cases}$$

We first consider the interval $(-\infty, 0)$. Since $-p'' = f(p)$, multiplying by p' and integrating yields

$$\frac{1}{2}\big(p'(x)\big)^2 + F(p(x)) = F(1).$$

Thus, $p'(x) = 0$ if and only if $p(x) = 1$. However, the maximum principle forbids this situation because 1 is a super-solution, so p cannot touch it.

Now consider $x \in (L, +\infty)$. Similarly, we obtain

$$\frac{1}{2}\Big(p'(x)\Big)^2 + F(p(x)) = 0.$$

Hence, p' can vanish only if $p = 0$ or $p = \theta_c$. Since $p = 0$ is impossible, the only remaining possibility is $p = \theta_c$.

Assume by contradiction that there exists $x_1 > L$ such that $p(x_1) = \theta_c$ and $p'(x_1) = 0$. Since $p(L) < \theta_c$, the function p increases on (L, x_1) and decreases after x_1, meaning that x_1 would be a maximum with value $p(x_1) = \theta_c > 0$.

By the strong maximum principle, such an interior maximum would force p to be constant on $(L, +\infty)$, which is impossible because $\lim_{x\to+\infty} p(x) = 0$. Therefore, p' never vanishes on $(L, +\infty)$. Since $p \geq 0$ and $\lim_{x\to+\infty} p(x) = 0$, it follows that p is strictly decreasing on $(L, +\infty)$.

We now turn to the interval $(0, L)$. Define

$$x_m = \inf\{x > 0 : p'(x) = 0\}.$$

Suppose by contradiction that $x_m \leq L$. There are two possible cases.

Either $p(x_m) \leq \theta_c$. In this case we introduce

$$E(x) = \frac{1}{2}\Big(p'(x)\Big)^2 + F(p(x)) + C^2 G(p(x)), \quad G(p) = \int_0^p g(u)\,du.$$

Differentiating gives

$$E'(x) = -C\Big(p'(x)\Big)^2 \leq 0,$$

then E is decreasing. At x_m, since $p'(x_m) = 0$, we have

$$E(x_m) = F(p(x_m)) + C^2 G(p(x_m)).$$

At $x = L$, using the transmission condition

$$p'(L^-) = p'(L^+) - Cg(p(L)),$$

and the fact that

$$\tfrac{1}{2}\Big(p'(L^+)\Big)^2 + F(p(L)) = 0,$$

we obtain after simplification

$$E(L) = Cg(p(L))\sqrt{-2F(p(L))} + \tfrac{C^2}{2} g(p(L))^2 + C^2 G(p(L)).$$

To analyze the sign of $E(L) - E(x_m)$, we distinguish two cases: $p(x_m) < p(L)$ and $p(x_m) > p(L)$.

$\star$ If $p(x_m) < p(L)$,

$$E(L) - E(x_m) = Cg(p(L))\sqrt{-2F(p(L))} + \tfrac{C^2}{2} g(p(L))^2 - F(p(x_m)) + C^2 \int_{p(x_m)}^{p(L)} g(u)\,du.$$

Since $0 \leq p(x_m) \leq p(L)$, and $p(L) < \frac{s_f}{s_h}$ with $g(u) > 0$ for all $0 < u < \frac{s_f}{s_h}$, the integral is nonnegative, which implies $E(L) \geq E(x_m)$. This contradicts the fact that E is decreasing and $x_m \leq L$.

$\star$ If $p(x_m) > p(L)$,

Since $p'(x_m) = 0$ with $p(x_m) > p(L)$, the function must increase before x_m and decrease after. But on $(-\infty, 0)$, p is already decreasing. For p to increase before x_m, there must exist another point before x_m where $p' = 0$, contradicting the definition of x_m as the first zero of p'. Hence this case is impossible.

We are left with $\theta_c \leq p(x_m) \leq 1$. Since $p(L) < \theta_c$, it follows that $p(x_m) > p(L)$. In this case, we fall back to the previous case, which leads to a contradiction. Hence $p^{'} < 0$ on $(0, L)$. Because $0 \leq p \leq 1$ and because of its limits at $+\infty$ and $-\infty$, p necessarily decreases at $(-\infty, 0) \cup (L, +\infty)$. □

4.4 Proofs of Main Results

In this section, we provide the proofs of the main results presented in Section 4.2.

4.4.1 No blocking for small variations

In this subsection, we present the proof of Lemma 27.

Proof.

We consider the following equation.

$$\begin{aligned} &\partial_t p - \partial_{xx} p - 2\frac{K^{'}}{K}\partial_x p \\ &= \frac{p(1-p)}{(1-s_f)p + (1-p)(1-s_h p)} \left(p\left(s_h \left(\delta d_u - \frac{K^{''}}{K} \right) \right) - d_u(s_f + \delta - 1) \right). \end{aligned} \tag{4.5}$$

Let $0 < A < s_h \delta d_u$ and define

$$f_A(p) = \frac{p(1-p)}{(1-s_f)p + (1-p)(1-s_h p)} \left(pA - d_u(s_f + \delta - 1) \right),$$

satisfies condition $\int_0^1 f_A(p)\, dp > 0$, it is possible since $F(1) > 0$. Then, there exists $c_A > 0$ and and a decreasing function ϕ_A satisfying

$$\begin{cases} -\phi_A^{''} - c_A \phi_A^{'} = f_A(\phi_A), \\ \phi_A(-\infty) = 1, \quad \phi_A(+\infty) = 0, \\ \phi_A^{'} < 0. \end{cases}$$

Assume $\left| \frac{K^{''}}{K} \right| \leq s_h \delta d_u - A$ and $2\left| \frac{K^{'}}{K} \right| < c_A$. Let $p_A(t, x) = \phi_A(x - c_A t)$ with $c_A > 0$. Then

$$\partial_t p_A - \partial_{xx} p_A - 2\frac{K^{'}}{K} \cdot \partial_x p_A = -2\frac{K^{'}}{K}\phi_A^{'} - \phi_A^{''} = \left[c_A - 2\frac{K^{'}}{K} \right] \phi_A^{'} + f_A(\phi_A).$$

Since $2\left|\frac{K^{'}}{K}\right| < c_A$ and $\phi_A^{'} < 0$, it follows that

$$\partial_t p_A - \partial_{xx} p_A - 2\frac{K^{'}}{K} \cdot \partial_x p_A < f_A(\phi_A) = f_A(p_A).$$

Finally, using $\left|\frac{K^{''}}{K}\right| \leq s_h \delta d_u - A$, we have

$$\partial_t p_A - \partial_{xx} p_A - 2\frac{K^{'}}{K} \cdot \partial_x p_A < \frac{p(1-p)}{(1-s_f)p + (1-p)(1-s_h p)} \left(p\left(s_h \left(\delta d_u - \frac{K^{''}}{K} \right) \right) - d_u(s_f + \delta - 1) \right).$$

Therefore, p_A is a sub-solution of equation (4.5), which implies that there is no blocking for $\frac{K^{'}}{K}$ and $\frac{K^{''}}{K}$ sufficiently small.

□

4.4.2 Proof of Theorem 9

Now, we proceed to the proof of Theorem 9, which establishes the existence of stationary solutions.
To get a better description of $B(f)$, we use a shooting method. We separate the study of equation (4.4) on $(0, L)$ by introducing

$$p(0) = \beta, \quad p(L) = \alpha.$$

We now face a problem that is slightly differently formulated:
for $\frac{s_f}{2s_h} < \alpha < \frac{s_f}{s_h} < \beta < 1$, we aim to find C and $L > 0$ such that

$$\begin{cases} -p^{''} - Cp^{'} - C^2 g(p) = f(p), \\ p(0) = \beta, \ \ p(L) = \alpha, \\ p'(0^-) - p'(0^+) = Cg(p(0)) = Cg(\beta), \\ p'(L^-) - p'(L^+) = -Cg(p(L)) = -Cg(\alpha), \\ \frac{1}{2}p^{'}(0^-)^2 + F(\beta) = F(1), \quad \frac{1}{2}p^{'}(L^+)^2 + F(\alpha) = 0. \end{cases} \tag{4.6}$$

There is an evident and direct link between equations (4.4) and (4.6).

Lemma 30.
Let $C, L > 0$. If $(C, L) \in B(f)$, then there exists (α, β) such that (4.6) has a solution. Conversely, if there exist α, β, C, and L such that (4.6) has a solution, then this solution is also a solution of (4.4).

Proof.
Let C and L be positive constants. If $(C, L) \in B(f)$, then the problem (4.4) admits a solution denoted by p, which satisfies the following equations:

$$\begin{cases} -p^{''} - Cp^{'} - C^2 g(p) = f(p), & on \ \ ]0, L[, \\ -p^{''} = f(p), & on \ \ [0, L]^c, \\ p'(0^-) - p'(0^+) = Cg(p(0)), \\ p'(L^-) - p'(L^+) = -Cg(p(L)), \\ p(-\infty) = 1, \ p(+\infty) = 0, \ p > 0. \end{cases}$$

Thus, the first equation of problem (4.6) is satisfied. It remains to demonstrate the existence of α and β that fulfill the conditions:

$$p(0) = \beta,\ \ p(L) = \alpha,\ \ \frac{1}{2}p^{'}(0^{-})^2 + F(\beta) = F(1),\ \ \frac{1}{2}p^{'}(L^{+})^2 + F(\alpha) = 0.$$

Since the problem (4.6) is well-posed in the space of real functions that are twice continuously differentiable on $[0, L]$ and on $[0, L]^c$, we can find $\alpha, \beta > 0$ such that $p(0) = \beta$ and $p(L) = \alpha$.

It is straightforward to demonstrate that $\frac{1}{2}p^{'}(0^{-})^2 + F(\beta) = F(1)$ and $\frac{1}{2}p^{'}(L^{+})^2 + F(\alpha) = 0$. The proof of these equations is direct and intuitive.

In conclusion, we can establish the existence of α and β that fulfill the conditions in Equation (4.6) and ensure the solvability of the problem. Similarly, to reverse the statement, we can employ a similar line of reasoning.

□

Lemma 31 (Existence of a Solution)**.**

Let $\frac{s_f}{2s_h} < \alpha < \frac{s_f}{s_h} < \beta < 1$, with $\alpha < \theta_c$. Assume that assumption 26 is satisfied.

Under these conditions, there exist unique constants $C = \gamma(\alpha, \beta)$ and $L = \lambda(\alpha, \beta)$ such that the system (4.6) *has a solution.*

Proof.

Here, we employ a shooting argument. Let p_α be a unique (by the Cauchy-Lipschitz theorem) decreasing (by similar arguments as in Lemma 29) solution to

$$\begin{cases} -p_\alpha^{''} - Cp_\alpha^{'} - C^2 g(p_\alpha) = f(p_\alpha), \\ p_\alpha(L) = \alpha, \ \ \frac{1}{2}p_\alpha^{'}(L^{+})^2 + F(\alpha) = 0, \\ {p_\alpha}'(L^{-}) - {p_\alpha}'(L^{+}) = -Cg(p_\alpha(L)). \end{cases} \tag{4.7}$$

Since p_α is decreasing, we may invert it and define $X_\alpha :]p_\alpha(L), p_\alpha(0)[\to]0, L[$ such that $p_\alpha(X_\alpha(p)) = p$. Moreover, we introduce the function:

$$w_\alpha(p) = \frac{F(1)}{F(1) + Cg(\beta)\sqrt{2(F(1) - F(\beta))} - Cg(\alpha)\sqrt{-2F(\alpha)}} \Bigg(\frac{1}{2}p_\alpha^{'}(X_\alpha(p))^2 + F(p) - \frac{C^2}{2}g(p)^2 - Cg(\alpha)\sqrt{-2F(\alpha)} \Bigg).$$

Consequently, the following system of equations holds:

$$\begin{cases} \frac{dw_\alpha}{dp} = CJ\sqrt{2(\frac{w_\alpha(p)}{J} - F(p)) + C^2 g(p)^2 + 2Cg(\alpha)\sqrt{-2F(\alpha)}} \\ \qquad\qquad -C^2 J g(p)[1 + g'(p)], \\ w_\alpha(\alpha) = 0. \end{cases} \tag{4.8}$$

Where $J = \frac{F(1)}{F(1) + Cg(\beta)\sqrt{2(F(1) - F(\beta))} - Cg(\alpha)\sqrt{-2F(\alpha)}}$ is positive. In what follows, we assume that $\sqrt{J}$, satisfies the following condition:

$$\sqrt{J} < \frac{C(\beta - \alpha) - \sqrt{2}\sqrt{F(1) + C\left(g(\beta)\sqrt{2(F(1) - F(\beta))} - g(\alpha)\sqrt{-2F(\alpha)}\right)}}{C^2(\beta - \alpha)\max R},$$

where the function R is defined by

$$R(p) = \frac{g(p)(1+g^{'}(p))}{\sqrt{2w_\alpha}},$$

with w_α being positive (which will be shown later).

Equation (4.8) has a solution as long as $w_\alpha \geq JF(p)$. On the interval (α, θ_c), we have $F(p) \leq 0$ by definition of θ_c. Consequently, on (α, θ_c), equation (4.8) has at least one solution.

Next, we consider $\theta_c \leq p_0 \leq 1$ and denote by (α, p_0) the largest interval within $(\alpha, 1)$ for which equation (4.8) has a solution.

The question now is whether it is possible to choose a value for C such that $w_\alpha(\beta) = F(1)$ holds for $\alpha < \frac{s_f}{s_h} < \beta < 1$? Before answering this question, we need to show that w_α is positive. Since we have $p \geq \alpha$ and $w_\alpha(\alpha) = 0$, to prove that w_α is positive, it suffices to show that w_α is increasing. we have

$$\frac{dw_\alpha}{dp} = CJ\sqrt{2(\frac{w_\alpha(p)}{J} - F(p)) + C^2g(p)^2 + 2Cg(\alpha)\sqrt{-2F(\alpha)}} \\ -C^2Jg(p)[1+g'(p)].$$

This is equivalent to

$$\frac{dw_\alpha}{dp} = CJ\left(\sqrt{2\left(\frac{w_\alpha(p)}{J} - F(p)\right) + C^2g(p)^2 + 2Cg(\alpha)\sqrt{-2F(\alpha)}} \right. \\ \left. -Cg(p)[1+g'(p)]\right).$$

The sign of $w_\alpha^{'}$ depends on the sign of $1+g^{'}$. If $1+g^{'}$ is positive, in this case, for simplicity, we will show that $1+g^{'} < 1$.
Considering

$$g^{'}(p) = \\ \frac{\left(-s_hp(1-p)\left((1-s_hp)(1-p)+(1-s_f)p\right) + (s_hp-s_f)\left(-s_fp^2+2p-1\right)\right)}{\left((1-s_f)p+(1-p)(1-s_hp)\right)^2}.$$

After straightforward calculations, it's found that :

$$-s_hp(1-p)\left((1-s_hp)(1-p)+(1-s_f)p\right) + (s_hp-s_f)\left(-s_fp^2+2p-1\right) < 0,$$

for all $\frac{s_f}{2s_h} < p$ and $s_f \leq 1-s_h$. Then we obtain that $1+g^{'} < 1$. Hence, we have:

$$\sqrt{2\left(\frac{w_\alpha(p)}{J} - F(p)\right) + C^2g(p)^2 + 2Cg(\alpha)\sqrt{-2F(\alpha)}} \geq Cg(p) \geq Cg(p)[1+g'(p)].$$

Implies that

$$\sqrt{2\left(\frac{w_\alpha(p)}{J} - F(p)\right) + C^2g(p)^2 + 2Cg(\alpha)\sqrt{-2F(\alpha)}} - Cg(p)[1+g'(p)] \geq 0.$$

For the second case, when $1 + g^{'}$ is negative, the same reasoning applies, and hence $w_{\alpha}^{'}$ is positive.

In conclusion, since $w_{\alpha}^{'}$ is positive, w_{α} is increasing, thus $w_{\alpha}(p) > w_{\alpha}(\alpha) = 0$, so w_{α} is positive.

Now let us return to our question: is it possible to choose a value for C such that $w_{\alpha}(\beta) = F(1)$ holds for $\alpha < \frac{s_f}{s_h} < \beta < 1$?. Here, we evaluate:

$$w_{\alpha}(\beta) = J\left(\frac{1}{2}p_{\alpha}^{'}(X_{\alpha}(\beta))^2 + F(\beta) - \frac{C^2}{2}g(\beta)^2 - Cg(\alpha)\sqrt{-2F(\alpha)}\right).$$

$$F(\beta) = \int_0^{\beta} f(p)dp.$$

We can rewrite the derivative of

$$w_{\alpha}^{'}(p) = CJ\sqrt{2\left(\frac{w_{\alpha}(p)}{J} - F(p)\right) + C^2g(p)^2 + 2Cg(\alpha)\sqrt{-2F(\alpha)}} \\ -C^2Jg(p)[1 + g'(p)].$$

To address our question, we will consider two cases.

• We first show that for $C = \min\left(\frac{\sqrt{-2F(\alpha)}}{g(\alpha)}, \frac{F(1)}{\left(g(\alpha)\sqrt{-2F(\alpha)} - g(\beta)\sqrt{2(F(1)-F(\beta))}\right)}\right)$, $w_{\alpha}(\beta) > F(1)$:

We note that on the interval (α, θ_c), the function $F(p)$ is negative, i.e., $F(p) < 0$. Consequently, we can estimate the derivative as follows:

$$\begin{aligned} w_{\alpha}^{'}(p) &= CJ\sqrt{2(\frac{w_{\alpha}(p)}{J} - F(p)) + C^2g(p)^2 + 2Cg(\alpha)\sqrt{-2F(\alpha)}} \\ &\quad - C^2Jg(p)[1 + g'(p)] \\ &> C\sqrt{J}\sqrt{2w_{\alpha}(p)} - C^2Jg(p)[1 + g'(p)]. \end{aligned}$$

By integrating both sides over (α, p), we get:

$$\sqrt{2w_{\alpha}(p)} > C\sqrt{J}(p - \alpha) - C^2J\int_{\alpha}^{p} R(u)du,$$

Thus, evaluating at $p = \beta$, we obtain:

$$\sqrt{2w_{\alpha}(\beta)} > C\sqrt{J}(\beta - \alpha) - C^2J(\beta - \alpha)\max_{p\in(\alpha,\beta)} R(p) > \sqrt{2F(1)}.$$

Since $\sqrt{J} < \frac{C(\beta-\alpha) - \sqrt{2}\sqrt{F(1) + C\left(g(\beta)\sqrt{2(F(1)-F(\beta))} - g(\alpha)\sqrt{-2F(\alpha)}\right)}}{C^2(\beta-\alpha)\max R}$.

Choosing $C = \min\left(\frac{\sqrt{-2F(\alpha)}}{g(\alpha)}, \frac{F(1)}{\left(g(\alpha)\sqrt{-2F(\alpha)} - g(\beta)\sqrt{2(F(1)-F(\beta))}\right)}\right)$ ensures that $w_{\alpha}(\beta) > F(1)$.

• Then we show that for C small enough $w_{\alpha}(\beta) < F(1)$:

If we consider $F(\theta_1) = \min_{[0,1]} F$, we obtain:

$$w'_\alpha(p) \le C\sqrt{2\left(\frac{w_\alpha(p)}{J} - F(\theta_1)\right) + C^2 \max_{[0,1]} g(p)^2 + 2Cg(\alpha)\sqrt{-2F(\alpha)}} - C^2 J g(p)(1 + g'(p)).$$

Integrating this inequality over (α, p), we get:

$$\begin{aligned} w_\alpha(p) \le JF(\theta_1) - \frac{J}{2}C^2 \max_{[0,1]} g(p)^2 - JCg(\alpha)\sqrt{-2F(\alpha)} \\ + \left(\frac{C}{\sqrt{2J}}(p-\alpha) - C^2\frac{\sqrt{J}}{\sqrt{2}}\int_\alpha^p \frac{g(u)}{\eta}(1+g'(u))du \right. \\ \left. + \sqrt{\frac{J}{2}}\sqrt{-2F(\theta_1) + C^2 \max_{[0,1]} g(p)^2 + 2Cg(\alpha)\sqrt{-2F(\alpha)}}\right)^2. \end{aligned}$$

Where $\eta = \sqrt{2(\frac{w_\alpha(p)}{J} - F(\theta_1)) + C^2 \max_{[0,1]} g(p)^2 + 2Cg(\alpha)\sqrt{-2F(\alpha)}}$.
Therefore:

$$\begin{aligned} w_\alpha(\beta) \le JF(\theta_1) - \frac{J}{2}C^2 \max_{[0,1]} g(p)^2 - JCg(\alpha)\sqrt{-2F(\alpha)} \\ + \left(\frac{\sqrt{2}C}{\sqrt{J}}(\beta-\alpha) - C^2\frac{J}{\sqrt{2}}\int_\alpha^\beta \frac{g(u)}{\eta}(1+g'(u))du \right. \\ \left. + \sqrt{\frac{J}{2}}\sqrt{-2F(\theta_1) + C^2 \max_{[0,1]} g(p)^2 + 2Cg(\alpha)\sqrt{-2F(\alpha)}}\right)^2. \end{aligned}$$

Therefore, we can choose C small enough such that $w_\alpha(\beta) < F(1)$.

• Next, we prove that w_α is increasing with respect to C.

We define $z_C(p) = \frac{dw_\alpha(p)}{dC}$. From equation (4.8), we have:

$$\begin{aligned} \frac{dz_C(p)}{dp} &= \frac{d}{dp}(\frac{dw_\alpha}{dC}) = \frac{d}{dC}(\frac{dw_\alpha}{dp}) \\ &= J\left(\sqrt{2(\frac{w_\alpha(p)}{J} - F(p) + \frac{C^2}{2}g(p)^2 + Cg(\alpha)\sqrt{-2F(\alpha)})}\right. \\ &\quad \left. - 2Cg(p)(1+g'(p))\right) \\ &\quad + CJ'\left(\sqrt{2(\frac{w_\alpha(p)}{J} - F(p) + \frac{C^2}{2}g(p)^2 + Cg(\alpha)\sqrt{-2F(\alpha)})}\right. \\ &\quad \left. - Cg(p)(1+g'(p))\right). \end{aligned}$$

Equivalent to

$$\begin{cases} \frac{dz_C(p)}{dp} = \tilde{J} z_C(p) + J[\sqrt{2(\frac{w_\alpha(p)}{J} - F(p) + \frac{C^2}{2} g(p)^2 + Cg(\alpha)\sqrt{-2F(\alpha)})} \\ \qquad\qquad -2Cg(p)(1+g^{'}(p))], \\ z_C(\alpha) = 0. \end{cases}$$

where

$$J^{'} = \frac{-F(1)(g(\beta)\sqrt{2(F(1)-F(\beta))} - g(\alpha)\sqrt{-2F(\alpha)})}{(F(1) + Cg(\beta)\sqrt{2(F(1)-F(\beta))} - Cg(\alpha)\sqrt{-2F(\alpha)})^2},$$

and

$$\tilde{J} = \frac{-(g(\beta)\sqrt{2(F(1)-F(\beta))} - g(\alpha)\sqrt{-2F(\alpha)})}{F(1) + Cg(\beta)\sqrt{2(F(1)-F(\beta))} - Cg(\alpha)\sqrt{-2F(\alpha)}}.$$

Near $p = \alpha$, the solution of this equation is positive. It remains positive for all $p \in (\alpha, \beta)$ because if $z_C(p)$ becomes too small the equation tells us that its derivative is positive, since $g(\alpha)C < \sqrt{-2F(\alpha)}$.

Therefore, $\frac{dz_C(p)}{dp} \geq 0$, indicating that z_C is increasing, and consequently, $z_C(p) \geq z_C(\alpha) = 0$. This implies that the solution w_α is increasing with respect to C, meaning that for each β, there exists a unique $C = \gamma(\alpha, \beta)$ such that $w_\alpha(\beta) = F(1)$. We can rename this solution as $w_{\alpha,\beta}$ so that

$$\begin{cases} \frac{dw_{\alpha,\beta}}{dp} = CJ\sqrt{2(\frac{w_{\alpha,\beta}(p)}{J} - F(p)) + C^2 g(p)^2 + 2Cg(\alpha)\sqrt{-2F(\alpha)}} \\ \qquad\qquad -C^2 J g(p)[1+g'(p)], \\ w_{\alpha,\beta}(\alpha) = 0, \ w_{\alpha,\beta}(\beta) = F(1) \end{cases} \tag{4.9}$$

To recover the value of L such that $w_{\alpha,\beta}$ comes from a solution p_α of (4.8), with

$$p_\alpha(0) = \beta \ \ and \ \ \frac{1}{2} p_\alpha^{'}(0^-)^2 + F(p_\alpha(0)) = F(1).$$

We simply need to note that $L = \int_\beta^\alpha X_\alpha^{'}(p)dp$. To calculate it from $w_{\alpha,\beta}$, we observe that

$$X_\alpha^{'}(p) = \frac{1}{p_\alpha^{'}(X_\alpha(p))}.$$

Therefore, we define

$$\lambda(\alpha, \beta) = \int_\alpha^\beta \frac{1}{\sqrt{2(\frac{w_{\alpha,\beta}(p)}{J} - F(p) + \frac{C^2}{2} g(p)^2 + Cg(\alpha)\sqrt{-2F(\alpha)}}} dp$$

Recall that $p_\alpha^{'} < 0$ on $]0, L[$, so $L = \lambda(\alpha, \beta)$ is uniquely defined.

Before moving on to the second objective, let us state some useful properties of the functions $\gamma(\alpha, \beta)$ and $\lambda(\alpha, \beta)$ defined in the lemma 31. These properties will be demonstrated immediately afterward. First, we denote $\xi = \frac{s_f}{2s_h}$.

Corollary 32.

1. *The functions γ and λ are continuous on (α, β), $\xi < \alpha < \frac{s_f}{s_h} < \beta < 1$, $\alpha < \theta_c$.*
2. *$\gamma(\alpha, \beta)$ is increasing in α and decreases in β. $\lambda(\alpha, \beta)$ is increasing in β.*
3. *The functions γ and λ satisfy the following properties: $\gamma(\alpha, \beta) \to +\infty$ as $\beta \searrow \alpha$, $\lambda(\alpha, \beta) \to +\infty$ as $\beta \to 1$, and $\lambda(\alpha, \beta) \to 0$ as $\beta - \alpha \to 0$.*

Our objective now is to demonstrate that for a given couple (C, L), it is possible to find values α and β such that C is equal to $\gamma(\alpha, \beta)$ and L is equal to $\lambda(\alpha, \beta)$. We first note that the limit of $\gamma(\alpha, \beta)$ as α approaches ξ and β approaches 1 can be established based on the monotonic properties described in corollaire 32. Furthermore, it is worth noting that $\gamma(\alpha, \beta)$ is bounded from below by c_*. Consequently, for any $\alpha \in (\xi, \theta_c)$ and $\beta \in (\xi, 1)$, the following limits hold:

$$\lim_{\beta \to 1} \gamma(\alpha, \beta) = C_\alpha, \quad \lim_{\alpha \to \xi} \gamma(\alpha, \beta) = C_\beta$$

Let $C > c_*$. Our aim is to demonstrate the existence of a unique $\alpha \in (\xi, \theta_c)$ such that $C_\alpha = C$. We observe that the function $\alpha \mapsto C_\alpha$ is continuous and increasing, as stated in corollaire 32. Therefore, it is sufficient to prove that the limit as α approaches θ_c of C_α is infinite. Once this condition is established, defining α_c as the value satisfying $C_{\alpha_c} = C$ will yield the desired result.

Similarly, we will demonstrate the existence of a unique $\beta \in (\xi, 1)$ such that $C_\beta = C$. Once again, we observe that the function $\beta \mapsto C_\beta$ is continuous, decreasing. Therefore, it suffices to prove that $\lim_{\beta \to \xi} C_\beta = +\infty$.

We now aim to show that $C_{\theta_c} = C_2 = +\infty$, where $C_{\theta_c} = \lim_{\alpha \to \theta_c} C_\alpha$ and $C_2 = \lim_{\beta \to \xi} C_\beta$. The fact that $C_2 = +\infty$ is a direct consequence of corollaire 32. Next, assuming, by contradiction, that $C_{\theta_c} < +\infty$, we proceed to find a solution to the following system:

$$\begin{cases} -p'' - C_{\theta_c} p' - C_{\theta_c}^2 g(p) = f(p), & on \ \ ]0\,;L[, \\ -p'' = f(p), & on \ \ [0\,;L]^c, \\ p'(0^-) - p'(0^+) = C g(p(0)), \\ p'(L^-) - p'(L^+) = -C g(p(L)), \\ p(-\infty) = 1, \ p(+\infty) = 0, \ p > 0. \end{cases}$$

By multiplying by p' and integrating over $(L, +\infty)$, we obtain:

$$-\int_L^{+\infty} p''(x) p'(x) = \int_L^{+\infty} f(p(x)) p'(x) dx.$$

Implies that

$$\frac{1}{2} p'(L^+)^2 = \int_L^{+\infty} f(p(x)) p'(x) dx.$$

Letting $u(x) = p(x)$, we have:

$$\frac{1}{2} p'(L^+)^2 = -\int_0^{p(L)} f(u) du.$$

Since $p'(L^+) = p'(L^-) + C g(p(L))$, then:

$$\frac{1}{2}(p'(L^+))^2 = \frac{1}{2}(p'(L^-))^2 + Cp'(L^-)g(p(L)) + \frac{1}{2}C^2 g(p(L))^2.$$

This yields:

$$\frac{1}{2}(p'(L^-))^2 + Cp'(L^-)g(p(L)) + \frac{1}{2}C^2 g(p(L))^2 = -F(p(L)).$$

Which implies:

$$p'(L^-) + \frac{1}{2}Cg(p(L)) = 0.$$

On the other hand,

$$p'(L^-) + \frac{1}{2}Cg(p(L)) = p'(L^+) - \frac{1}{2}Cg(p(L)).$$

Which further implies:

$$p'(L^+) = \frac{1}{2}Cg(p(L)).$$

Absurd since p is decreasing over $(L, +\infty)$ and $\frac{1}{2}Cg(p(L)) > 0$. Therefore, we conclude that $C_{\theta_c} = C_2 = +\infty$. According to Corollaire 32, for any $\alpha \in (\xi, \theta_c)$, there exists a unique $\beta > \alpha$ such that $\lambda(\alpha, \beta) = L$. □

Proof of Theorem 9.

Theorem 9 is a direct consequence of Lemmas 30 and 31. □

Before moving on to the proof of the final main results, we prove the properties presented in Corollary 32.

Proof of Corollary 32.

1. We have $w'_{\alpha,\beta}(p) = J\gamma(\alpha,\beta)H(w_{\alpha,\beta}(p), p) - \gamma(\alpha,\beta)^2 Jg(p)[1 + g'(p)]$, where $w(\alpha) = 0$, $w(\beta) = F(1)$, and

$$H(w_{\alpha,\beta}(p), p) = \sqrt{2\left(\frac{w_{\alpha,\beta}(p)}{J} - F(p)\right) + C^2 g(p)^2 + 2Cg(\alpha)\sqrt{-2F(\alpha)}}$$

   is a solution of a differential equation with boundary conditions.

   On the set $(\alpha, \beta), \xi < \alpha < \frac{s_f}{s_h} < \beta < 1$, $\alpha < \theta_1$, the functions H and g are continuous, which implies the continuity of w with respect to γ and, consequently, the continuity of γ with respect to β (when $w(\alpha) = 0$) and with respect to α (when $w(\beta) = F(1)$). This implies the continuity of λ.

2. ⋆ Let $\xi < \alpha < \frac{s_f}{s_h} < \beta < 1$, $\alpha < \theta_1 < \theta_c$, $C = \gamma(\alpha, \beta)$, and w be the solution to (4.9) associated with C and β. Similarly, let $\tilde{\beta} > \beta$, $\tilde{C} = \gamma(\alpha, \tilde{\beta})$, and $\tilde{w}$ be the solution to (4.9) associated with $\tilde{C}$ and $\tilde{\beta}$ (i.e., $\tilde{w}(\tilde{\beta}) = F(1)$). We assume by contradiction that $\tilde{C} \geq C$. Then, $\tilde{w}$ is a supersolution to the equation satisfied by w with the initial condition $\tilde{w}(\alpha) = 0$. Hence, $\tilde{w} > w$ over $[\alpha, \beta]$, which implies $\tilde{w}(\beta) > w(\beta) = F(1) = \tilde{w}(\tilde{\beta})$. This implies that $\tilde{w}$ is decreasing, which contradicts the fact that $\tilde{w}$ is increasing. Therefore, we conclude that $\tilde{C} \leq C$. Since $w(\alpha) = \tilde{w}(\alpha) = 0$, it follows that $w \geq \tilde{w}$ on the interval

(α, β).

$\star$ We can calculate :

$$\int_\alpha^{\tilde{\beta}} \frac{1}{\sqrt{2(\frac{\tilde{w}(p)}{J} - F(p) + \frac{\tilde{C}^2}{2} g(p)^2 + \tilde{C} g(\alpha)\sqrt{-2F(\alpha)})}} dp$$
$$> \int_\alpha^{\beta} \frac{1}{\sqrt{2(\frac{w(p)}{J} - F(p) + \frac{C^2}{2} g(p)^2 + C g(\alpha)\sqrt{-2F(\alpha)})}} dp$$

which demonstrates the monotonicity of the function λ.

$\star$ Let $\xi < \alpha < \frac{s_f}{s_h} < \beta < 1$, $C = \gamma(\alpha, \beta)$, and w be the solution to (4.9) associated with C and α. Similarly, let $\tilde{\alpha} > \alpha$, $\tilde{C} = \gamma(\tilde{\alpha}, \beta)$, and $\tilde{w}$ be the solution to (4.9) associated with $\tilde{C}$ and $\tilde{\alpha}$ (i.e., $\tilde{w}(\tilde{\alpha}) = 0$).

Suppose by contradiction that $\tilde{C} \leq C$. This implies that $\tilde{w} < w$ on $[\alpha, ; \beta]$, which further implies that $\tilde{w}(\alpha) < w(\alpha) = 0 = \tilde{w}(\tilde{\alpha})$.

Therefore, $\tilde{w}$ is decreasing, which contradicts the fact that $\tilde{w}$ is increasing. Hence, γ is increasing in α.

3.

$\star$ As β approaches α, $C = \gamma(\alpha, \beta) \to +\infty$. Indeed, we have already proven it above:

$$w_\alpha(p) \leq \frac{J}{2} F(\theta_1) - \frac{J}{2} C^2 \max_{[0,1]} g(p)^2 - JCg(\alpha)\sqrt{-2F(\alpha)}$$
$$+ \left(\frac{\sqrt{2}C}{\sqrt{J}} (p - \alpha) - C^2 \frac{J}{\sqrt{2}} \int_\alpha^p \frac{g(u)}{\eta} (1 + g'(u)) du \right.$$
$$\left. + \sqrt{\frac{J}{2}} \sqrt{-2F(\theta_1) + C^2 \max_{[0,1]} g(p)^2 + 2Cg(\alpha)\sqrt{-2F(\alpha)}} \right)^2.$$

Taking $p = \beta$, we obtain:

$$w_\alpha(\beta) \leq JF(\theta_1) - \frac{J}{2} C^2 \max_{[0,1]} g(p)^2 - JCg(\alpha)\sqrt{-2F(\alpha)}$$
$$+ \left(\frac{\sqrt{2}C}{\sqrt{J}} (\beta - \alpha) - C^2 \frac{J}{\sqrt{2}} \int_\alpha^\beta \frac{g(u)}{\eta} (1 + g'(u)) du \right.$$
$$\left. + \sqrt{\frac{J}{2}} \sqrt{-2F(\theta_1) + C^2 \max_{[0,1]} g(p)^2 + 2Cg(\alpha)\sqrt{-2F(\alpha)}} \right)^2.$$

If $\gamma(\alpha, \beta)$ does not tend to $+\infty$ as $\beta \to \alpha$, then this function would be bounded, as it is monotonic. Therefore, by taking the limit in the inequality, we obtain

$$F(1) < 0.$$

This contradicts the fact that $F(1) = \int_0^1 f(t)dt > 0$. Thus, we conclude that $\gamma(\alpha, \beta) \to +\infty$ as $\beta \to \alpha$.

$\star$ As β approaches 1, $\lambda(\alpha,\beta) \to +\infty$. Indeed, we observe that the function $\gamma(\alpha,\cdot)$ is decreasing and bounded from below by c_*. Therefore, it converges to a limit C_∞ as $\beta \to 1$. Since $\lambda(\alpha,\cdot)$ is increasing, if it does not diverge to $+\infty$, then it converges to a limit λ_∞. Consider the system of equations:

$$\begin{cases} -p'' - \gamma(\alpha,\beta)p' - \gamma(\alpha,\beta)^2 g(p) = f(p), \\ \frac{1}{2}p'(0)^2 + F(\beta) = F(1),\ \frac{1}{2}p'(L)^2 + F(\alpha) = 0. \end{cases}$$

If $\beta \to 1$, then we obtain the following system of equations:

$$\begin{cases} -p'' - C_\infty p' - C_\infty^2 g(p) = f(p), \\ \frac{1}{2}p'(0)^2 + F(1) = F(1), \quad \frac{1}{2}p'(\lambda_\infty)^2 + F(\alpha) = 0. \end{cases}$$

This implies $p'(0) = 0$, which in turn gives $p \equiv 1$ by uniqueness. However, this contradicts $\frac{1}{2}p'(\lambda_\infty)^2 + F(\alpha) = 0$. Therefore, we conclude that $\lambda(\alpha,\cdot) \to +\infty$ as $\beta \to 1$.

$\star$ As β approaches α, $\lambda(\alpha,\beta) \to 0$. We know that

$$2\left(\frac{w(p)}{J} - F(p) + \frac{C^2}{2}g(p)^2 + Cg(\alpha)\sqrt{-2F(\alpha)}\right) > 2Cg(\alpha)\sqrt{-2F(\alpha)}.$$

Therefore,

$$\lambda(\alpha,\beta) = \int_\alpha^\beta \frac{1}{\sqrt{2\left(\frac{w(p)}{J} - F(p) + \frac{C^2}{2}g(p)^2 + Cg(\alpha)\sqrt{-2F(\alpha)}\right)}} dp$$

$$\leq \int_\alpha^\beta \frac{dp}{\sqrt{2Cg(\alpha)\sqrt{-2F(\alpha)}}} = \frac{\beta - \alpha}{\sqrt{2Cg(\alpha)\sqrt{-2F(\alpha)}}}.$$

If $\beta \to \alpha$, we deduce that $\lambda(\alpha,\beta) \to 0$.

□

Having established the properties, we now proceed with the proof of the final main result, which is Proposition 28.

Proof of Proposition 28.

The result follows directly from the maximum principle, given that $\bar{P}$ is a barrier and $p^{ini} \leq \bar{P}$. Therefore, the solution remains bounded by $\bar{P}$ for all $t \geq 0$, implying that the spreading stops. □

The results of Theorem 9 and Proposition 28 conclude that if the initial positive solution is smaller than the stationary solution, it can never reach or exceed the stationary solution. Indeed, the stationary solution acts as a barrier to propagation. The term 'blocking' is therefore justified, as it describes the situation where the solution consistently remains below the stationary solution, thus confirming the phenomenon of propagation blocking.

4.5 Numerical simulations

We performed numerical simulations of Mathematical Model (3.4) to illustrate our theoretical results. We used the parameter values listed in Table 4.1 below, which were estimated based on the conditions identified in the theoretical results.

Parameters	Interpretations	Values
s_f	A dimensionless parameter that reflects the reduced fecundity of infected mosquitoes	0.015
F_u	Fecundity	1
d_u	Mortality rate of non-infected mosquitoes	0.30
d_i	Mortality rate of infected mosquitoes	0.315
δ	The ratio $\frac{d_i}{d_u}$	1.05
s_h	Cytoplasmic incompatibility parameter	0.7

Table 4.1: Specified parameter values for the model. The values used in the simulations are inspired by those presented in [24].

We performed numerical simulations of the system in a one-dimensional space. The simulations spanned a time interval from $t = 0$ to $T = 600$ days. The numerical domain used was the interval $[-40, 40]$, representing a total width of 80 units. This domain was discretized using a semi-implicit finite difference scheme with 2000 spatial points, resulting in a spatial step size of $dx = \frac{2L}{2000}$. A time step of $dt = 0.7$. The implicit scheme efficiently handled the complex terms in the system.

Neumann boundary conditions were applied at the edges of the domain, ensuring consistent behavior at the boundaries.

In these simulations, the function $K(x)$, which directly influences the propagation dynamics, was defined as follows:

$$K(x) = \begin{cases} A, & \text{for } x < 0, \\ Ae^{Cx}, & \text{for } x \in [0, \frac{L}{2}], \\ Ae^{CL}, & \text{for } x > \frac{L}{2}. \end{cases}$$

The constant C, which appears in the exponential expression of $K(x)$, plays a crucial role in determining the propagation dynamics. As demonstrated in Lemma 3.2, small values of C allow continuous propagation. For instance, with $C = 0.0001$, the results illustrate uninterrupted propagation, as shown in Figures 4.1 and 4.2.

In a second simulation, we studied a propagation blocking scenario by extending the simulation duration to $T = 800$ days. A moderately high value of C, sufficiently large to cause blocking but not excessive to avoid unrealistic numerical behaviors, was used. Specifically, we set $C = 0.4$. The observed blocking can be explained by the exponential nature of the function $K(x)$, where higher values of C effectively limit propagation. The results illustrate the blocking of propagation, as shown in Figures 4.3 and 4.4.

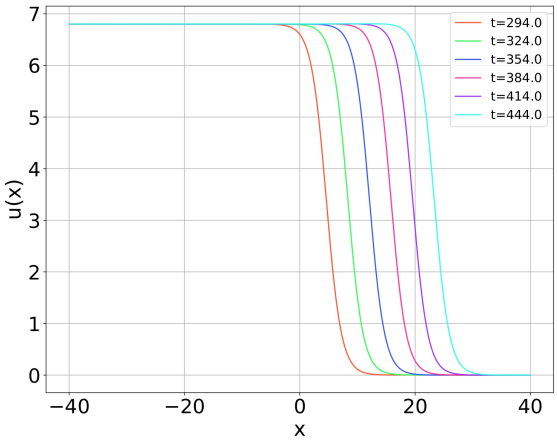

Figure 4.1: Propagation of Infected Mosquitoes at Constant Speed Over Time.

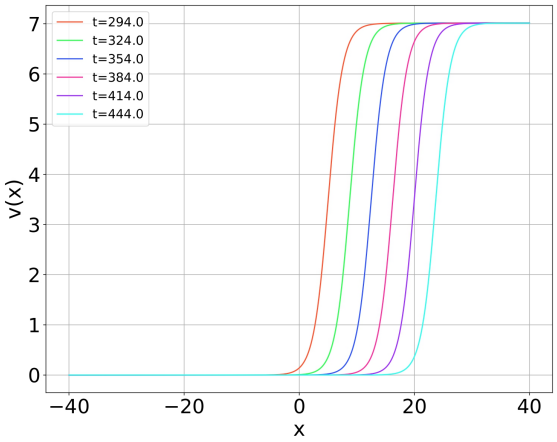

Figure 4.2: Propagation of Non-Infected Mosquitoes at Constant Speed Over Time.

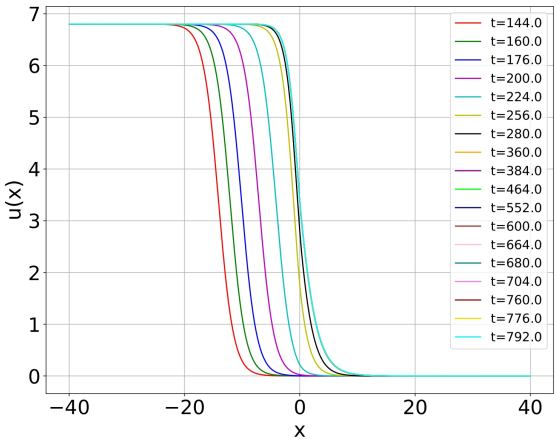

Figure 4.3: Blocking of Infected Mosquito Propagation.

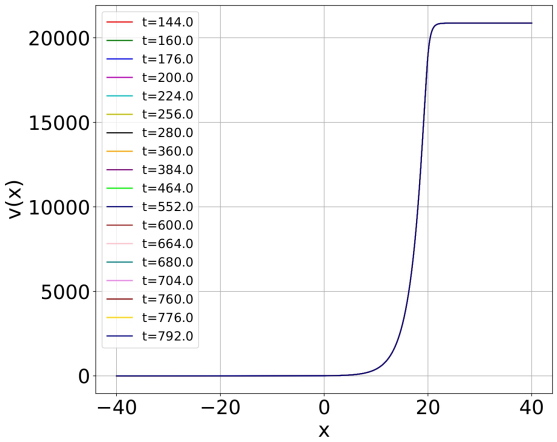

Figure 4.4: Blocking of Non-Infected Mosquito Propagation.

4.6 Conclusion

Our work has contributed to deepening the understanding of strategies to control mosquito-borne disease epidemics. A mathematical model describing the introduction of the endosymbiotic bacterium *Wolbachia* was used to analyze the spatial propagation mechanisms of the replacement of the mosquito population. While propagation already exists when the carrying capacity K is constant, our study focused on the potential blocking of this propagation in heterogeneous environments.

More specifically, we investigated scenarios where the environmental carrying capacity varies significantly across different regions of the spatial domain. Our results highlighted that such environmental heterogeneity can pose a major obstacle to the effective replacement of mosquito populations with *Wolbachia*-carrying populations. These findings are of great importance for the development of targeted control strategies.

Part III

Intracellular Signaling and Compartmentalization

Abstract

The results presented in this chapter stem from a collaboration with Claire Alamichel, Juan Calvo, Erwan Hingant, Nathan Quiblier, and Romain Yvinec. They were obtained during my participation in CEMRACS 2022 and have been published in the journal ESAIM [1].

We present a novel approach to modeling receptor-activated signaling pathways that take into account the compartmentalization of receptors and their effectors, both on the cell surface and in dynamic intracellular vesicles called endosomes. The first building block of the model concerns compartment dynamics. It takes into account creation of de novo endosomes, i.e. endocytosis, and further recycling of endosomes to the cell surface or degradation, as well as fusion of endosomes via coagulation dynamics. The second building block concerns biochemical reactions on the cell surface and within intra-cellular compartments. Both building blocks are coupled by the transfer of molecules that occurs at each event that modifies the compartments.

The model is formulated as a integro-partial differential equation, with transport and coagulation operators, and source terms, coupled to an integro-differential equation. In this work, we prove sufficient conditions to obtain exponential ergodicity for the size distribution of intracellular compartments. We further design a finite volume scheme to simulate our model. Finally, we show two application cases that show qualitative agreement with recently published data, proving that our model can help capture the spatio-temporal complexity of receptor-activated signaling pathway.

CHAPTER 5

MODELING COMPARTMENTALIZATION WITHIN INTRACELLULAR SIGNALING PATHWAY

"Do what you can, with what you have, where you are."

Theodore Roosevelt

5.1 Introduction

G Protein Coupled Receptors (GPCR) are a large class of transmembrane receptors: they are proteins located at the cell surface (plasma membrane) that are specialized in receiving (binding to) extracellular molecules, called ligand. The ligand-bound receptor will subsequently affect biochemical changes through the plasma membrane towards intracellular molecules. GPCR thus play a key role in the signal transduction, which allows long range cell communications mediated by ligand (*e.g.* hormones, cytokines, growth factors *etc*) and leads to major changes in the metabolism and activity of a cell [61, 77]. In addition, GPCR form an important class of targeted pharmaceutical agents in many different physiological contexts.

A receptor-activated signalling pathway, or biochemical cascade, is a chain of biochemical events activated by a receptor upon ligand binding. A series of signal transducers, or effector molecules, are activated within a reaction network (with typically many feedbacks and/or feedforward loops) and ultimately leads to a cell response, *e.g.* changes in gene expression, cell growth, metabolism [51]. Recently, it has been shown that GPCR are pleiotropic: they are able to selectively activate different signalling pathways. Distinct biochemical events can indeed be modulated by the nature of the ligand (either native physiological ligand or pharmaceutical agent) and the specific 3D conformational structured adopted by the ligand-bound receptor. This pleiotropy sheds light into important cell regulation mechanisms that need to be taken into account to design efficient therapeutic strategies [50].

GPCR do not permanently stay at the plasma membrane. Rather, an important desensitization mechanism of signaling pathways is receptor endocytosis. Receptor endocytosis is the internalization inside the cell of a vesicle surrounded by an area of cell membrane which contains receptor (and other) molecules. Endocytosis is an active form of transport of molecules. The vesicles, called endosomes, and their molecular content, can further be degraded by cell machinery through hydrolytic enzymes, or be partly recycled back to the plasma membrane. These spatial movements induce, upon ligand binding, an heterogeneous

population of receptors spread out between plasma membrane and a dynamic population of endosomes with distinct micro-environment. Within the context of receptor-activated signalling pathways, the processes of endocytosis, degradation and/or recycling are commonly referred to receptor trafficking, and provide further cell regulation mechanisms of signaling pathways [15]. Key evidence have indeed shown that the intra-cellular traffic of internalized receptors has a major impact in cell response to a given stimuli [48, 87].

In this work, we will focus our applications on a specific class of receptors that share in common the activation of the same effector molecule, the cyclic adenosine monophosphate (cAMP). For a number of GPCR among this class, including the Beta-2 Adrenergic Receptors (β2AR) [52], the parathyroid hormone receptor (PTHR) [47], the luteinizing hormone receptor (LHR) [64], or the follicle-stimulating hormone receptor (FSHR) [79], after ligand binding, the production of cAMP occurs first at the plasma membrane and later on from a highly dynamic pool of endosomes following internalization of the receptor by endocytosis. This spatio-temporal dimension of signaling has been found to have a significant impact on physiological functions, such as the control of serum calcium by PTHR signaling [97], or the resumption of meiosis by LHCGR signaling [64].

Thus, to faithfully represent the complexity of signalling pathways, we need to take into account the dynamic of the transient pool of specialised endosomes [83, 15, 88] following receptor stimulation, and its role on the reaction networks involved in the signalling pathways. The current biological hypothesis is that the endosomal compartments provide a dynamic and heterogeneous compartmentalised structure that allows specialised effector molecules to be separated from the bulk cytoplasm (physically separated through a lipid bilayer) in order to have a proper function of the cell response.

Classical ways to model the dynamic behaviour of signalling pathways use Chemical Reaction Networks [46], either in a deterministic formalism using ordinary differential equations [31], or in a stochastic formalism (typically when few molecules are present) using continuous-time Markov chains [9]. Both approaches typically assume the law of mass action and an idealised homogeneous environment. When spatial dynamics is important to take into account, one may use reaction-diffusion models to represent for instance spatial gradients [51], or compartmental models, to physically represent segregation between static compartments [93]. Note that in most applied literature, like in the field of epidemiology (*e.g.* SIR model), compartmental models refers to finite-dimensional dynamical systems where one variable is associated to each compartment, and the model described fluxes between compartments.

Up to our knowledge, relatively few works have addressed the issue of representing explicitly the segregation of molecules in a dynamic environment. The peculiarity of receptor trafficking at play within signalling pathways is that the endosomal compartments are created upon receptor activation, and their number, their size and their molecular content evolved dynamically, within a similar time scale than that of the signalling pathways activation. A first attempt of defining such models, within the context of signalling pathways, dates back to [33] and uses a deterministic population dynamics formalism to follow a population of compartments, structured by their size and molecular content, and which undergo coagulation-fragmentation like dynamics, representing endocytosis, fusion, fission, recycling and degradation. Recently, a stochastic counterpart has been proposed by [25, 72, 8]. To the best of our knowledge, a model that represents the chemical reactions that take place both at plasma membrane and within a dynamic population of endosomal compartment has never been considered and represents a novelty of our current work.

In this work, we define and study the long-time behavior and numerical schemes of minimal deterministic models that can represent compartmentalised signalling pathways, taking inspiration from [33]. Furthermore, we provide two simple examples of our model that show

that this model is able to represent qualitatively main experimental observations on cAMP signaling from [47, 97].

5.2 Modelling compartmentalised signalling pathways

The first objective is to be able to define a model to simulate the endosomal compartment dynamics from their size structure perspective only. We adopt a deterministic population dynamic approach, where individuals are structured by a single positive variable (their size). From biological observations, the main processes that shape the size distribution of the endosomal population include:

- Endocytosis: creation of a de-novo compartment from the cell membrane;
- Removal of compartment: either recycling back to the cell membrane, or degradation through lysosomal pathways;
- Fusion: binary coagulation of compartments.

Let $g = g(t, r)$ be the population density of endosomal compartments at time $t \in \mathbb{R}^+$ and size (volume) $r \in \mathbb{R}^+$. The evolution equation for g, that takes into account the three mechanisms above is given by, for all $t > 0$ and $r > 0$:

$$\frac{\partial g(t,r)}{\partial t} = \underbrace{Q(g,g)(t,r)}_{\text{coagulation}} + \underbrace{\alpha(r)}_{\text{endocytosis}} - \underbrace{\gamma(r)g(t,r)}_{\text{removal}}, \tag{M1}$$

where

$$Q(g,g)(t,r) = \frac{1}{2}\int_0^r \kappa(r-r',r')g(t,r-r')g(t,r')\mathrm{d}r' - \int_0^\infty \kappa(r,r')g(t,r)g(t,r')\mathrm{d}r' . \tag{5.1}$$

In the sequel, we denote $g(0, r) = g_0(r)$ the initial condition of Eq. (M1). A similar equation may be found in [33, 2]. The coagulation operator is quadratic: two compartments of respective size r, r' fuse in one compartment of size $r + r'$ at rate $\kappa(r, r')$. One obtains Eq. (5.1) by considering all compartments that reach size r and all that leave size r. The kernel $\kappa \geq 0$ is symmetric ($\kappa(r, r') = \kappa(r', r)$), such that the coagulation operator Eq. (5.1) preserves mass ($\int rQ(g, g)(r)dr = 0$). In particular, we have (at least formally),

$$\frac{\mathrm{d}}{\mathrm{d}t}\int_0^\infty rg(t,r)dr = \int_0^\infty r\alpha(r)\mathrm{d}r - \int_0^\infty \gamma(r)rg(t,r)\mathrm{d}r . \tag{5.2}$$

Endocytosis is a zero-order process at rate α (source term), compartment removal is a first-order process and occurs at a rate γ. In the sequel, model (M1) will be referred as our 1D model.

The second modelling step is to include molecular content into Eq. (M1). One may first think as an additional one dimensional structure variable. The first example we have in mind is the quantity of (active) receptor within each compartment, which is of primary interest to represent receptor trafficking within cells (see application in subsection 5.5.1). The second example we have in mind is the production of cAMP effector molecules, both at the plasma membrane and within each endosomes (see application in subsection 5.5.2). Thanks to this second structuring variable, besides compartment dynamics, we aim to represent:

- Biochemical reactions inside each compartment. Reaction rates are dependent on local abundances of molecular species, as well as the size (and more generally other physical variable like pH) of the compartment.
- Biochemical reactions that occur at the plasma membrane.
- Molecular conservation laws that may hold at each event that modifies the compartments, in particular between membrane and compartments. Hence we will now distinguish between compartment degradation and compartment recycling.

Let $f = f(t, r, a)$ be the population density of compartments at time $t \in \mathbb{R}^+$, size (volume) $r \in \mathbb{R}^+$ and molecular content $a \in \mathbb{R}^+$. Let also $M = M(t) \in \mathbb{R}^+$ be the molecular quantity at the plasma membrane. The joint evolution equation for f, M is , for all $t > 0$, $r > 0$ and $a > 0$,

$$\frac{\partial f(t,r,a)}{\partial t} + \underbrace{\frac{\partial \left(V(r,a) f(t,r,a)\right)}{\partial a}}_{\text{reactions}} = \underbrace{\tilde{Q}(f,f)(t,r,a)}_{\text{coagulation}} + \underbrace{\alpha(r,a,M(t))}_{\text{endocytosis}} - \underbrace{\gamma(r,a) f(t,r,a)}_{\text{degradation}} - \underbrace{\lambda(r,a) f(t,r,a)}_{\text{recycling}}, \tag{M2a}$$

$$\frac{\mathrm{d}M(t)}{\mathrm{d}t} = \underbrace{J_M(M(t))}_{\text{reactions}} - \underbrace{\int_0^\infty \int_0^\infty a\alpha(r,a,M(t))\mathrm{d}a\mathrm{d}r}_{\text{endocytosis}} + \underbrace{\int_0^\infty \int_0^\infty a\lambda(r,a) f(t,r,a)\mathrm{d}a\mathrm{d}r}_{\text{recycling}}, \tag{M2b}$$

where

$$\tilde{Q}(f,f)(t,r,a) = \frac{1}{2}\int_0^r \int_0^a \kappa(r-r',r') f(t,r-r',a-a') f(t,r',a')\mathrm{d}a'\mathrm{d}r' - \int_0^\infty \int_0^\infty \kappa(r,r') f(t,r,a) f(t,r',a')\mathrm{d}a'\mathrm{d}r' . \tag{5.3}$$

In the sequel, we denote $f(0,r,a) = f_0(r,a)$ and $M(0) = M_0$ the initial conditions of Eqs. (M2a)-(M2b).

In Eq. (M2a), the extension of the coagulation and endocytosis processes to include the second structuring variable a is clear. Note that we chose the coagulation kernel to be dependent on the size of the compartments (not their molecular content), for the sake of simplicity. The removal terms are now splitted in two: the degradation occurs at rate γ, and the recycling occur at rate λ. The transport term represents the biochemical reactions that modify the molecular content within each compartment, and which occur at rate $V(r,a)$. Also, the endocytosis rate α is necessarily dependent on the molecular content of the plasma membrane M, to avoid negative values for M, e.g. $\alpha(r,a,0) = 0$. In Eq. (M2b), J_M represent biochemical reactions that occur at the plasma membrane, and the two integral terms represent the molecules that are lost or gained at the plasma membrane through respectively

the endocytosis or recycling processes. The Eq. (M2b) on the scalar variable M was not present in [33] and, to the best of our knowledge, it is a novelty of our model. Still interpreting the molecular content as a quantity of receptors, it allows to represent conservation laws of receptors between plasma membrane and endosomal compartments, giving a satisfactory representation of the biological concept of receptor *trafficking*: receptors (together with other molecules) undergo directed movement back-and-forth between plasma membrane and intra-cellular endosomal compartments. In particular, we have (at least formally),

$$\begin{aligned}\frac{\mathrm{d}}{\mathrm{d}t}\left(\int_0^\infty\int_0^\infty rf(t,r,a)\mathrm{d}r\mathrm{d}a\right) &= \int_0^\infty\int_0^\infty r\alpha(r,a,M(t))\mathrm{d}r\mathrm{d}a \\ &\quad -\int_0^\infty\int_0^\infty \gamma(r,a)rf(t,r,a)\mathrm{d}r\mathrm{d}a \\ &\quad -\int_0^\infty\int_0^\infty \lambda(r,a)rf(t,r,a)\mathrm{d}r\mathrm{d}a\,,\end{aligned} \tag{5.4}$$

and

$$\begin{aligned}\frac{\mathrm{d}}{\mathrm{d}t}\left(\int_0^\infty\int_0^\infty af(t,r,a)\mathrm{d}r\mathrm{d}a + M(t)\right) &= J_M(M(t)) \\ &\quad +\int_0^\infty\int_0^\infty V(r,a)f(t,r,a)\mathrm{d}r\mathrm{d}a - \int_0^\infty\int_0^\infty \gamma(r,a)af(t,r)\mathrm{d}r\mathrm{d}a\,.\end{aligned} \tag{5.5}$$

The choice of the rate functions α, γ, λ and κ mainly governs the compartment size dynamics. In [33, 2], the authors consider a one-dimensional model (M1) with constant coagulation kernel, constant first-order rate γ, and exponentially decaying source rate $\alpha(r) = Ce^{-r/a_0}$. The choice of the rate functions V and J_M will mainly impact the molecular content at the plasma membrane and within compartments. Its choice may be guided by the underlying chemical reactions that take place at the plasma membrane and within compartments. Linear or polynomial functions may thus be suitable to represent mass action kinetic law.

In the sequel, the model given by Eqs. (M2a)-(M2b) will be referred as our 2D model.

In the remaining, in Eq. (M1), Eqs. (M2a)-(M2b), all rate functions and initial conditions are nonnegative. Further, we do not address in this paper the well-posedness of solutions of either Eq. (M1) or Eqs. (M2a)-(M2b) and rather take for granted that a unique sufficiently smooth nonnegative solution is given.

5.3 Long time behavior of the 1D model (M1)

In this section we provide sufficient conditions so that Eq. (M1) exhibits a unique globally stable steady state. The large-time behaviour of this equation -also known as *coagulation equation with source and efflux* [18], has been studied first in [34] with drift, in [23, 60] without efflux, in [85] with a bounded coagulation kernel and in [37] with a singular coagulation kernel. Here, we limit ourselves to give a self-contained proof of exponential stability of the steady state in L^1 with bounded coagulation kernel. We mainly use a contraction argument, taking inspiration from [21].

Theorem 10.

Let g_0, α, κ, γ nonnegative. Assume α is integrable, κ and γ are bounded and morevover $\inf\gamma = \gamma_0 > 0$. *If*

$$3\|\kappa\|_{L^\infty}\|\alpha\|_{L^1} < \gamma_0^2\,, \tag{5.6}$$

then there exists a unique nonnegative stationary solution in $L^1(\mathbb{R}_+)$ of Eq. (M1)*, denoted by g_∞. Moreover,*

$$\|g_\infty\|_{L^1} \le \tfrac{\|\alpha\|_{L^1}}{\gamma_0}\,,$$

and for every solution $g \in C(\mathbb{R}_+, L^1(\mathbb{R}_+))$ we have

$$\lim_{t\to+\infty} \|g(t) - g_\infty\|_{L^1} = 0\,.$$

The convergence is at least exponential with rate $\frac{\gamma_0^2 - 3\|\kappa\|_{L^\infty}\|\alpha\|_{L^1}}{\gamma_0} > 0$.

We do not expect condition (5.6) to be optimal. See the discussion in Section 5.4.2. We assume here that well-posedness of a unique nonegative solution $g \in C(\mathbb{R}_+, L^1(\mathbb{R}_+))$ of Eq. (M1) is given. We note that this implicitly imposes conditions on the rate functions and the initial condition, which will at least need to be nonnegative and integrable. See [17] for more details.

Proof. First we prove existence and uniqueness of a stationary solution g_∞ thanks to a Banach fixed point argument. Let us define

$$X = \left\{ g \in L^1(\mathbb{R}_+) \,:\, g \geq 0,\ \|g\|_{L^1} \leq \frac{\|\alpha\|_{L^1}}{\gamma_0} \right\}.$$

Consider a constant $K \geq \|\gamma\|_{L^\infty} + \|\kappa\|_{L^\infty}\frac{\|\alpha\|_{L^1}}{\gamma_0}$. For $g \in X$ we define

$$T_K g = \frac{1}{K}\left(\alpha - \gamma g + Q(g,g) + Kg\right).$$

The operator T_K is well-defined since $Q(g,g)$ is also well-defined for any integrable g provided that κ is bounded [21, Lemma 3]. We aim to apply Banach's fixed point theorem for T_K on X -which is a closed subset of the Banach space $L^1(\mathbb{R}_+)$; this will give a stationary solution of Eq. (M1). Let $g \in X$, we have that

$$T_K g \geq \frac{1}{K}\left(K - \|\gamma\|_{L^\infty} - \|\kappa\|_{L^\infty}\|g\|_{L^1}\right) g\,. \tag{5.7}$$

Indeed, g and α are positive and κ is bounded, thus

$$Q(g,g) \geq -g(r)\int_0^\infty \kappa(r,r')g(r')\mathrm{d}r' \geq -\|\kappa\|_{L^\infty}\|g\|_{L^1} g(r)\,,$$

which leads to Eq. (5.7) thanks to the boundedness of γ. The fact that $\|g\|_{L^1} \leq \frac{\|\alpha\|_{L^1}}{\gamma_0}$ and the condition on K entail the positivity of $T_K f$. Then, because

$$\int_0^\infty Q(g,g)\,\mathrm{d}r = -\frac{1}{2}\int_0^\infty\int_0^\infty \kappa(r',r)g(r')g(r)\mathrm{d}r'\mathrm{d}r \leq 0\,,$$

we deduce that

$$\begin{aligned}\|T_K g\|_{L^1} &= \int_0^\infty \frac{1}{K}\left(\alpha(r) - \gamma g(r) + Q(g,g)(r) + Kg(r)\right)\mathrm{d}r \\ &\leq \frac{\|\alpha\|_{L^1}}{K} + \frac{K-\gamma_0}{K}\|g\|\,.\end{aligned}$$

But $K \geq \|\gamma\|_{L^\infty} \geq \gamma_0$, thus, for $g \in X$,

$$K\|T_K g\|_{L^1} \leq \|\alpha\|_{L^1} + (K-\gamma_0)\frac{\|\alpha\|_{L^1}}{\gamma_0} \leq K\frac{\|\alpha\|_{L^1}}{\gamma_0}\,,$$

and we conclude that $T_K g$ belongs to X. We now show that T_K is a contraction on X. Let g and h in X. It is straightforward to check that

$$\|T_K g - T_K h\|_{L^1} \leq (1 - \frac{\gamma_0}{K})\|g - h\|_{L^1} + \frac{1}{K}\|Q(g,g) - Q(h,h)\|_{L^1} .$$

By a simple computation (see e.g. [21, Lemma 3] or [85, 17]),

$$\|Q(g,g) - Q(h,h)\|_{L^1} \leq \frac{3}{2}\|\kappa\|_{L^\infty}(\|g\|_{L^1} + \|h\|_{L^1})\|g - h\|_{L^1} \tag{5.8}$$

$$\leq 3\|\kappa\|_{L^\infty}\frac{\|\alpha\|_{L^1}}{\gamma_0}\|g - h\|_{L^1}. \tag{5.9}$$

Thus, we have

$$\|T_K g - T_K h\|_{L^1} \leq \left(1 + \frac{1}{K}(3\|\kappa\|_{L^\infty}\frac{\|\alpha\|_{L^1}}{\gamma_0} - \gamma_0)\right)\|g - h\|_{L^1} .$$

Then the hypothesis Eq. (5.6) allows us to conclude that there exists a unique fixed point to T_K in X. Moreover, this is the unique stationary solution which is positive and belongs to L^1. Indeed, assume we have a positive stationary solution $g \notin X$ i.e. in L^1 satisfying $\gamma_0 \int g > \|\alpha\|_{L^1}$. Then

$$0 = \int_0^\infty (\alpha(r) - \gamma(r)g(r) + Q(g,g)(r))\, \mathrm{d}r \leq \|\alpha\|_{L^1} - \gamma_0 \int_0^\infty g(r)\, \mathrm{d}r < 0 ,$$

which is a contradiction.

We now turn to the proof of asymptotic stability. Let $g \in C(\mathbb{R}_+, L^1(\mathbb{R}_+))$ be a nonnegative solution to Eq. (M1) in the sense of distributions and let $g_\infty \in L^1(\mathbb{R}_+)$ be the stationary solution. We first provide a bound on g. We have

$$\begin{aligned}\frac{d}{dt}\int_0^\infty g(t,r)\mathrm{d}r &= \|\alpha\|_{L^1} - \gamma_0 \int_0^\infty g(t,r)\mathrm{d}r + \int_0^\infty Q(g,g)(t,r)\mathrm{d}r \\ &\leq \|\alpha\|_{L^1} - \gamma_0 \int_0^\infty g(t,r)\mathrm{d}r .\end{aligned}$$

Thus,

$$\|g(t,\cdot)\|_{L^1} \leq \|g(0,\cdot)\|_{L^1} e^{-\gamma_0 t} + \frac{\|\alpha\|_{L^1}}{\gamma_0} .$$

It is a classical computation that

$$\frac{\partial}{\partial_t}|g - g_\infty| = -\gamma(r)|g - g_\infty| + (Q(g,g) - Q(g_\infty, g_\infty))\, sign(g - g_\infty).$$

Thus, using Eq. (5.8),

$$\begin{aligned}&\frac{\mathrm{d}}{\mathrm{d}t}\|g(t,\cdot) - g_\infty\|_{L^1} \\ &\leq \left[-\gamma_0 + \frac{3}{2}\|\kappa\|_{L^\infty}\left(\|g(0,\cdot)\|_{L^1} e^{-\gamma_0 t} + \frac{\|\alpha\|_{L^1}}{\gamma_0} + \|g_\infty\|_{L^1}\right)\right]\|g(t,\cdot) - g_\infty\|_{L^1} \\ &\leq \left(3\|\kappa\|_{L^\infty}\frac{\|\alpha\|_{L^1}}{\gamma_0} - \gamma_0 + \frac{3}{2}\|\kappa\|_{L^\infty}\|g(0,\cdot)\|_{L^1} e^{-\gamma_0 t}\right)\|g(t,\cdot) - g_\infty\|_{L^1}.\end{aligned}$$

We conclude that

$$\|g(t,\cdot) - g_\infty\|_{L^1} \leq \|g(0,\cdot) - g_\infty\|_{L^1} e^{\frac{3\|\kappa\|_{L^\infty}}{2\gamma_0}\|g(0,\cdot)\|_{L^1} - \frac{\gamma_0^2 - 3\|\kappa\|_{L^\infty}\|\alpha\|_{L^1}}{\gamma_0}t} ,$$

which ends the proof. □

5.4 Numerical scheme for 1D and 2D models

In this section, we detail our Finite Volume numerical scheme used to simulate our models, and numerically illustrate their properties. In order to tackle the complexity of the model, we decided to construct a conservative scheme that preserves moments of the solution. To that, we use of the finite volume scheme framework, after reformulating the coagulation operator in a divergence form in the spirit of [16, 42]. The transport term is treated by an up-wind scheme. Remaining terms are approximated in a standard way. Time is treated by a first order Euler explicit approximation.

5.4.1 Finite volume scheme

We want to write a numerical scheme of the 2D model, Eqs. (M2a)-(M2b) using a finite volume method.

First we can rmk that, for $r > 0$ and $a > 0$, we can rewrite our Eq. (M2a) in the following conservative form [16]

$$\begin{aligned}\partial_t f(t,r,a) =& \frac{1}{ra}\partial_r\partial_a \mathcal{C}(f)(t,r,a) - \partial_a\left(V(r,a) f(t,r,a)\right) \\ &+ \alpha(r,a,M(t)) - \lambda(r,a) f(t,r,a) - \gamma(r,a) f(t,r,a),\end{aligned} \tag{5.10}$$

where

$$\mathcal{C}(f)(t,r,a) = \int_0^r \int_0^a r'a' \tilde{Q}(f,f)(t,r',a') \mathrm{d}a' \mathrm{d}r'.$$

From Eq. (5.10), we will first detail the truncation we use (step (i)) and the discretization (step (ii)). Then, we detail the finite volume approximation of the coagulation and first-order transport operator in the right-hand side of Eq. (5.10) (step (iii)). We finally sum-up the numerical scheme in the last step (step (iv)).

(i) Truncation. As in [42, 16], to study our equation, we will truncate the size variable to a maximal value $R > 0$ and the quantity of reactants variable to a maximal value $A > 0$ and we will choose a truncation of the functional $\mathcal{C}$. We chose the following truncation, given by, for any $r \leq R$ and $a \leq A$,

$$\begin{aligned}&\mathcal{C}_{\mathrm{c}}^{RA}(f)(t,r,a) = \\ &\frac{1}{2}\int_0^r\int_0^a r'a' \int_0^{r'}\int_0^{a'} \kappa(r'-r'',r'') f(t,r'-r'',a'-a'') f(t,r'',a'') \,\mathrm{d}a''\mathrm{d}r''\mathrm{d}a'\mathrm{d}r' \\ &- \int_0^r\int_0^a r'a' f(t,r',a') \int_0^{R-r'}\int_0^{A-a'} \kappa(r',r'') f(t,r'',a'') \,\mathrm{d}a''\mathrm{d}r''\mathrm{d}a'\mathrm{d}r'.\end{aligned} \tag{5.11}$$

The truncation in Eq. (5.11) ensures that no cluster of size larger than R and molecular content larger than A arise. It can be obtained from Eq. (5.3) using the truncated kernel $\kappa(r,r')\mathbb{1}_{r+r'<R}\mathbb{1}_{a+a'<A}$ instead of $\kappa(r,r')$. The equation we will numerically approximate is a truncated version of Eq. (5.10) on the time interval $[0,T]$, where $T > 0$. We then look at the equation, for any $0 < t < T$, $0 < r \leq R$ and $0 < a \leq A$,

$$\begin{aligned}\partial_t f^{RA}(t,r,a) =& \frac{1}{ra}\partial_r\partial_a \mathcal{C}_{\mathrm{c}}^{RA}\left(f^{RA}\right)(t,r,a) - \partial_a\left(V(r,a) f^{RA}(t,r,a)\right) \\ &+ \alpha(r,a,M(t)) - \lambda(r,a) f^{RA}(t,r,a) - \gamma(r,a) f^{RA}(t,r,a).\end{aligned} \tag{5.12}$$

Heuristically, we expect f^{RA} to be close to f as long as the mass of f outside $[0,R/2]\times[0,A/2]$ is small (so that coagulation that leads to compartment of size larger than R and molecular

content larger than A are unlikely). We call Eq. (5.12) a conservative truncation of Eq. (5.10) because the choice of the truncation of the coagulation operator does not lead to a loss of mass in the first moments. In particular, f^{RA} satisfies, at least formally, (compare to Eqs. (5.4)-(5.5)),

$$\begin{aligned}\frac{\mathrm{d}}{\mathrm{d}t}\left(\int_0^\infty\int_0^\infty r f^{RA}(t,r,a)\mathrm{d}r\mathrm{d}a\right) &= \int_0^\infty\int_0^\infty r\alpha(r,a,M)\mathrm{d}r\mathrm{d}a \\ &\quad - \int_0^\infty\int_0^\infty \gamma(r,a) r f^{RA}(t,r,a)\mathrm{d}r\mathrm{d}a \\ &\quad - \int_0^\infty\int_0^\infty \lambda(r,a) r f^{RA}(t,r,a)\mathrm{d}r\mathrm{d}a\,,\end{aligned} \tag{5.13}$$

and

$$\begin{aligned}\frac{\mathrm{d}}{\mathrm{d}t}\left(\int_0^\infty\int_0^\infty a f^{RA}(t,r,a)\mathrm{d}r\mathrm{d}a + M(t)\right) &= J_M(M(t)) \\ &\quad + \int_0^\infty\int_0^\infty V(r,a) f^{RA}(t,r,a)\mathrm{d}r\mathrm{d}a \\ &\quad - \int_0^\infty\int_0^\infty \gamma(r,a) a f^{RA}(t,r)\mathrm{d}r\mathrm{d}a\,.\end{aligned} \tag{5.14}$$

We choose to use a conservative truncation for our scheme in order to construct a scheme that preserves the conservation properties (5.13)-(5.14), as we will verify it in the case of pure coagulation.

(ii) Grids definition. Let $I^r \in \mathbb{N}$. We discretize the size interval $[0,R]$ into I^r intervals. We denote by $\left(r_{i-\frac{1}{2}}\right)_{i\in\{1,\dots,I^r+1\}}$ a regular mesh of $[0,R]$ with size step Δr and we set

$$r_i = \frac{r_{i-\frac{1}{2}} + r_{i+\frac{1}{2}}}{2} = \left(i - \frac{1}{2}\right)\Delta r, \quad i \in \{1,\dots,I^r\}\,.$$

Let $I^a \in \mathbb{N}$. We discretize the size interval $[0,A]$ into I^a intervals. We denote by $\left(a_{j-\frac{1}{2}}\right)_{j\in\{1,\dots,I^a+1\}}$ a regular mesh of $[0,A]$ with step Δa and we set

$$a_j = \frac{a_{j-\frac{1}{2}} + a_{j+\frac{1}{2}}}{2} = \left(j - \frac{1}{2}\right)\Delta a, \quad j \in \{1,\dots,I^a\}\,.$$

For all $i \in \{1,\dots,I^r\}$ and $j \in \{1,\dots,I^a\}$, we set

$$\Lambda_{ij} = \left[r_{i-\frac{1}{2}}, r_{i+\frac{1}{2}}\right] \times \left[a_{j-\frac{1}{2}}, a_{j+\frac{1}{2}}\right].$$

Let $\Delta t > 0$ be the time step. We discretize $[0,T]$ by the set of points $\{t^n = n\,\Delta t,\ n \in \{0,\dots,N\}\}$, where $N = \left\lfloor \frac{T}{\Delta t} \right\rfloor$.

(iii) Finite volume approximation. For all $n \in \{0,\dots,N\}$, $i \in \{1,\dots,I^r\}$ and $j \in \{1,\dots,I^a\}$, we denote $f^n_{i,j}$ an approximation of the function f^{RA} at the point (t^n, r_i, a_j). We will recursively calculate $f^n_{i,j}$ such that

$$f^n_{i,j} \approx \frac{1}{\Delta r \Delta a}\int_{\Lambda_{ij}} f^{RA}\left(t^n, r, a\right)\mathrm{d}a\mathrm{d}r.$$

Similarly, we denote by M^n an approximation of $M(t^n)$. First, we write the explicit forward Euler scheme in time associated to the Eq. (5.12). For all $n \in \{0, \dots, N-1\}$, we have

$$\begin{aligned}\frac{f^{RA}(t^{n+1},r,a) - f^{RA}(t^n,r,a)}{\Delta t} =& \frac{1}{ra}\partial_r\partial_a \mathcal{C}_{\mathrm{c}}^{RA}\left(f^{RA}\right)(t^n,r,a) \\ &- \partial_a\left(V(r,a)\, f^{RA}(t^n,r,a)\right) \\ &+ \alpha(r,a,M^n) - \lambda(r,a)\, f^{RA}(t^n,r,a) \\ &- \gamma(r,a)\, f^{RA}(t^n,r,a) + O(\Delta t).\end{aligned} \tag{5.15}$$

For each $i \in \{1, \dots, I^r\}$ and $j \in \{1, \dots, I^a\}$, we will integrate Eq. (5.15) over Λ_{ij}. We first deal with the coagulation operator. Approximating ra by the constant $r_{i-\frac{1}{2}} a_{j-\frac{1}{2}}$ on Λ_{ij}, and integrating, we obtain

$$\begin{aligned}&\int_{\Lambda_{ij}} \frac{1}{ra}\partial_r\partial_a \mathcal{C}_{\mathrm{c}}^{RA}\left(f^{RA}\right)(t^n,r,a)\,\mathrm{d}a\mathrm{d}r \\ &\approx \frac{1}{r_{i-\frac{1}{2}} a_{j-\frac{1}{2}}}\Bigg(\mathcal{C}_{\mathrm{c}}^{RA}\left(f^{RA}\right)\left(t^n, r_{i+\frac{1}{2}}, a_{j+\frac{1}{2}}\right) - \mathcal{C}_{\mathrm{c}}^{RA}\left(f^{RA}\right)\left(t^n, r_{i-\frac{1}{2}}, a_{j+\frac{1}{2}}\right) \\ &\quad - \mathcal{C}_{\mathrm{c}}^{RA}\left(f^{RA}\right)\left(t^n, r_{i+\frac{1}{2}}, a_{j-\frac{1}{2}}\right) + \mathcal{C}_{\mathrm{c}}^{RA}\left(f^{RA}\right)\left(t^n, r_{i-\frac{1}{2}}, a_{j-\frac{1}{2}}\right)\Bigg).\end{aligned} \tag{5.16}$$

Using a change of variable $r' - r'' \to r'$ in Eq. (5.11), and decomposing the first two integrals in telescopic sums we have,

$$\begin{aligned}&\mathcal{C}_{\mathrm{c}}^{RA}\left(f^{RA}\right)\left(t^n, r_{i+\frac{1}{2}}, a_{j+\frac{1}{2}}\right) = \\ &\frac{1}{2}\sum_{k=1}^{i}\sum_{m=1}^{j}\int_{r_{k-\frac{1}{2}}}^{r_{k+\frac{1}{2}}}\int_{a_{m-\frac{1}{2}}}^{a_{m+\frac{1}{2}}}\int_0^{r_{i+\frac{1}{2}}-r'}\int_0^{a_{j+\frac{1}{2}}-a'} (a'+a'')(r'+r'')\,\kappa(r',r'') \\ &\qquad\qquad \times f^{RA}(t^n,r',a')\, f^{RA}(t^n,r'',a'')\,\mathrm{d}a''\mathrm{d}r''\mathrm{d}a'\mathrm{d}r' \\ &- \sum_{k=1}^{i}\sum_{m=1}^{j}\int_{r_{k-\frac{1}{2}}}^{r_{k+\frac{1}{2}}}\int_{a_{m-\frac{1}{2}}}^{a_{m+\frac{1}{2}}} r'a' f^{RA}(t^n,r',a')\int_0^{R-r'}\int_0^{A-a'} \kappa(r',r'') \\ &\qquad\qquad \times f^{RA}(t^n,r'',a'')\,\mathrm{d}a''\mathrm{d}r''\mathrm{d}a'\mathrm{d}r'.\end{aligned}$$

Further, setting $\kappa_{k,k'} = \dfrac{1}{\Delta r^2}\displaystyle\int_{r_{k-\frac{1}{2}}}^{r_{k+\frac{1}{2}}}\int_{r_{k'-\frac{1}{2}}}^{r_{k'+\frac{1}{2}}} \kappa(r,r')\,\mathrm{d}r'\mathrm{d}r$, and approximating again product terms ra by their left value on Λ_{ij}, we approximate $\mathcal{C}_{\mathrm{c}}^{RA}$ by:

$$\begin{aligned}&\mathcal{C}_{\mathrm{c}}^{RA}\left(f^{RA}\right)\left(t^n, r_{i+\frac{1}{2}}, a_{j+\frac{1}{2}}\right) \\ &\approx \frac{1}{2}(\Delta r \Delta a)^2 \sum_{k=1}^{i}\sum_{m=1}^{j}\sum_{k'=1}^{i-k+1}\sum_{m'=1}^{j-m+1}\left(a_{m-\frac{1}{2}} + a_{m'-\frac{1}{2}}\right)\left(r_{k-\frac{1}{2}} + r_{k'-\frac{1}{2}}\right)\kappa_{k,k'} f^n_{k,m} f^n_{k',m'} \\ &\quad - (\Delta r \Delta a)^2 \sum_{k=1}^{i}\sum_{m=1}^{j}\sum_{k'=1}^{I^r-k+1}\sum_{m'=1}^{I^a-m+1} a_{m-\frac{1}{2}} r_{k-\frac{1}{2}} \kappa_{k,k'} f^n_{k,m} f^n_{k',m'},\end{aligned} \tag{5.17}$$

Plugging this latter approximation (5.17) into Eq. (5.16), we finally define the approximation of the coagulation operator, as

$$\begin{aligned}Q^n_{i,j}(f,f) = (\Delta r \Delta a)^2 \Bigg(&\frac{1}{2}\sum_{k=1}^{i}\sum_{m=1}^{j}\kappa_{k,i-k+1} f^n_{k,m} f^n_{i-k+1,j-m+1} \\ &- f^n_{i,j}\sum_{k=1}^{I^r-i+1}\sum_{m=1}^{I^a-j+1}\kappa_{i,k} f^n_{k,m}\Bigg).\end{aligned} \tag{5.18}$$

Note that the approximation $Q_{i,j}^n$ of $\tilde{Q}\left(f^{RA}, f^{RA}\right)$ is conservative (in the sense that it preserves the first moments in r and a), as we will show in the next section. Then, we use an upwind approximation for the transport term, together with an integration of transport velocity over r using the midpoint rule:

$$\begin{aligned}
&\int_{\Lambda_{ij}} \partial_a \left(V(r,a) f^{RA}(t,r,a)\right) da dr \\
&\quad = \int_{r_{i-\frac{1}{2}}}^{r_{i+\frac{1}{2}}} \left(V\left(r, a_{j+\frac{1}{2}}\right) f^{RA}\left(t, r, a_{j+\frac{1}{2}}\right)\right) \mathrm{d}r - \int_{r_{i-\frac{1}{2}}}^{r_{i+\frac{1}{2}}} \left(V\left(r, a_{j-\frac{1}{2}}\right) f^{RA}\left(t, r, a_{j-\frac{1}{2}}\right)\right) \mathrm{d}r \\
&\qquad \approx W_{i,j+\frac{1}{2}} f^{RA}\left(t, r_i, a_{j+\frac{1}{2}}\right) \Delta r - W_{i,j-\frac{1}{2}} f^{RA}\left(t, r_i, a_{j-\frac{1}{2}}\right) \Delta r \\
&\qquad \approx \Delta r \cdot \left[A^{\mathrm{up}}\left(W_{i,j+\frac{1}{2}}, f_{i,j}^n, f_{i,j+1}^n\right) - A^{\mathrm{up}}\left(W_{i,j-\frac{1}{2}}, f_{i,j-1}^n, f_{i,j}^n\right)\right], \quad (5.19)
\end{aligned}$$

where $W_{i,j-\frac{1}{2}} = \frac{1}{2}\left(V\left(r_{i+\frac{1}{2}}, a_{j-\frac{1}{2}}\right) + V\left(r_{i-\frac{1}{2}}, a_{j-\frac{1}{2}}\right)\right)$, $f_{i,0}^n = f_{i,I^r+1}^n = 0$, and the operator A^{up} is

$$A^{\mathrm{up}}(u, f_+, f_-) = \begin{cases} u f_+ & \text{if } u \geq 0, \\ u f_- & \text{if } u < 0. \end{cases}$$

(iv) Finite volume scheme. Finally, the scheme of the model (M2a)-(M2b) is given by:

- Initialization: For $i \in \{1, \ldots, I^r\}$ and $j \in \{1, \ldots, I^a\}$ we set

$$f_{i,j}^0 = \frac{1}{\Delta r \Delta a} \int_{\Lambda_{ij}} f(0, r, a) \, da dr.$$

- Time iteration: For all $n \in \{1, \ldots, N\}$, $i \in \{1, \ldots, I^r\}$ and $j \in \{1, \ldots, I^a\}$, using Eqs. (5.18)-(5.19), and an explicit forward Euler scheme in time for M, we set:

$$\begin{aligned}
f_{i,j}^{n+1} = f_{i,j}^n &+ \frac{\Delta t}{\Delta r \Delta a} Q_{i,j}^n(f, f) \qquad (5.20) \\
&- \frac{\Delta t}{\Delta a}\left[A^{\mathrm{up}}\left(W_{i,j+\frac{1}{2}}, f_{i,j}^n, f_{i,j+1}^n\right) - A^{\mathrm{up}}\left(W_{i,j-\frac{1}{2}}, f_{i,j-1}^n, f_{i,j}^n\right)\right] \\
&+ \frac{\Delta t}{\Delta r \Delta a}\Bigg[\int_{\Lambda_{ij}} \alpha(r, a, M^n) \, da dr - f_{i,j}^n \int_{\Lambda_{ij}} \lambda(r, a) \, da dr \\
&- f_{i,j}^n \int_{\Lambda_{ij}} \gamma(r, a) \, da dr\Bigg].
\end{aligned}$$

$$M^{n+1} = M^n + \Delta t \, J_M(M^n) - \Delta t \int_0^R \int_0^A a' \alpha(r', a', M^n) \, da' dr' \qquad (5.21)$$

$$+ \Delta t \sum_{i=1}^{I^r} \sum_{j=1}^{I^a} f_{i,j}^n \int_{\Lambda_{ij}} a \lambda(r, a) \, da dr. \qquad (5.22)$$

The remaining integrals in Eq. (5.20) are calculated using an automatic adaptive numerical integration method, detailed in [36] and implemented in the Julia package HCubature.

Remark 5. *With the same tools, we can write a scheme in dimension 1 for model* (M1)*, noticing that if we set* $h(t,r) = rg(t,r)$ *we have*

$$\partial_t h(t,r) = -\partial_r J(g)(t,r) + r\alpha(r, M(t)) - \gamma(r) h(t,r),$$

where $J(g)$ *is defined as follows*

$$J(g)(t,r) = \int_0^r \int_{r-r'}^{\infty} r'\kappa(r', r'') g(t,r') g(t,r'') \mathrm{d}r''\mathrm{d}r'.$$

A conservative truncation is then given by:

$$J_c^R(g)(t,r) = \int_0^r \int_{r-r'}^{R-r'} r'\kappa(r', r'') g(t,r') g(t,r'') \mathrm{d}r'' \mathrm{d}r'.$$

5.4.2 Numerical tests

In this section, we will investigate the behavior of the numerical scheme given by Eq. (5.20) in some particular cases. We aim to verify the conservation laws satisfied by the numerical scheme, the consistency and convergence properties of the numerical scheme, as well as to illustrate the long-time behavior we proved in Theorem 10.

Conservation laws and consistency. First, we will evaluate the numerical scheme in the case of a pure coagulation model ($\alpha = \gamma = \lambda = V = J_M = 0$). We consider the pure coagulation equation:

$$\partial_t f(t,r,a) = \tilde{Q}(f(t), f(t))(r,a), \quad \text{with } t > 0, r > 0 \text{ and } a > 0. \tag{5.23}$$

The discrete equation associated to Eq. (5.23) is given by, as a special case of Eq. (5.20) when $\alpha = \gamma = \lambda = V = J_M = 0$,

$$f_{i,j}^{n+1} = f_{i,j}^n + \frac{\Delta t}{\Delta r \Delta a} Q_{i,j}^n(f,f), \quad n \in \{1,\dots,N\}, \quad i \in \{1,\dots,I^r\} \text{ and } j \in \{1,\dots,I^a\}. \tag{5.24}$$

and where $Q_{i,j}^n$ is defined in Eq. (5.18). We remark that we keep the same properties on the moments dynamics for the two Eqs. (5.23) and (5.24). For some test function φ, we define $H(\varphi, t)$ the moment of f associated with the function φ at time $t > 0$,

$$H(\varphi, t) := \int_0^{\infty} \int_0^{\infty} \varphi(r,a) f(t,r,a) \mathrm{d}a\mathrm{d}r,$$

and $H^n(\varphi)$ its discrete analogue moment, associated with the function φ at time t^n with $n \in \{1,\dots,N\}$,

$$H^n(\varphi) := \Delta r \Delta a \sum_{i=1}^{I^r} \sum_{j=1}^{I^a} \varphi\left(r_{i-\frac{1}{2}}, a_{j-\frac{1}{2}}\right) f_{i,j}^n. \tag{5.25}$$

Then

$$\begin{aligned}
\frac{\mathrm{d}}{\mathrm{d}t} H(\varphi, t) &= \frac{\mathrm{d}}{\mathrm{d}t}\left[\int_0^{\infty} \int_0^{\infty} \varphi(r,a) f(t,r,a) \mathrm{d}a\mathrm{d}r\right] \\
&= \int_0^{\infty} \int_0^{\infty} \varphi(r,a) \tilde{Q}(f(t), f(t))(r,a) \mathrm{d}a\mathrm{d}r \\
&= \frac{1}{2} \int_0^{\infty} \int_0^{\infty} \int_0^{\infty} \int_0^{\infty} [\varphi(r+r', a+a') - \varphi(r,a) - \varphi(r',a')] \\
&\qquad \times \kappa(r,r') f(t,r,a) f(t,r',a') \mathrm{d}a'\mathrm{d}r'\mathrm{d}a\mathrm{d}r,
\end{aligned}$$

and similarly

$$\frac{H^{n+1}(\varphi)-H^{n}(\varphi)}{\Delta t}=\frac{(\Delta r\Delta a)^{2}}{2}\sum_{i=1}^{I^{r}}\sum_{j=1}^{I^{a}}\sum_{k=1}^{I^{r}-i+1}\sum_{m=1}^{I^{a}-j+1}\Big[\varphi\left(r_{i+k-1-\frac{1}{2}},a_{j+m-1-\frac{1}{2}}\right)$$
$$-\varphi\left(r_{i-\frac{1}{2}},a_{j-\frac{1}{2}}\right)-\varphi\left(r_{k-\frac{1}{2}},a_{m-\frac{1}{2}}\right)\Big]\kappa_{i,k}f_{i,j}^{n}f_{k,m}^{n}.$$

Thus choosing $\varphi(r,a)=r$ or $\varphi(r,a)=a$, we have that the first-order moments are constant in time both at the discrete and continuous levels, consistently with Eqs. (5.4)-(5.5) and Eqs. (5.13)-(5.14) for the pure coagulation case. We also have that the zeroth-order moments are non-increasing functions of time in both cases.

For the pure coagulation model given by Eq. (5.23), choosing an affine kernel $\kappa(r,r')=K_0+K_1(r+r')$ leads to a closed moment equation in the form of an ODE system. Indeed, in such case, it is easy to see that we have the following ODE system for the moments of order 0 and 1:

$$\begin{cases}\dfrac{\mathrm{d}}{\mathrm{d}t}H(1,t)=-\dfrac{1}{2}K_0\left(H(1,t)\right)^{2}-K_1H(1,t)\,H(r,t)\,,\\[2ex]\dfrac{\mathrm{d}}{\mathrm{d}t}H(r,t)=0,\\[2ex]\dfrac{\mathrm{d}}{\mathrm{d}t}H(a,t)=0.\end{cases}\tag{5.26}$$

Eq. (5.26) is of the form of a Bernoulli differential equation, and its analytical solution can be computed. The pure coagulation case with an affine kernel is thus an appropriate setting to compare analytical solutions with moments associated to our numerical scheme (5.24) calculated by Eq. (5.25). For this purpose, we introduce the following notation, for $x>0$:

$$\mathcal{N}_x(\mu,\sigma)=\frac{1}{\sqrt{2\pi}\sigma}e^{-\frac{1}{2}\left(\frac{x-\mu}{\sigma}\right)^{2}}\mathbf{1}_{x>0}\,.\tag{5.27}$$

We approximate the pure coagulation Eq. (5.23) using the scheme Eq. (5.24) with the following numerical parameters:

$$T=1\,,\Delta t=10^{-4}\,,\quad R=A=10\,,\Delta r=\Delta a=0.25\,.\tag{5.28}$$

We study two cases. The first one is the case of a constant kernel with the following model parameters:

$$\begin{aligned}&f_0(r,a)=0.5\cdot\left[\mathcal{N}_r(1.5,0.15)\times\mathcal{N}_a(0.5,0.3)+\mathcal{N}_r(0.5,0.3)\times\mathcal{N}_a(1.5,0.15)\right]\,,\\&\kappa(r,r')=0.5\,.\end{aligned}\tag{5.29}$$

The second one is the case of an affine kernel with the following model parameters:

$$\begin{aligned}&f_0(r,a)=0.5\cdot\left[\mathcal{N}_r(1.5,0.15)\times\mathcal{N}_a(0.5,0.3)+\mathcal{N}_r(0.5,0.3)\times\mathcal{N}_a(1.5,0.15)\right]\,,\\&\kappa(r,r')=0.5+0.1\,(r+r')\,.\end{aligned}\tag{5.30}$$

As expected, we recover from our numerical scheme (5.24) that the moment of order 0 is a nonincreasing function and the moments of order 1 are constant (Figure 5.1). Moreover, we also observed that these numerical results are very close to the analytical solutions directly computed from Eq. (5.26) (Figures 5.2 and 5.3). Relative error of moments of order 0 are increasing through time, as expected from the fact that the size-truncation of the numerical scheme (5.24) implies more and more error as compartments gets bigger in pure-coagulation dynamics.

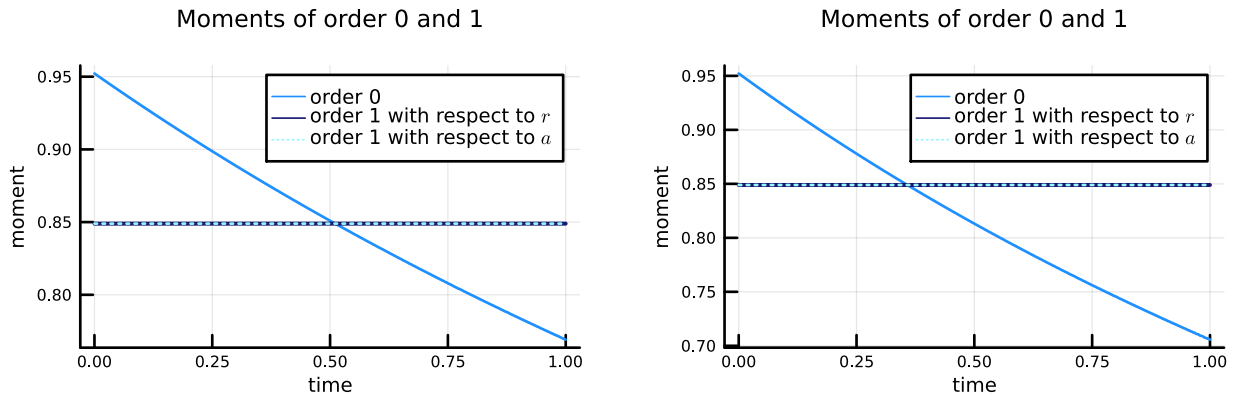

Figure 5.1: *Time evolution of the moments of order* 0 *and* 1 *(see inserted legend) computed from our pure coagulation numerical scheme* (5.24)*, with the constant kernel and the model parameters* (5.29) *for the left picture and with the constant kernel and the model parameters* (5.30) *for the right one. The results are obtained with the numerical parameters* (5.28)*. In both cases, the moment of order* 0 *is a nonincreasing function and the moments of order* 1 *are constant. With the choice of our initial condition, both moments of order* 1 *in* r *and* a *superimposed.*

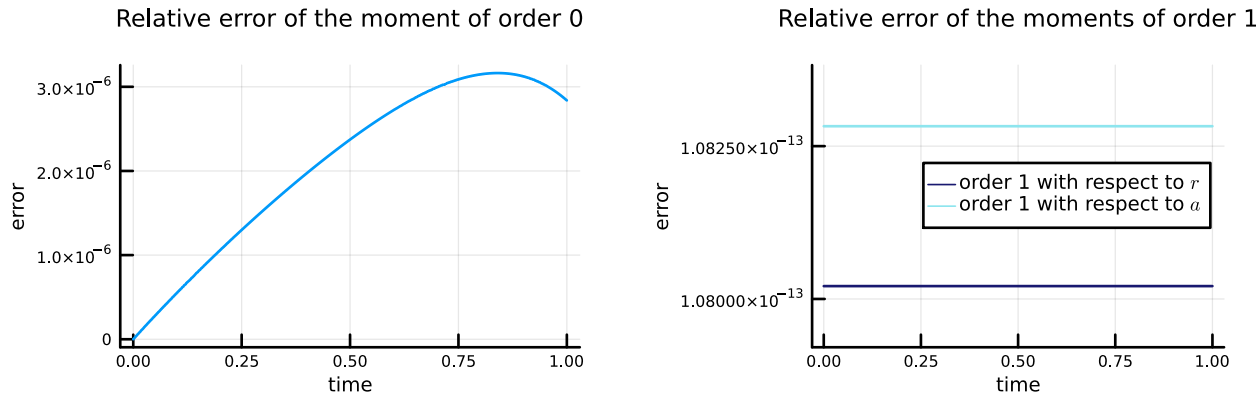

Figure 5.2: *Relative error of the moments of order 0 (left panel) and 1 (right panel) between moments computed from our pure coagulation numerical scheme* (5.24) *and from the analytical solution of the ODE system Eq.* (5.26)*, in the case of a constant kernel* (5.29) *with the same parameters as in the left panel of Figure 5.1.*

Convergence. We now investigate the convergence property of our numerical scheme given by Eq. (5.20) in a more general setting. We want to illustrate the convergence of the numerical scheme as the size steps Δr and Δa decreases to 0. Regarding stability, we expect the numerical scheme to be conditionally stable for small enough $\frac{\Delta t}{\Delta r \Delta a}$ as our scheme is a first-order finite volume scheme, but the proof of stability is out of the scope of this paper. See for instance [16] for stability results on the coagulation part. We thus fix a small enough time step Δt and choose $\Delta r = \Delta a = h$ with linearly decreasing h in a $log2$ scale, namely $h_m = \frac{h_0}{2^m}$ for integers m from 0 to 11 and $h_0 = \frac{1}{2}$. The finite volume size is then decreasing from h_0^2 to $\left(\frac{h_0}{2^{11}}\right)^2$. We choose the finest solution as reference solution and compare the solutions defined on the coarser grids to this reference solution with the following different norms, defined for a function f and $k, l \in \mathbb{N}$ as follows:

$$\|f\|_{k,l} = \int_0^R \int_0^A r^k a^l \left| f\left(r, a\right) \right| \mathrm{d}a\mathrm{d}r.$$

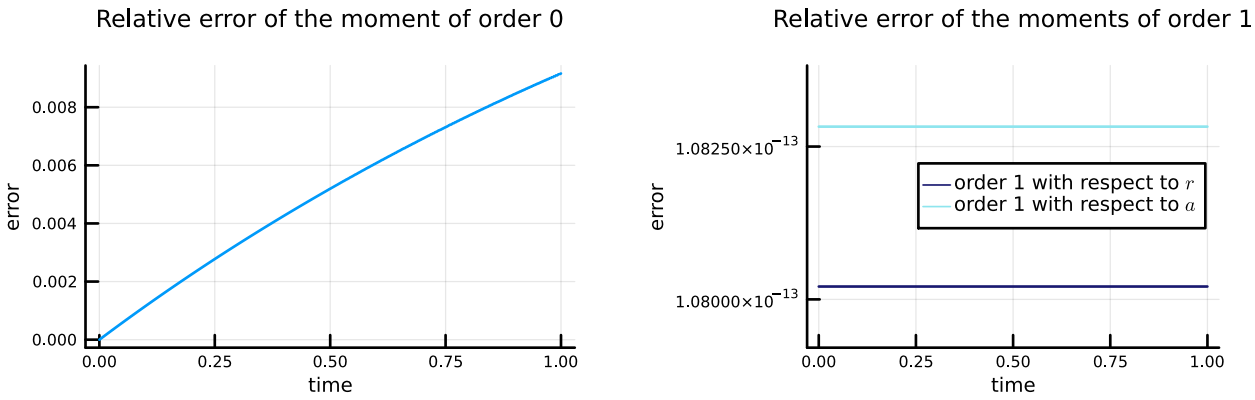

Figure 5.3: *Relative error of the moments of order 0 (left panel) and 1 (right panel) between moments computed from our pure coagulation numerical scheme* (5.24) *and from the analytical solution of the ODE system Eq.* (5.26)*, in the case of an affine kernel* (5.30) *with the same parameters as in the right panel of Figure 5.1.*

Those moment-based norms are natural within the context of coagulation equations, see e.g. Eqs. (5.13)-(5.14). The fact that the grids are nested allows to compute the following errors, for $m \in \{0, ...10\}$,

$$\|E(h_m, t^n)\|_{k,l} = h_{11}^2 \sum_{i=1}^{R/h_{11}} \sum_{j=1}^{A/h_{11}} r_{i-\frac{1}{2}}^k a_{j-\frac{1}{2}}^l \mid f_{i,j}^{n,h_m} - f_{i,j}^{n,h_{11}} \mid , \tag{5.31}$$

where the value of $f_{i,j}^{n,h_m}$ are extended from the coarser grid to the finer grid by taking its value constant over the subdomains defined by the finer grid. We compute the errors defined in Eq. (5.31) up to second order moments ($0 \leq k + l \leq 2$) in two different cases as we detail now. For that aim, we introduce the notation, for $x > 0$,

$$\mathcal{P}_x(\bar{x}, \epsilon) = \left(\frac{\bar{x} + \epsilon - x}{\bar{x} + \epsilon} \right)^{\frac{1}{3}} \left(\frac{x}{\bar{x}} \right)^{\frac{2}{3}} . \tag{5.32}$$

(i) Case 1 We approximate the pure coagulation case Eq. (5.23) (Figure 5.4) with the numerical parameters

$$\Delta t = 0.0005 \, , \quad R = A = 3 \, , \Delta r = \Delta a = h_m \, , \tag{5.33}$$

and the model parameters

$$\begin{aligned} f_0 \left(r, a \right) &= 0.5 \cdot \left[\mathcal{N}_r \left(1.5, 0.15 \right) \times \mathcal{N}_a \left(0.5, 0.3 \right) + \mathcal{N}_r \left(0.5, 0.3 \right) \times \mathcal{N}_a \left(1.5, 0.15 \right) \right] \, , \\ \kappa \left(r, r' \right) &= 0.5 \, . \end{aligned} \tag{5.34}$$

(ii) Case 2 We approximate the general case Eqs. (M2a)-(M2b) (Figure 5.5), with the model parameters

$$\begin{aligned}
f_0(r,a) &= 0.5 \cdot \Big[\mathcal{N}_r(1.5, 0.15) \times \mathcal{N}_a(0.5, 0.3) \\
&\qquad + \mathcal{N}_r(0.5, 0.3) \times \mathcal{N}_a(1.5, 0.15)\Big], \\
M_0 &= 20, \\
\kappa(r,r') &= 0.5, \\
\alpha(r,a,M) &= 0.1 \cdot M \cdot [\mathcal{N}_r(0.6, 0.01) \times \mathcal{N}_a(0.3, 0.05) + \mathcal{N}_r(0.3, 0.05) \times \mathcal{N}_a(0.6, 0.01)], \\
\gamma(r,a) &= 20(r-5)^4 \mathbf{1}_{r>5} + 10^{-5}, \\
\lambda(r,a) &= 10^{-2} \cdot \mathcal{P}_r(10, 0), \\
V(r,a) &= 0, \\
J_M(M) &= 0,
\end{aligned} \tag{5.35}$$

and the same numerical parameters as in Eq. (5.33). In both cases, we observe that the error decreases linearly (in log-log scale) when the size of the discretization step h does. For both cases, the order of the scheme appears to be 1.

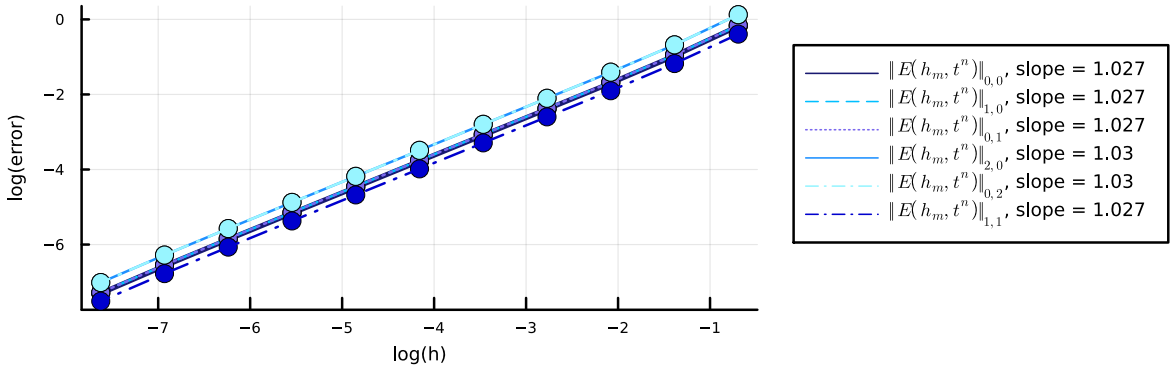

Figure 5.4: *Illustration of the convergence of the numerical scheme* (5.24) *in the case of the pure coagulation (case 1, numerical and model parameters given by Eqs.* (5.33)-(5.34)*) . We plot the error as a function of the grid size h, in log-log scale, using the six different norms* $\|E(h_m,t^n)\|_{k,l}$ *defined in Eq.* (5.31) *for* $0 \leq k+l \leq 2$ *(see inserted legend).*

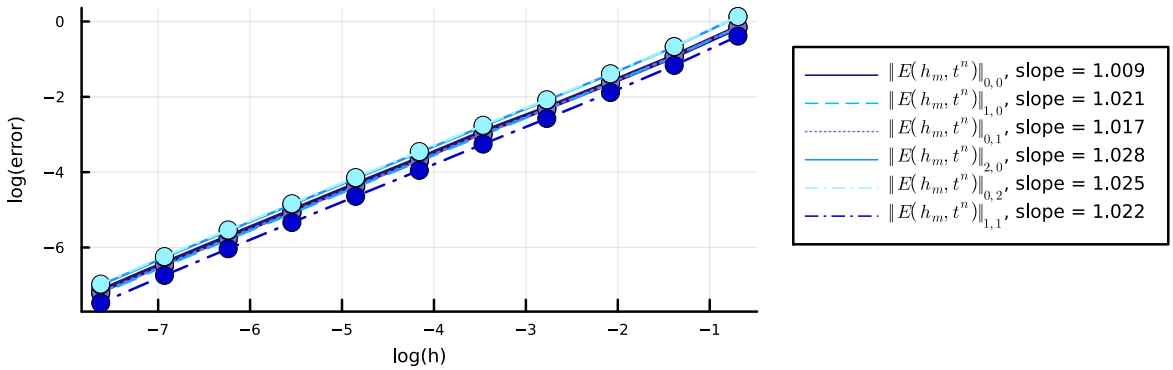

Figure 5.5: *Illustration of the convergence of the numerical scheme* (5.20) *in case 2 (numerical and model parameters given by Eqs.* (5.33)-(5.35)*). See legend of Figure 5.4.*

Long-time behavior. Finally, we we illustrate the long-time behavior of the numerical solutions and test the optimality of the conditions from the long time behavior given in Theorem 10 for the one dimensional model (M1), with the numerical parameters

$$\Delta t = 0.05\,, \quad R = 5\,, I^r = 301\,, \tag{5.36}$$

and the model parameters

$$\begin{aligned} f_0\,(r,a) &= 0.5 \cdot \mathcal{N}_r(0.2, 0.15)\,, \\ \kappa\,(r,r') &= 1\,, \\ \alpha\,(r,M) &= M \cdot \mathcal{N}_r(0.6, 0.1)\,. \end{aligned} \tag{5.37}$$

We show in Figure 5.6 two cases. In the first one (left hand-side), we use $\gamma\,(r) = \sqrt{3.1}$ together with Eq. (5.37), for which the condition Eq. (5.6) of Theorem 10 is satisfied. In the second one (right hand-side), we use $\gamma\,(r) = 0.7$ together with Eq. (5.37), for which the condition Eq. (5.6) is not satisfied. In both cases, the curves for $t = 10$ and $t = 50$ are superimposed, and we observe that the solution seems to converge to a stationary state. Numerically, while we verify the conclusion of Theorem 10 holds true, it seems that the condition Eq. (5.6) is too restrictive since the scheme stays stable in a wider range of parameters such that the condition Eq. (5.6) is not satisfied.

5.5 Applications

In this section we provide two applications of our 2D model given by Eqs. (M2a)-(M2b), that show good qualitative agreement with published experimental data on receptor-activated signaling pathways. Our simulations also provide additional insight, which calls for new experiments.

5.5.1 Receptor trafficking

The 2D model given by Eqs. (M2a)-(M2b) is ideally suited to model receptor trafficking from plasma membrane to endocytic comparments. As detailed in the introduction, the GPCR are typically located at the surface of the cells, on the plasma membrane. Upon ligand binding, the GPCR activate several signalling pathways as well as their own internalization through endocytosis. The vesicles still carry the internalised receptors on their surface. Endosomes are then sorted thanks to complex processes which are not yet fully understood,

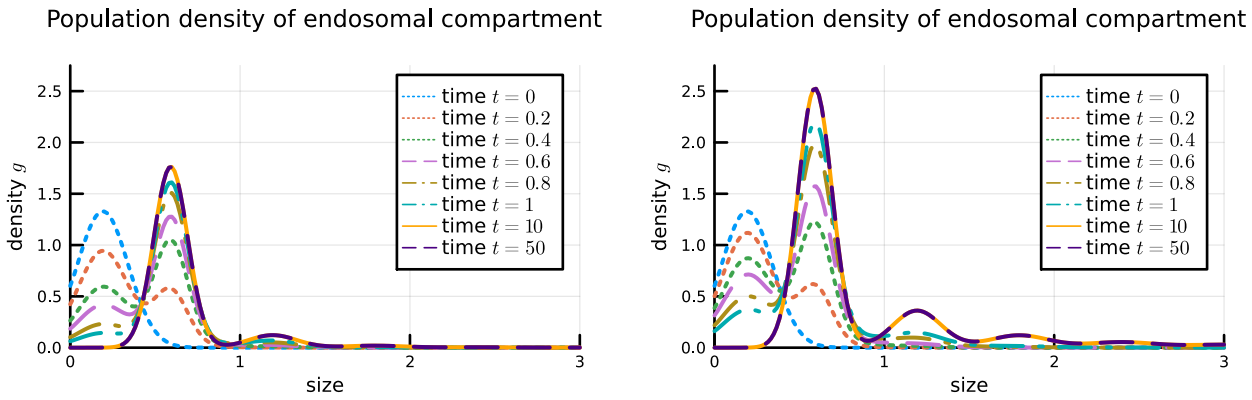

Figure 5.6: *Size-distribution of the population density g of endosomal compartement for model* (M1) *at different times (see inserted legend) and parameters given by Eqs.* (5.36)-(5.37). *On the left hand-side the condition Eq.* (5.6) *is satisfied ($\gamma(r) = \sqrt{3.1}$) whereas on the right hand-side the condition Eq.* (5.6) *is not satisfied ($\gamma(r) = 0.7$). In both cases, the curves for $t = 10$ and $t = 50$ are superimposed.*

but that depends both on the nature of the receptor and the ligand. Internalized receptors can indeed commit to several endosomal compartments of different kinds, and be recycled at the cell surface, which could impact on the kinetic profile of the receptor and its signalling pathways. Consequently, endocytosis regulate receptor cell surface density and signaling profile, and endosomal targeting of receptors may produce specificity in the signaling pathways. In particular, it has been shown [47] that the LHR and the B2AR are two GPCR that undergo divergent trafficking to distinct endosomal compartments. B2AR traffics mostly to early endosomes (EEs) and LHR to pre-early endosomes (pre-EEs). In short, the authors in [47] demonstrate that LHR endosome sizes increased over time quickly before reaching a plateau, producing a small endosome population (400-500 nm of diameter). The mean B2AR endosome sizes are bigger (1200-1400 nm of diameter). They also see that B2AR was more internalized than LHR in percentage but both receptors are equally recycled. The objective of this section is to provide numerical simulations of our model (M2a)-(M2b) that can reproduce these two distinct scenarios.

In order to compare qualitatively our model with the experimental results presented in [47], we choose the following parametrization (we recall definitions in Eqs. (5.27)-(5.32)):

$$\begin{aligned} f_0(r,a) &= 0\,, \\ M_0 &= 7.2 \times 10^{-4}\,, \\ \kappa(r,r') &= K_0\,, \\ \alpha(r,a,M) &= \overline{\alpha}\mathcal{N}_r(200,10) \times \mathcal{N}_a(r,0.5) \times M\,, \\ \gamma(r,a) &= 10^{-5} + 2 \times 10^1 \times \left(\frac{r-1950}{50}\right)^4 \mathbf{1}_{\{r>1950\}}\,, \\ \lambda(r,a) &= 10^{-2} \times \mathcal{P}_r(2000,0)\,, \\ V(r,a) &= 0\,, \\ J_M(M) &= 0\,, \end{aligned} \tag{5.38}$$

which we interpret as follows. Endosomes fuse at a constant coagulation kernel κ, whose rate will depend on the receptor. Endosomes are created with a size following a Gaussian law and with a quantity of reactant proportional to their size, and the rate $\overline{\alpha} > 0$ will depend on

the receptor. Small endosomes are degraded at constant (low) rate, and degradation rates quickly increases for endosomes large enough. Endosomes recycling increase with the surface of endosomes and decreases with their volume ($\lambda \propto r^{\frac{2}{3}} - r$). We don't consider reactions, e.g. V and J_M are taken as null functions.

For the numerical scheme, we take

$$T = 30, \Delta t = 10^{-1}, \quad I^r = I^a = 30, R = A = 2000. \tag{5.39}$$

To explain the qualitative differences between LHR and B2AR trafficking observed in [47], we tested two hypotheses here.

- (H1) In the first hypothesis (Figure 5.7), we modify only the internalization rate $\overline{\alpha} > 0$ between LHR and B2AR, with a higher internalization rate for the B2AR, keeping all the remaining parameters the same. This hypothesis is in line with [47]. LHR and B2AR affect only the endocytosis rate as follows (refer to Eq. (5.38)):

Parameters	K_0	$\overline{\alpha}$
LHR	5×10^{-1}	8×10^{-5}
B2AR	5×10^{-1}	3×10^{-4}

(5.40)

- (H2) In the second hypothesis (Figure 5.8), both the internalization rate and the coagulation rate are higher for the B2AR compared to the LHR (H2). LHR and B2AR affect the internalization and the coagulation rate as follows:

Parameters	K_0	$\overline{\alpha}$
LHR	5×10^{-3}	8×10^{-5}
B2AR	5×10^{-1}	3×10^{-4}

(5.41)

In [47], mean and variance of the size of the endosomal populations are measured at different time after ligand stimulation, as well as the internalization ratio, which corresponds to the fraction of internalised receptors among the total number of receptors initially present at the plasma membrane. Consistently, we define in the model the internalization ratio as $\frac{\|f\|_{0,1}(t)}{M_0}$. In both hypotheses the internalization ratio is well reproduced by the model, compared to [47]. The major discrepancy of the first hypothesis with the experiments is the variance in size of the endosomal population, which seems too high compared to experimentation. Furthermore the production of large endosomes with LHR seems too high and similar to the ones of B2AR (Figure 5.7). In the second hypothesis, however, these two discrepancies are not present anymore (Figure 5.8). These results indicate that the differences in endosome dynamics between LHR and B2AR signaling pathways seem not only due to a difference in internalization rate, but probably also to the coagulation dynamics inside cells. Difference in coagulation dynamics may be explained by differences in endosomes sorting and/or differences in molecular composition of endosomes, which are believed to be of different nature between LHR and B2AR vesicles [47].

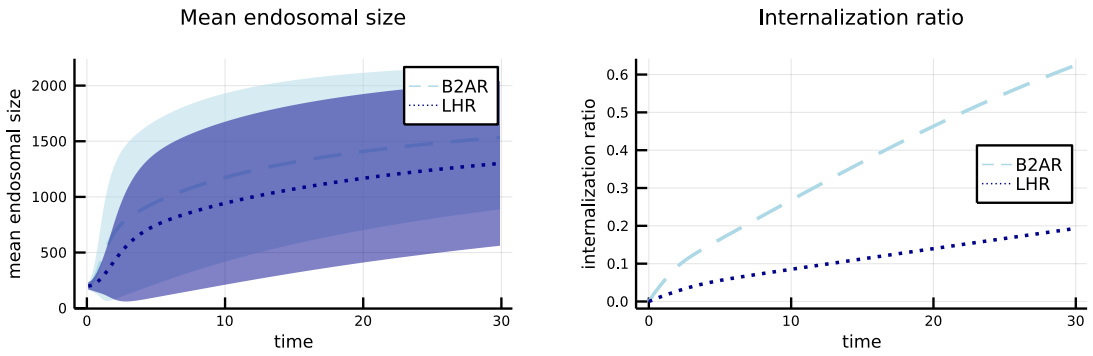

Figure 5.7: *Time evolution of the endosomal size (left panel) and internalization ratio (right panel). We numerically simulate the 2D model given by Eqs.* (M2a)-(M2b) *with parameters given by.* (5.38)-(5.39)-(5.40) *(LHR and B2AR affect only the internalization rate). On the left panel, the dashed blue (resp. dotted purple) line represents the mean endosomal size for B2AR (resp. LHR), that corresponds to* $\|f\|_{1,0}(t)/\|f\|_{0,0}(t)$*, and the shaded light area represents its standard deviation. On the right panel, the dashed blue (resp. dotted purple) line represents the internalization ratio for B2AR (resp. LHR), that corresponds to* $\frac{\|f\|_{0,1}(t)}{M_0}$.

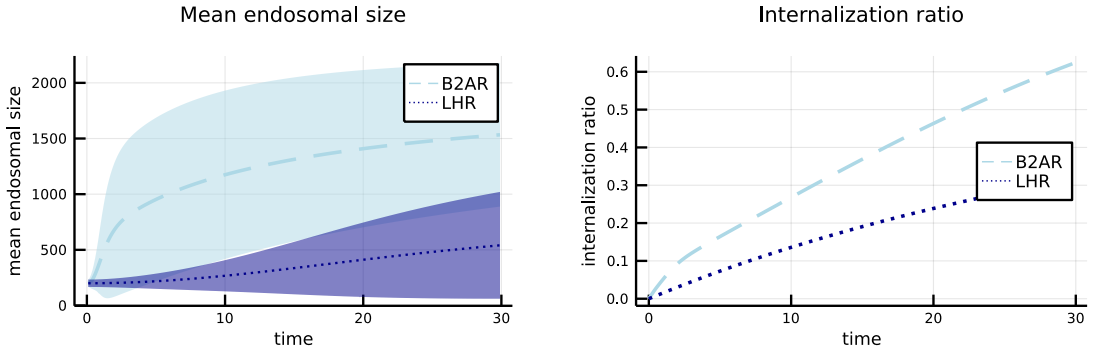

Figure 5.8: *Time evolution of the endosomal size (left panel) and internalization ratio (right panel). We numerically simulate the 2D model given by Eqs.* (M2a)-(M2b) *with parameters given by.* (5.38)-(5.39)-(5.41) *(LHR and B2AR affect the internalization and the coagulation rate). See legend of Figure 5.7 for details.*

5.5.2 Second effector signaling

The second application of our model we present here concerns the efficacy of second messenger molecules production as a function of the localization of the active receptor. We focus on the production of cAMP induced by the activation of the PTHR. Recent discoveries find that the PTHR may engage cAMP signaling not only at the cell's plasma membrane but also in early endosomes after receptor internalization through endocytosis [87]. Furthermore, the full-length parathyroid hormone (LA-PTH) induces through the activation of PTHR an augmentation of production of cAMP in the endosomes, whereas the ligand PTH 7D (PTHR peptide ligand through amino acid epimerization at position 7 of PTH^{1-34}) induces the production of cAMP at the plasma membrane. In White's paper [97], the authors show that even if the production place is different, the total amount of cAMP stays the same after some time, a phenomenon that could be named location-biased, and that can have implications for the cellular response. The objective of this section is to provide numerical simulations of our model (M2a)-(M2b) that can reproduce these two distinct scenarios.

We could reproduce qualitatively these observations with our model following this parametriza-

tion:

$$
\begin{aligned}
f_0(r,a) &= 0\,,\\
M_0 &= 0\,,\\
\kappa(r,r') &= 2\times 10^{-1}\,,\\
\alpha(r,a,M) &= \mathcal{N}_r(200,10)\times\mathcal{N}_a(0,0.1))\times M\,,\\
\gamma(r,a) &= \mathcal{P}_r(2000,100)\mathbf{1}_{\{r\le 1950\}} + 2\times 10^2\times\left(\frac{r-1950}{50}\right)^4\mathbf{1}_{\{r>1950\}}\,,\\
\lambda(r,a) &= 10^{-2}\times\mathcal{P}_r(2000,100)\,,\\
V(r,a) &= \left(v_s\mathbf{1}_{\{\epsilon\le r\le\bar r\}} + v_l\mathbf{1}_{\{\bar r<r\}}\right)\times\left(1-\frac{a}{pr}\right)\,,\quad \epsilon = 10/3, \bar r = 500\,,\\
J_M(M) &= v_M\times\left(\frac{\bar M - M}{\bar M}\right)\,,
\end{aligned}
\tag{5.42}
$$

which we interpret as follows. Endosomes fuse via a constant coagulation kernel, and are created with a size following a Gaussian law and with a quantity of reactant, independently of the size, taken as a positive fraction of the quantity M present at the plasma membrane. Endosomes recycling and degradation increase with the surface of endosomes and decrease with their volume (λ and $\gamma \propto r^{\frac{2}{3}} - r$). cAMP is produced at the plasma membrane at constant rate and linearly degraded, where both the saturation $\bar M$, and the production rate v_M may depend on the ligand. cAMP is produced in endosomes at two different rates, v_s, for the endosomes smaller than $\bar r$ and v_l, for larger endosomes. Also the amount of saturation depends linearly on the size of the endosomes (caracterized by a portion p of r). Here v_s, v_l and p may depend on the ligand.

For the numerical scheme, we take

$$
\Delta t = 3^{-2},\quad I^r = I^a = 30, R = 2000, A = 30\,. \tag{5.43}
$$

We have two different hypotheses to explain the different qualitative behaviour of the two ligand LA-PTH and PTH 7D described above:

- (H1) Suppose LA-PTH and PTH 7D differs in cAMP production kinetics only in terms of rate (Figure 5.9), with a higher rate for LA-PTH at the plasma membrane ($v_M^{PTH7D} < v_M^{LA-PTH}$), and a higher rate for PTH 7D in the endosomes ($v_s^{LA-PTH} < v_s^{PTH7D}$ and $v_l^{LA-PTH} < v_l^{PTH7D}$).

Parameters	v_s	v_l	p	v_M	$\bar M$
LA-PTH	0.05	0.02	1/20	3.5	10
PTH 7D	5	2	1/20	0.035	10

(5.44)

- (H2) Suppose LA-PTH and PTH 7D differs in cAMP production kinetics not only in terms of rate but also in terms of saturation (Figure 5.10) with $\bar M^{LA-PTH} > \bar M^{PTH^{7D}}$ and $p^{PTH^{7D}} > p^{LA-PTH}$.

Parameters	v_s	v_l	p	v_M	$\bar M$
LA-PTH	0.5	0.2	1/200	3.5	10
PTH 7D	5	2	1/20	0.35	1

(5.45)

With both hypotheses, we observe a much more efficient cAMP production at the plasma membrane with LA-PTH and a much more efficient cAMP production in the endosomes with PTH 7D (Figures 5.9 and 5.10). Consistently with the observation in [97], both total responses have similar magnitude for the time period of the numerical simulation.

However, from the numerical simulation presented in figures 5.9 and 5.10, the cAMP production has already reached a "stable" state at $T = 20$ for LA-PTH, while it keeps increaseasing for PTH 7D. Therefore, a longer time measurement could discriminate between both ligands.

Also we could notice a fine kinetic difference between the responses induces by LA-PTH and PTH 7D with the two hypotheses. Indeed, PTH 7D leads to a convex kinetic production of cAMP during the early dynamics, which switches to a concave kinetic at later time. Whereas with LA-PTH the production stays concave all time long. Of course this behaviour may be quite complicated to observe experimentally due to the accuracy of the measures.

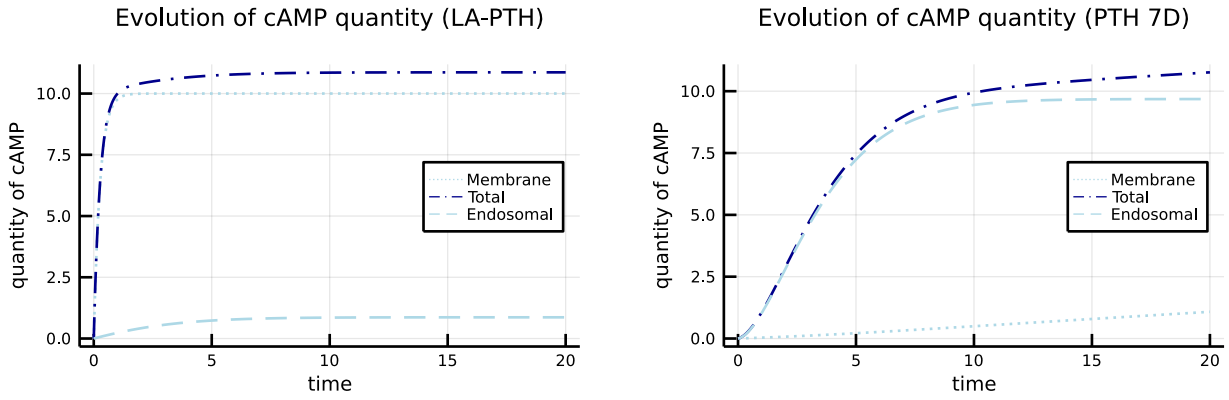

Figure 5.9: *Time evolution of the cAMP production for the LA-PTH ligand (left panel) and the PTH-7D ligand (right panel). We numerically simulate the 2D model given by Eqs.* (M2a)-(M2b) *with parameters given by.* (5.42)-(5.43)-(5.44) *(cAMP kinetic parameters differ between PTH 7D and LA-PTH only by the production rate). In both panels, the dotted blue line shows the endosomal quantity of cAMP, given by* $\|f\|_{0,1}(t)$*, the dashed blue line shows the cAMP quantity at the plasma membrane, given by* $M(t)$*, and the dashed-dotted purple line shows the total cAMP quantity* $(\|f\|_{0,1}(t) + M(t))$*.*

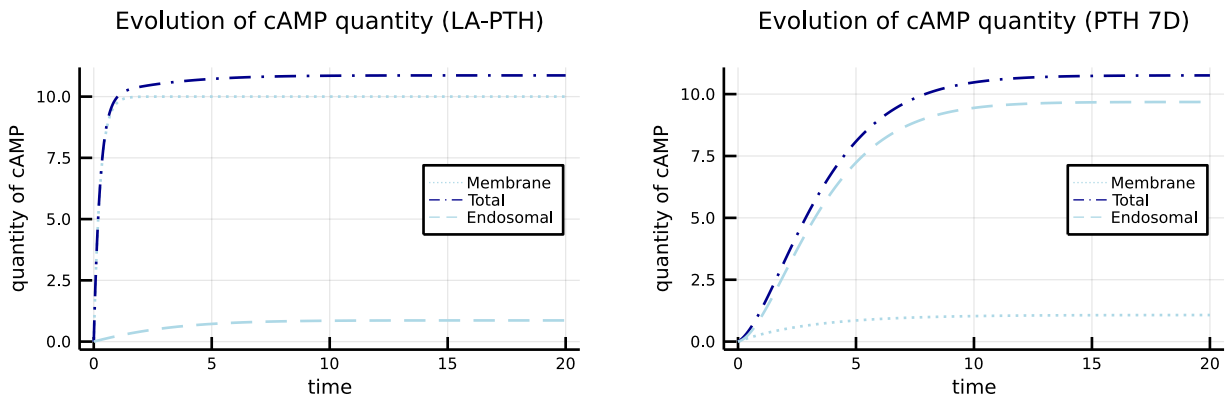

Figure 5.10: *Time evolution of the cAMP production for the LA-PTH ligand (left panel) and the PTH-7D ligand (right panel). We numerically simulate the 2D model given by Eqs.* (M2a)-(M2b) *with parameters given by.* (5.42)-(5.43)-(5.45) *(cAMP kinetic parameters differ between PTH 7D and LA-PTH both by the production rate and capacity of production.). See legend of Figure 5.9 for details.*

BIBLIOGRAPHY

[1] Claire Alamichel et al. “Modeling compartmentalization within intracellular signaling pathway”. In: *ESAIM: Proceedings and Surveys* 77 (2024), pp. 100–122.

[2] Dmitri V Alexandrov et al. “Dynamics of intracellular clusters of nanoparticles”. In: *Cancer Nanotechnology* 13.1 (2022), p. 15.

[3] Safaa Al-Ali. “Modélisation mathématique des maladies inflammatoires chroniques de l’intestin”. PhD thesis. Université Paris XIII, 2022.

[4] Safaa Al-Ali et al. “Automatic bleeding and ulcer detection from limited quality annotations in ulcerative colitis”. In: *Inflammatory Bowel Diseases* 28.Supplement_1 (2022), S19–S20.

[5] Safaa Al-Ali et al. “Detection of ulcerative colitis lesions from weakly annotated colonoscopy videos using bounding boxes”. In: *Gastrointestinal Disorders* 6.1 (2024), pp. 292–307.

[6] Luís Almeida et al. “Optimal releases for population replacement strategies: application to wolbachia”. In: *SIAM Journal on Mathematical Analysis* 51.4 (2019), pp. 3170–3194.

[7] Luke Alphey et al. “Genetic control of Aedes mosquitoes”. In: *Pathogens and global health* 107.4 (2013), pp. 170–179.

[8] David F Anderson and Aidan S Howells. “Stochastic reaction networks within interacting compartments”. In: *Bulletin of Mathematical Biology* 85.10 (2023), p. 87.

[9] David F Anderson and Thomas G Kurtz. *Stochastic analysis of biochemical systems*. Vol. 674. Springer, 2015.

[10] Donald G Aronson and Hans F Weinberger. “Nonlinear diffusion in population genetics, combustion, and nerve pulse propagation”. In: *Partial Differential Equations and Related Topics: Ford Foundation Sponsored Program at Tulane University, January to May, 1974*. Springer, 2006, pp. 5–49.

[11] Célestine M Atyame et al. “Stable coexistence of incompatible Wolbachia along a narrow contact zone in mosquito field populations”. In: *Molecular Ecology* 24.2 (2015), pp. 508–521.

[12] Nicholas H Barton. “The effects of linkage and density-dependent regulation on gene flow”. In: *Heredity* 57.3 (1986), pp. 415–426.

[13] Nick H Barton and Michael Turelli. “Spatial waves of advance with bistable dynamics: cytoplasmic and genetic analogues of Allee effects”. In: *The American Naturalist* 178.3 (2011), E48–E75.

[14] Samir Bhatt et al. “The global distribution and burden of dengue”. In: *Nature* 496.7446 (2013), pp. 504–507.

[15] Marc R Birtwistle and Boris N Kholodenko. “Endocytosis and signalling: a meeting with mathematics”. In: *Molecular oncology* 3.4 (2009), pp. 308–320.

[16] Jean-Pierre Bourgade and Francis Filbet. “Convergence of a finite volume scheme for coagulation-fragmentation equations”. In: *Mathematics of Computation* 77.262 (2008), pp. 851–882.

[17] José Alfredo Cañizo Rincón et al. “Some problems related to the study of interaction kernels: coagulation, fragmentation and diffusion in kinetic and quantum equations”. In: (2006).

[18] Dongho Chae and PB Dubovskii. “Existence and uniqueness for spatially inhomogeneous coagulation equation with sources and effluxes”. In: *Zeitschrift für angewandte Mathematik und Physik ZAMP* 46.4 (1995), pp. 580–594.

[19] Alexander D Chalmers et al. “Bifurcation and dynamics in a mathematical model of early atherosclerosis: How acute inflammation drives lesion development”. In: *Journal of mathematical biology* 71 (2015), pp. 1451–1480.

[20] Matthew HT Chan and Peter S Kim. “Modelling a Wolbachia invasion using a slow–fast dispersal reaction–diffusion approach”. In: *Bulletin of Mathematical Biology* 75 (2013), pp. 1501–1523.

[21] J-F Collet and T Goudon. “Lifshitz-Slyozov equations: the model with encounters”. In: *Transport theory and statistical physics* 28.6 (1999), pp. 545–573.

[22] Jacques Cosnes et al. “Epidemiology and natural history of inflammatory bowel diseases”. In: *Gastroenterology* 140.6 (2011), pp. 1785–1794.

[23] Pavel B. Dubovskĭi. *Mathematical theory of coagulation*. National Univ., 1994.

[24] Michel Duprez et al. “Optimization of spatial control strategies for population replacement, application to Wolbachia”. In: *ESAIM: Control, Optimisation and Calculus of Variations* 27 (2021), p. 74.

[25] Lorenzo Duso and Christoph Zechner. “Stochastic reaction networks in dynamic compartment populations”. In: *Proceedings of the National Academy of Sciences* 117.37 (2020), pp. 22674–22683.

[26] Heverton Leandro Carneiro Dutra et al. “From lab to field: the influence of urban landscapes on the invasive potential of Wolbachia in Brazilian Aedes aegypti mosquitoes”. In: *PLoS neglected tropical diseases* 9.4 (2015), e0003689.

[27] W El Hajj, N El Khatib, and V Volpert. “Inflammation propagation modeled as a reaction–diffusion wave”. In: *Mathematical Biosciences* 365 (2023), p. 109074.

[28] N El Khatib, Stéphane Génieys, and Vitaly Volpert. “Atherosclerosis initiation modeled as an inflammatory process”. In: *Mathematical Modelling of Natural Phenomena* 2.2 (2007), pp. 126–141.

[29] Nader El Khatib et al. “Reaction–diffusion model of atherosclerosis development”. In: *Journal of mathematical biology* 65 (2012), pp. 349–374.

[30] Lawrence C Evans. "Partial differential". In: *American Mathematical Society, Providence, RI, USA* (2010).

[31] Martin Feinberg. "Foundations of chemical reaction network theory". In: (2019).

[32] Ronald Aylmer Fisher. "The wave of advance of advantageous genes". In: *Annals of eugenics* 7.4 (1937), pp. 355–369.

[33] Lionel Foret et al. "A general theoretical framework to infer endosomal network dynamics from quantitative image analysis". In: *Current Biology* 22.15 (2012), pp. 1381–1390.

[34] Herbert Gajewski. "On a first order partial differential equation with nonlocal nonlinearity". In: *Mathematische Nachrichten* 111.1 (1983), pp. 289–300.

[35] Robert A Gardner. "Existence and stability of travelling wave solutions of competition models: a degree theoretic approach". In: *Journal of Differential equations* 44.3 (1982), pp. 343–364.

[36] Alan C Genz and Aftab Ahmad Malik. "Remarks on algorithm 006: An adaptive algorithm for numerical integration over an N-dimensional rectangular region". In: *Journal of Computational and Applied mathematics* 6.4 (1980), pp. 295–302.

[37] Debdulal Ghosh, Jayanta Paul, and Jitendra Kumar. "On equilibrium solution to a singular coagulation equation with source and efflux". In: *Journal of Computational and Applied Mathematics* 422 (2023), p. 114909.

[38] Penelope A Hancock and H Charles J Godfray. "Modelling the spread of Wolbachia in spatially heterogeneous environments". In: *Journal of The Royal Society Interface* 9.76 (2012), pp. 3045–3054.

[39] Penelope A Hancock, Steven P Sinkins, and H Charles J Godfray. "Strategies for introducing Wolbachia to reduce transmission of mosquito-borne diseases". In: *PLoS neglected tropical diseases* 5.4 (2011), e1024.

[40] Danielle Hilhorst, Sébastien Martin, and Masayasu Mimura. "Singular limit of a competition–diffusion system with large interspecific interaction". In: *Journal of Mathematical Analysis and Applications* 390.2 (2012), pp. 488–513.

[41] Danielle Hilhorst et al. "Relative compactness in $L\hat{}p$ of solutions of some 2m components competition-diffusion systems". In: *Discrete and continuous dynamical systems* 21.1 (2008), pp. 233–244.

[42] Erwan Hingant and Mauricio Sepúlveda. "Derivation and mathematical study of a sorption-coagulation equation". In: *Nonlinearity* 28.10 (2015), p. 3623.

[43] Ary A Hoffmann et al. "Stability of the w Mel Wolbachia infection following invasion into Aedes aegypti populations". In: *PLoS neglected tropical diseases* 8.9 (2014), e3115.

[44] Ary A Hoffmann et al. "Successful establishment of Wolbachia in Aedes populations to suppress dengue transmission". In: *Nature* 476.7361 (2011), pp. 454–457.

[45] Harriet Hughes and Nicholas F Britton. "Modelling the use of Wolbachia to control dengue fever transmission". In: *Bulletin of mathematical biology* 75 (2013), pp. 796–818.

[46] Brian P Ingalls. *Mathematical modeling in systems biology: an introduction*. MIT press, 2013.

[47] Frederic Jean-Alphonse et al. “Spatially restricted G protein-coupled receptor activity via divergent endocytic compartments”. In: *Journal of Biological Chemistry* 289.7 (2014), pp. 3960–3977.

[48] Frédéric Jean-Alphonse and AC Hanyaloglu. “Regulation of GPCR signal networks via membrane trafficking”. In: *Molecular and cellular endocrinology* 331.2 (2011), pp. 205–214.

[49] Timothy H Keitt, Mark A Lewis, and Robert D Holt. “Allee effects, invasion pinning, and species’ borders”. In: *The American Naturalist* 157.2 (2001), pp. 203–216.

[50] Terry Kenakin. “Biased receptor signaling in drug discovery”. In: *Pharmacological reviews* 71.2 (2019), pp. 267–315.

[51] Boris N Kholodenko. “Cell-signalling dynamics in time and space”. In: *Nature reviews Molecular cell biology* 7.3 (2006), pp. 165–176.

[52] Hyunbin Kim et al. “Spatiotemporal characterization of GPCR activity and function during endosomal trafficking pathway”. In: *Analytical Chemistry* 93.4 (2021), pp. 2010–2017.

[53] A Kolmogoroff, I Petrovsky, and N Piscounoff. “Study of the diffusion equation with growth of the quantity of matter and its application to a biology problem”. In: *Dynamics of curved fronts*. Elsevier, 1988, pp. 105–130.

[54] AN Kolmogorov, IG Petrovskii, and NS Piskunov. “Étude de l’equations de la chaleur, de la matiére et son application á un probleme biologique”. In: *Bull. Moskov. Gos. Univ. Mat. Mekh* 1 (1937), p. 125.

[55] Tal Korem et al. “Growth dynamics of gut microbiota in health and disease inferred from single metagenomic samples”. In: *Science* 349.6252 (2015), pp. 1101–1106.

[56] S. Latrach, Nicolas Vauchelet, and Hatem Zaag. “Study of Wave Blocking in a Population Replacement Technique”. In submission. 2024.

[57] S. Latrach et al. “Mathematical study of the spread and Blocking in inflammatory bowel disease”. submitted. 2024.

[58] Douglas A Lauffenburger and Clinton R Kennedy. “Analysis of a lumped model for tissue inflammation dynamics”. In: *Mathematical biosciences* 53.3-4 (1981), pp. 189–221.

[59] Douglas A Lauffenburger and Clinton R Kennedy. “Localized bacterial infection in a distributed model for tissue inflammation”. In: *Journal of mathematical biology* 16 (1983), pp. 141–163.

[60] Philippe Laurençot. “Stationary solutions to Smoluchowski’s coagulation equation with source”. In: *arXiv preprint arXiv:2006.15879* (2020).

[61] Robert J Lefkowitz. “A brief history of G-protein coupled receptors (Nobel Lecture).” In: *Angewandte Chemie International Edition* 52.25 (2013).

[62] Peter CJ Leijh et al. “Kinetics of intracellular killing of Staphylococcus aureus and Escherichia coli by human granulocytes”. In: *European journal of immunology* 10.10 (1980), pp. 750–757.

[63] Wing-Cheong Lo, Razvan I Arsenescu, and Avner Friedman. “Mathematical model of the roles of T cells in inflammatory bowel disease”. In: *Bulletin of mathematical biology* 75.9 (2013), pp. 1417–1433.

[64] Sandra Lyga et al. “Persistent cAMP signaling by internalized LH receptors in ovarian follicles”. In: *Endocrinology* 2016.1 (2016), pp. 63–71.

[65] H Mayer, KS Zaenker, and U An Der Heiden. “A basic mathematical model of the immune response”. In: *Chaos: An Interdisciplinary Journal of Nonlinear Science* 5.1 (1995), pp. 155–161.

[66] Ian Morilla et al. “Singular manifolds of proteomic drivers to model the evolution of inflammatory bowel disease status”. In: *Scientific Reports* 10.1 (2020), p. 19066.

[67] Gregoire Nadin et al. “A Turing mechanism in order to explain the patchy nature of Crohn’s disease”. In: *Journal of Mathematical Biology* 83.2 (2021), pp. 1–17.

[68] Grégoire Nadin, Martin Strugarek, and Nicolas Vauchelet. “Hindrances to bistable front propagation: application to Wolbachia invasion”. In: *Journal of Mathematical Biology* 76 (2018), pp. 1489–1533.

[69] Tran Hien Nguyen et al. “Field evaluation of the establishment potential of w MelPop Wolbachia in Australia and Vietnam for dengue control”. In: *Parasites & vectors* 8 (2015), pp. 1–14.

[70] Kevin Penner, Bard Ermentrout, and David Swigon. “Pattern formation in a model of acute inflammation”. In: *SIAM Journal on Applied Dynamical Systems* 11.2 (2012), pp. 629–660.

[71] Benoît Perthame. *Parabolic equations in biology. Lecture notes on mathematical modelling in the life sciences*. 2015.

[72] Tobias Pietzsch, Lorenzo Duso, and Christoph Zechner. “Compartor: a toolbox for the automatic generation of moment equations for dynamic compartment populations”. In: *Bioinformatics* 37.17 (2021), pp. 2782–2784.

[73] Consul Porras et al. “A PDE approach of inflammatory phase dynamics in diabetic wounds.” In: (2014).

[74] Ahmed Rebai et al. “Unsupervised physics-informed neural network in reaction-diffusion biology models (Ulcerative colitis and Crohn’s disease cases) A preliminary study”. In: *arXiv preprint arXiv:2302.07405* (2023).

[75] A Reynolds et al. “A reduced mathematical model of the acute inflammatory response”. In: *I* (2006), pp. 220–236.

[76] Angela Reynolds et al. “A reduced mathematical model of the acute inflammatory response: I. Derivation of model and analysis of anti-inflammation”. In: *Journal of theoretical biology* 242.1 (2006), pp. 220–236.

[77] Susanne Roth et al. “G Protein–Coupled Receptor Signaling Networks from a Systems Perspective”. In: *Molecular Pharmacology* 88.3 (2015), pp. 604–616.

[78] Peter A Ryan et al. “Establishment of wMel Wolbachia in Aedes aegypti mosquitoes and reduction of local dengue transmission in Cairns and surrounding locations in northern Queensland, Australia”. In: *Gates open research* 3 (2019).

[79] Niamh Sayers and Aylin C Hanyaloglu. “Intracellular follicle-stimulating hormone receptor trafficking and signaling”. In: *Frontiers in endocrinology* 9 (2018), p. 653.

[80] Joshua G Schraiber et al. “Constraints on the use of lifespan-shortening Wolbachia to control dengue fever”. In: *Journal of theoretical biology* 297 (2012), pp. 26–32.

[81] Jacques Simon. “Compact sets in the space L p (O, T; B)”. In: *Annali di Matematica pura ed applicata* 146 (1986), pp. 65–96.

[82] Joel Smoller. *Shock waves and reaction—diffusion equations*. Vol. 258. Springer Science & Business Media, 2012.

[83] Alexander Sorkin and Mark Von Zastrow. "Endocytosis and signalling: intertwining molecular networks". In: *Nature reviews Molecular cell biology* 10.9 (2009), pp. 609–622.

[84] Martin Strugarek and Nicolas Vauchelet. "Reduction to a Single Closed Equation for 2-by-2 Reaction-Diffusion Systems of Lotka–Volterra Type". In: *SIAM Journal on Applied Mathematics* 76.5 (2016), pp. 2060–2080.

[85] María Ofelia Vásquez Ávila et al. "Ecuaciones en derivadas parciales para el análisis de modelos biopoliméricos". In: (2016).

[86] Pierre François Verhulst. *Recherches mathématiques sur la loi d'accroissement de la population*. Vol. 18. Hayez, 1845.

[87] Jean-Pierre Vilardaga, Frederic G Jean-Alphonse, and Thomas J Gardella. "Endosomal generation of cAMP in GPCR signaling". In: *Nature chemical biology* 10.9 (2014), pp. 700–706.

[88] Roberto Villaseñor, Yannis Kalaidzidis, and Marino Zerial. "Signal processing by the endosomal system". In: *Current opinion in cell biology* 39 (2016), pp. 53–60.

[89] Yoram Vodovotz. "Deciphering the complexity of acute inflammation using mathematical models". In: *Immunologic research* 36 (2006), pp. 237–245.

[90] Yoram Vodovotz et al. "Mathematical models of the acute inflammatory response". In: *Current opinion in critical care* 10.5 (2004), pp. 383–390.

[91] Aizik Isaakovich Vol pert, Vitaly A Volpert, and Vladimir A Volpert. *Traveling wave solutions of parabolic systems*. Vol. 140. American Mathematical Soc., 1994.

[92] TJPH Walker et al. "The w Mel Wolbachia strain blocks dengue and invades caged Aedes aegypti populations". In: *Nature* 476.7361 (2011), pp. 450–453.

[93] Jared C Weddell and Princess I Imoukhuede. "Integrative meta-modeling identifies endocytic vesicles, late endosome and the nucleus as the cellular compartments primarily directing RTK signaling". In: *Integrative Biology* 9.5 (2017), pp. 464–484.

[94] Hans F Weinberger, Mark A Lewis, and Bingtuan Li. "Analysis of linear determinacy for spread in cooperative models". In: *Journal of Mathematical Biology* 45.3 (2002), pp. 183–218.

[95] Katherine Wendelsdorf et al. "Model of colonic inflammation: immune modulatory mechanisms in inflammatory bowel disease". In: *Journal of theoretical biology* 264.4 (2010), pp. 1225–1239.

[96] John H Werren, Laura Baldo, and Michael E Clark. "Wolbachia: master manipulators of invertebrate biology". In: *Nature Reviews Microbiology* 6.10 (2008), pp. 741–751.

[97] Alex D White et al. "Spatial bias in cAMP generation determines biological responses to PTH type 1 receptor activation". In: *Science signaling* 14.703 (2021), eabc5944.

[98] Zhuoqun Wu, Jingxue Yin, and Chunpeng Wang. *Elliptic and parabolic equations*. World Scientific Publishing Company, 2006.

[99] Heng Lin Yeap et al. "Dynamics of the "popcorn" Wolbachia infection in outbred Aedes aegypti informs prospects for mosquito vector control". In: *Genetics* 187.2 (2011), pp. 583–595.

[100] Karma Yeshi et al. “Revisiting inflammatory bowel disease: pathology, treatments, challenges and emerging therapeutics including drug leads from natural products”. In: *Journal of clinical medicine* 9.5 (2020), p. 1273.